Università degli Studi di Ferrara

DOTTORATO DI RICERCA IN
SCIENZE DELL'INGEGNERIA

Ciclo XXX

Coordinatore: Prof. S. Trillo

Development and validation of Blind Deconvolution and Empirical Mode Decomposition techniques for impulsive fault diagnosis in rotating machines

Settore Scientifico Disciplinare ING/IND 13

Dottorando
Dott. Marco Buzzoni

Tutore
Chiar.mo Prof. Giorgio Dalpiaz

Anni 2014/2017

I always made an awkward bow
John Keats

to my family and Anna

PREFACE

I graduated in 2014 in Mechanical Engineering at the University of Ferrara discussing the thesis entitled "Analisi vibrazionale numerico-sperimentale di un trabatto per pasta alimentare" under the supervision of Prof. Dalpiaz. The results of my thesis [1] has been presented at "VIII Giornata di studio Ettore Funaioli". Immediately after, I started my Ph.D. in Engineering Science at the same university still under the supervision of Prof. G. Dalpiaz.

In the first year of my Ph.D., I have been involved on the development of a lumped parameter model based on the Eksergian's equation for the prediction of torsional oscillations and global vibration level of a linear vibratory feeder, pursuing the topic of my master's degree thesis. Over the three years of doctoral research, this research work led to further three publications, consisting of two conference papers [2, 3] and one journal paper [4].

[1] M. Buzzoni, E. Mucchi, and G. Dalpiaz. "Analisi vibrazionale numerica e sperimentale di un trabatto per pasta alimentare." In: *Giornata di studio Ettore Funaioli*. Bologna, 2014, pp. 153–166.

[2] M. Buzzoni, E. Mucchi, and G. Dalpiaz. "Improvement of the vibro-acoustic behaviour of vibratory feeders for pasta by modelling and experimental techniques." In: *Internoise 2016*. Hamburg, 2016, pp. 4005–4013.

[3] M. Buzzoni, M. Battarra, E. Mucchi, and G. Dalpiaz. "Noise and vibration improvements in vibratory feeders by analytical models and experimental analysis." In: *Internoise 2017*. Honk Kong, 2017, pp. 6749–6759.

[4] M. Buzzoni, B. M., E. Mucchi, and G. Dalpiaz. "Motion analysis of a linear vibratory feeder: Dynamic modeling and experimental verification." In: *Mechanism and Machine Theory* 114 (2017), pp. 98–110. ISSN: 0094-114X. DOI: http://dx.doi.org/10.1016/j.mechmachtheory.2017.04.006.

From the second half of the first year, I have been introduced on the research field of vibration-based diagnosis and monitoring of machines. In a first time, my researches focused on the characterization of piston slap phenomenon in IC diesel engines by means of vibration analysis taking advantage of cyclostationarity theory. In particular, the proposed procedure departs from the analysis of the Continuous Wavelet Transform in order to identify an

informative frequency band of piston slap phenomenon. This frequency band has been exploited as the input data in the further envelope analysis of the second-order cyclostationary part of the signal. The preliminary results of my studies about piston slap have been presented at the ISMA 2016 conference [5] whereas the complete research work has been published in Mechanical System and Signal Processing journal [6].

[5] M. Buzzoni, E. Mucchi, and G. Dalpiaz. "Piston slap noise reduction in IC engines : design improvements by advanced signal processing techniques." In: *ISMA2016*. Leuven, 2016.

[6] M. Buzzoni, E. Mucchi, and G. Dalpiaz. "A CWT-based methodology for piston slap experimental characterization." In: *Mechanical Systems and Signal Processing* 86.April 2016 (2017), pp. 16–28. ISSN: 08883270. DOI: 10.1016/j.ymssp.2016.10.005.

Consequently, my research activity focused on the detection and identification of impulsive faults. Firstly, I studied the Empirical Mode Decomposition algorithms for the fault diagnosis in multi-stage gearboxes. In particular, I have developed a methodology that combines the Empirical Mode Decomposition and the Time Synchronous Average in order to decompose the first-order cyclostationary part of the vibration signals related to an intermediate shaft of a multi-stage gearbox. The separated signals allow for the precise identification of the faulty gear even when the fault occurs in a stage having multiple (synchronous) gears. The results of this research work have been published to Shock and Vibration journal [7].

[7] M Buzzoni, E Mucchi, G D'Elia, and G Dalpiaz. "Diagnosis of Localized Faults in Multistage Gearboxes: A Vibrational Approach by Means of Automatic EMD-Based Algorithm." In: *Shock and Vibration* 2017 (2017), pp. 1–22. ISSN: 1070-9622. DOI: 10.1155/2017/8345704. URL: https://www.hindawi.com/journals/sv/2017/8345704/.

Then, in the wake of my studies about detection and identification of impulsive components through vibration analysis, I spent four months at the INSA of Lyon under the supervision of Prof. Antoni. In this period, I studied blind deconvolution algorithms with application to rotating machine diagnosis. Specifically, a novel BD algorithm has been developed and investigated based on a cyclostationary criterion. This research activity led to a novel method for extracting impulsive sources having (second-order) cyclostationary nature with a specific cyclic frequency. This methodology, compared with other blind deconvolution algorithms, proved to be superior on the extraction

of cyclostationary sources as well as on impulsive fault identification in gears and bearings.

On the grounds of the application of EMD algorithms and blind deconvolution methods for the diagnosis of localized faults in rotating machines, my thesis gathers and deepens the results and considerations achieved in these research activities.

Furthermore, I've recently collaborated with Prof. Castellani and his research group from the University of Perugia regarding the study of wake effects in a wind turbine farm through vibration analysis. The research focused on the characterization of the wake effects among wind turbines in series by analyzing the vibrations measured on the drive-line and on the nacelle. The results of this work have been published in Energies journal [8].

[8] F. Castellani, M. Buzzoni, D. Astolfi, G. D. Elia, G. Dalpiaz, and L. Terzi. "Wind Turbine Loads Induced by Terrain and Wakes : An Experimental Study through Vibration Analysis and Computational Fluid Dynamics †." In: *Energies* 10.11 (2017), pp. 1–19. DOI: 10.3390/en10111839.

Ferrara, 30/11/2017

Marco Buzzoni

ACKNOWLEDGMENTS

First of all, I would express my gratitude to my supervisor, Prof. Dalpiaz, for giving me the opportunity to start my Ph.D. on such a interesting field. I am also grateful to Prof. Mucchi and Dr. D'Elia for their useful suggestions and guidance.
I would like also to acknowledge Prof. Antoni for hosting me in his lab. It has been a sincere privilege and pleasure to collaborate with him in that short, but surely intense, period in Lyon.
I would also mention my thesis reviewers, Prof. Cadpessus and Prof. Fassois. Thanks for your kind words and your precious suggestions that have been very useful for improving this thesis.
I would thank all my colleagues who shared with me good and bad times, laughs and complaints. In these years, you have been more than just colleagues.
Last but not least, I'm very grateful to all those special people who supported me during this long and intense path. I particularly refer to my family, my girlfriend Anna and all my friends. Let me apologize, my friends, but you are too many to be mentioned one by one. I would like you to know that each contribution, small or big, has been fundamental for me. Every time you made me smile, I have made a step towards my goal. I'm pretty sure that all of this would never have been possible without you.
Thanks.

CONTENTS

LIST OF FIGURES

LIST OF TABLES

ACRONYMS

AR	Auto-Regressive
BD	Blind Deconvolution
CEEMDAN	Complete Ensemble Empirical Mode Decomposition with Adaptive Noise
CS1	First-order cyclostationary
CS2	Second-order cyclostationary
CYCBD	Maximum ICS2 Blind Deconvolution
CYCBDang	Maximum ICS2 Blind Deconvolution in the angle domain
DCS	Degree of cyclostationarity
EEMD	Ensemble Empirical Mode Decomposition
EMD	Empirical Mode Decomposition
EV	Eigenvalue
EVA	Eigenvalue Algorithm
FIR	Finite impulse response
HHT	Hilbert-Huang Transform
ICS	Indicator of cyclostationarity
IMF	Intrinsic mode function
IQR	Inter-quartile range
IRF	Impulse response function
MCKD	Maximum Correlated Kurtosis Deconvolution
MED	Minimum Entropy Deconvolution
MOMEDA	Multipoint Optimal Minimum Entropy Deconvolution Adjusted
OFM	Objective Function Method
OMEDA	Optimal Minimum Entropy Deconvolution Adjusted

SC	Spectral correlation
SES	Squared Envelope Spectrum
SIMO	Single-input-multi-output
SISO	Single-input-single-output
SNR	Signal-to-Noise Ratio
STFT	Short-time Fourier Transform
TSA	Time Synchronous Average

1

GENERAL INTRODUCTION

1.1 BACKGROUND

This thesis is focused on the diagnosis of rotating machines, with specific reference to rolling bearings and gears, by using the mechanical signature analysis. In this context, the terms "diagnosis" and "mechanical signature" assume a precise meaning. The term "diagnosis" refers to the detection and the localization of defects occurring in a mechanical system. The term "mechanical signature" refers to the characteristic vibration radiated by an operating machine, which can be recorded by using specific transducers. The basic concept behind the vibration analysis of mechanical systems is that any alteration – e.g. varying operating conditions, arising faults and so on, – is somehow reflected in the vibration signature. Thus, the vibrations generated by any operating machine can be exploited to extract a wide range of useful information about the system.

In the industrial scenario, the spread of vibration analysis can be quickly explained by the points of strength of this approach. Being non-intrusive and very reactive to the machine changes, the vibrational approach fits the needs of many applications and fields. The potential of this method consists in the number of heterogeneous information that is often contained in vibration signals allowing for the simultaneous extraction of data having various nature just from a single sensor. Some possible application fields of vibration signal analysis are: condition monitoring, fault detection, fault diagnosis, quality control, and so on [9].

There is another side of the coin. In fact, such information carried by vibration signals are often hidden and their extraction could not be a trivial task. De facto, the interpretation of mechanical vibration signals is frequently difficult

due to the background noise and several vibration contributions generated by the motion of the mechanical components, especially in complex mechanical systems.

Furthermore, vibration analysis is rooted on a fundamental limitation: the vibration transducers measure the response of the system to an excitation rather than the excitation itself. Since any structure acts - to a first approximation - as a linear time-invariant filter, the output of this "physical" filter actually is the measured vibration and not the source, which is the real origin of vibrations. Hence, the system response depends not merely on the excitation (often called source in this thesis), but also on the structural impulse response that relies upon the physical properties of the structure and the transducer position.

The aforementioned issues can be faced by processing the vibration signal with proper analysis techniques. Different strategies can be used according to the signal type (periodic, non-stationary, cyclostationary, etc). Many efforts have been made in the last four decades by the researchers in this direction in order to adapt and extend the general signal processing theory to mechanical applications. The number of works addressing this topic confirms the academic interest as well as the industrial one. In recent years, the vibration-based diagnosis has reached a satisfactory stage of maturity proposing several well established signal processing methodologies. Many methodologies have been designed with particular care about real applications guaranteeing consistency and effectiveness. Thanks to the advances achieved in the field of vibration-based diagnosis, the use of vibration analysis has spread in many fields and applications. Hereafter, a brief overview of some standard approaches is outlined.

1.2 VIBRATION-BASED DIAGNOSIS OF IMPULSIVE FAULTS

Gears and rolling bearings represent crucial components of many machines. In fact, the occurrence of faults in these components could lead to serious consequences to the whole system as high vibration level or breakdown. Thus, it has become essential to detect and diagnose the incipient faults in order to ensure the proper functioning of machines and avoid catastrophic failures. A survey about the consolidated signal processing techniques referenced to the identification of faults having impulsive nature is presented hereafter.

In general, gear faults and bearing faults can be divided into two main categories: localized faults and distributed faults. Overlooking the distributed faults that are not investigated in this thesis, the localized faults usually manifest in the form of cracks, spalls and pits, depending on the considered system and on the generation mechanism. Local gear faults typically occur on the tooth surface or on the tooth root such as: cracks in the gear tooth root, spalls, early stage pitting and certain manufacturing errors (such as burrs) [10]. On the other hand, the bearing faults can occur locally in the rolling elements or in the races, in particular in the early stage. The most common bearing faults are: localized pitting, spalls and brinelling [11].

The localized faults introduce non-stationary components into the measured vibration signal [9] in the form of a series of transients. Gears and bearings have different ways to generate these transients since the physical phenomena involved are dissimilar too. Regarding the gear faults, Mark [12, 13] demonstrated that two mating gears should exhibit a vibration signature containing only the tooth meshing harmonics. However, faults and tooth-to-tooth deviations from the perfect involute profile, commonly existing in real gears, produce contributions in the vibration signal. It is known that a reasonable way to model the vibration response due to a local gear fault in a spur gear train is by means of a local amplitude/phase modulation with a pure impulsive component [14, 15]. The vibration signature is a superposition of vibration components caused by the fault, dominant meshing vibrations and many other contributions, such as the effect of speed fluctuations. Thus, the presence of a gear fault is frequently masked by such interferences. Further, local bearing faults originally have been modeled using a deterministic approach, namely considering a Dirac comb convolved with the transfer function of the structure [16]. In general, the contributions of bearing faults are very weak with respect to other components as gear mesh vibrations. The detection of these impulsive components is further shrouded by modulation effects and variable transfer paths [17]. Moreover, random slip effects make things even more complicated.

In the last decade, a new perspective has taken hold: cyclostationarity proved to be a very effective framework for describing and processing vibration signals generated by gears and bearings (and many other mechanical systems). By noting that the occurrence rate and the amplitude of impulses are characterized by a certain level of randomness, a stochastic modeling of bear-

ing vibration signals has been proposed by Antoni and Randall [18, 19]. In fact, bearing fault signals exhibit random contributions having cyclic behavior. Specifically, it has been demonstrated that second-order cyclostationary (CS2) processes gives a more realistic description of involved random phenomena. Analogously, it has been proved that localized gear faults can be modeled by means of the cyclostationary framework as well. In this case, Capdessus et al. [20] shown that localized gear faults can be investigated by using first-order cyclostationary (CS1) tools as well as second-order ones.

Over the years, several consistent strategies have been proposed for the identification of localized faults in gears and rolling element bearings. On the basis of the previous considerations, two distinct families of signal processing techniques can be distinguished: the approaches exploiting the cyclostationary theory and the others. Regarding the gear diagnosis, the following traditional approaches are worth mentioning: order tracking techniques [21], scalar indicators (kurtosis, etc.) [22], cepstral analysis [23], demodulation analysis [24], time-frequency approaches [25, 26], synchronous averaging [27, 21], blind deconvolution algorithms [28], AR models [29] and methods based on spectral kurtosis [30]. The aforementioned approaches can be performed also for the bearing fault diagnosis. In particular, the envelope analysis (also called high-frequency resonance technique) [31] represented and is still representing the most common signal processing technique for bearing fault diagnosis. Well written references about the bearing fault diagnosis can be found in [32, 17].

The noteworthy cyclostationary tools are: the spectral correlation (SC) [33], the signal decomposition into CS1 part and CS2 part [34] and scalar indicators of cyclostationarity (ICS) [35]. Moreover, many connections and explanations have been established between the cyclostationary framework and the traditional approaches. In particular, it is relevant the connection between the envelope analysis (very effective but having an heuristic basis) and the integrated SC [36], the relationship between the TSA and the cyclostationarity at the first order [20] and the SC and the spectral kurtosis [37].

Finally, a general but complete dissertation about the fault diagnosis by using vibration analysis can be found in Ref [9].

1.3 RESEARCH OBJECTIVES

In the context of diagnosis of rotating machines, this research investigates two different aspects about impulsive fault detection and identification. The first one concerns the identification of impulsive sources just from noisy responses; the second one is about gear fault identification of multi-stage gearboxes, with specific regards to synchronous gears in intermediate stages.
As reported in Section 1.1, many approaches can be found in the specialized literature about identification of impulsive faults in gears and rolling bearings. In particular, the blind deconvolution (BD) methods can overcome the fact that vibration analysis, in general, deals with responses and not directly with excitations. Indeed, BD can recover an excitation to a linear system from a noisy observation (in a single-input-single-output system), which is a typical situation in the vibration-based diagnosis. For instance, the excitation force due to an incipient fault can be recovered from a measured vibration signal without the knowledge of the structural transfer function just using BD methods.
The most common BD algorithm used for machine diagnosis is based on the kurtosis maximization [38]. Only recently, two novel criteria [39, 40] have been proposed in order to improve the performances of BD algorithms when applied to rotating machine vibration signals. On this grounds, some aspects are still unclear or even not addressed:

- does an alternative to the optimization algorithms commonly used for BD exist?
- Is it possible to introduce a criterion explicitly based on cyclostationarity?
- What is the effectiveness of a cyclostationary criterion with respect to the others?
- How can be handled the non-constant regime cases by using BD algorithms?

Further, this thesis addresses also another complementary issue that is still not faced in the literature. De facto, even if many steps forward have been made on the fault diagnosis in multi-stage gearboxes, the fault identification is generally limited to establishing which stage pertains to the fault gear. The

identification of gear fault occurring in a wheel located in the intermediate shaft can be particularly complex due to the superposition of vibration signatures related to synchronous wheels. On these grounds, a method based on the Empirical Mode Decomposition (EMD) has been developed trying to answer to the following questions:

- is it possible to solve the issue previously described?
- Which EMD algorithm can deal with this problem?
- Which scalar indicator is the most effective in this circumstance?

All these questions have been carefully examined in this thesis. The possible answers are presented and supported by an extended discussion involving simulated and real signals.

1.4 METHODOLOGY AND ORGANIZATION OF THE THESIS

This thesis is organized into 4 chapters, where two different approaches for the detection and identification of impulsive components in the rotating machines are presented and discussed. The general research approach followed in this thesis involves an exhaustive validation including the use of both synthetic signals and real ones. Special attention has been paid on designing meaningful simulated signals, in agreement with the goal of the study. Furthermore, the practical application of all the proposed methodologies have been carefully addressed by means of extended experimental validations.
In Chapter 2, a novel BD method based on the generalized Rayleigh quotient and solved by means of an iterative eigenvalue decomposition algorithm is proposed. The peculiarity of this approach is that it can be easily adapted to arbitrary criteria. A new criterion based on (second-order) cyclostationarity maximization of the signal is proposed and compared with other BD methods existing in the literature. The cyclostationary BD method has been called CYCBD. Specifically, the following BD algorithms are taken into account: Minimum Entropy Deconvolution (MED), Optimal Minimum Entropy Deconvolution Adjusted (OMEDA), Maximum Correlated Kurtosis Deconvolution (MCKD) and Multi-point Optimal Minimum Entropy Deconvolution Adjusted (MOMEDA).

Foremost, the aforementioned BD methods are briefly summarized, highlighting strong points and limitations. Some original theoretical interpretations have been introduced as well. Firstly, the formulation based on the maximization of the kurtosis as well as higher-order statistics is deduced for single-input single-output (SISO) systems. Secondly, the SISO formulation based on the Indicator of Cyclostationarity (ICS) is proposed, i.e. the CYCBD. These formulations are given also in the case of Single-Input Multi-Output (SIMO) systems and for angle/time dependent signals.

Both benchmarking and validation have been performed taking into account synthetic signals and real ones in both constant and non-constant regimes. The synthetic signals are constituted of pure cyclostationary sources in complex environment in order to highlight the advantages of a cyclostationary BD criterion. The experimental signals concern two faulty conditions: a gear tooth spall and an outer race bearing fault. The gear fault data have been acquired from a dedicated test bench, taking into account different fault sizes and test conditions. The proposed method reliability has been assessed in terms of fault identification accuracy as well as fault severity. A diagnostic protocol for the gear tooth spall identification in multi-stage gearboxes based on CYCBD has also been proposed. The bearing fault data is related to a run-to-failure dataset, which may be found online in the NASA Prognostics Data Repository. Details can be found in the dedicated section. In this case, CYCBD and the BD methods have been compared in terms of bearing fault identification accuracy and prognostic capability.

The second part of this thesis, namely Chapter 3, deals with the identification of a localized gear fault occurring in a wheel located in the intermediate shaft of a multi-stage gearbox. The fundamental idea is to decompose the synchronous averaged signal referenced to the faulty (intermediate) stage into a set of representing signals containing the contribution of a single gear. In this way, it should be possible to establish which gear is the faulty one. The proposed methodology combines two well-known signal processing techniques: the EMD and the time synchronous average (TSA). Three different versions of the EMD algorithms are considered investigating which one returns the best output. The validation involves, again, simulated signals and experimental ones.

Finally, Chapter 4 outlines the concluding remarks summarizing results and significant aspects achieved in this thesis. Particular emphasis has been dedicated about the aspects of novelty and possible practical implications.

2

CYCLOSTATIONARY BLIND DECONVOLUTION FOR ROTATING MACHINE DIAGNOSIS

2.1 INTRODUCTION

The identification of impulsive faults may be difficult, particularly in the early stage, since the impulsive pattern characterizing the fault is often masked by the background noise, the dynamic response of the structure and other mechanical interferences. As mentioned in Section 1.1, impulsive sources cannot be directly measured. In fact, the original impulsive source is filtered by the impulse response function (IRF) of the system that frequently is unknown. For this purpose, BD techniques can be exploited in order to recover an impulsive pattern from noisy observations, even considering the effect of a unknown linear time-invariant system.

The mathematical problem behind BD is very general since a number of phenomena can be modeled as (linear) convolution mixtures with additive background noise. BD methods have been investigated and applied in a large number of fields and applications, such as image processing, telecommunications, seismic signal processing and rotating machinery, in order to blindly recover a source of interest. Indeed, in the field of seismic signal processing, Wiggins [41] pioneered BD by developing an iterative algorithm based on the maximization of the kurtosis (also called Varimax) in order to recover a spike-like source from a signal convolved with a unknown impulse response function. In the same field, Cabrelli [42] proposed another norm, called D-Norm, geometrically equivalent to the Varimax norm, which poses a direct solution to BD. In the literature, these methods are commonly known as Minimum Entropy Deconvolution (MED) and Optimal Minimum Entropy Deconvolution (OMED), respectively.

MED presents some drawbacks for the diagnosis of rotating machines such as the tendency to deconvolve a large single peak rather than periodic impulses and the inaptitude to deal with multiple faults. For these reasons, MED has been exploited in combination with other signal processing techniques in order to restrain some of its limitations.

Regarding the tooth fault detection, Endo and Randall [38] combined autoregressive (AR) models with MED in order to enhance the impulsive features of the vibration signal in the AR residual. This method has been further investigated by Endo et al. [43] in order to discriminate a gear tooth spall from a cracked tooth. A similar approach has been proposed by Sawalhi et al. [28] with regard of bearing diagnostics, taking advantage of the envelope spectrum driven by maximum spectral kurtosis. In a different way, the spectral kurtosis has been exploited also by He et al. [44] in order to extract multiple bearing faults.

Some authors explored higher-order statistics as well as various optimization algorithms. Lee and Nandi [45] analyzed the performance of BD via higher-order statistics (from the third to the sixth) considering impacting signals from a vibrating cantilever beam. The same authors [46] demonstrated also that Objetive Function Method (OFM) and EigenValue Method (EVA) give equivalent results considering the same experimental measurements. Another statistic, called Jarque-Bera statistic, combining both skewness and kurtosis (originally used in goodness-of-fit tests) has been investigated by Obuchowski et al. [47] for the gear fault identification in real vibration signals.

The need to design criteria dedicated to machine diagnosis led to the introduction of the correlated kurtosis and the Multi-Point D-Norm. BD via correlated kurtosis, also called MCKD, has been introduced by McDonald et al. [39] whereas BD via Multi-Point D-Norm (MOMEDA in short) has been proposed by McDonald and Zhao [40]. Both criteria try to enhance the impulsiveness of the vibration signal taking into account only a certain fault periodicity. In this way, the deconvolution of a periodic sequence of impulses is encouraged to meet the characteristic features of the vibration signals related to mechanical impulsive faults. In this direction it is worth mentioning the work of Miao et al. [48] who proposed an improved version of MCKD for bearing fault diagnosis that estimates automatically the fault period by using the auto-correlation function of the envelope.

Cyclostationarity has not been explicitly used for the design of BD criteria before now, although the importance to take advantage of cyclostationarity for diagnostics purpose [34] has been widely recognized. In fact, despite MCKD is a cyclostationary criterion, it has been proposed empirically, without explicit mention of cyclostationarity. Moreover, the definition of correlated kurtosis (that is the criterion of MCKD) entails some drawbacks that limit its application in many real applications. Thus, this research try to fill this gap exploiting cyclostationarity to design a simpler and more efficient criterion. Firstly, a novel iterative eigenvalue algorithm for BD based on the Rayleigh quotient is proposed. This algorithm differs from the EVA introduced by Jelonnek et al. [49] by the fact that it's not restricted to the use of fourth-order (cross) cumulants. Moreover, despite a similar approach have been investigated once by Zazo and Borrallo [50] in blind equalization problems, the proposed method is more general. In fact, the deconvolution process is guided by a weighting matrix which can be easily modified adapting the algorithm to arbitrary criteria. Then, criteria based on higher-order statistics have been deduced as well as criteria based on indicators of cyclostationarity (ICS), where the latter represent the very original part of this research. Indeed, in the literature only one other cyclostationary criterion can be found, i.e. the MCKD [39], whereas the others are based on extracting the most impulsive contribution (MED [41] and OMEDA [42]) or a periodic impulsive train (MOMEDA [40]). On these grounds, CYCBD can deal with cyclostationary sources and non-equispaced impulse trains, overcoming the limitations of the aforementioned BD methods.

Firstly, an introductory overview about several BD norms is given, pointing out some original considerations in order to explain advantages and limits of such techniques. Then, the performances of the proposed method rooted on a second-order cyclostationary criterion, called CYCBD, are compared with other BD methods, taking into account simulated signals as well as measured signals. Five different simulated examples have been investigated and discussed clarifying all the pros and cons described in the previous overview. The effectiveness of the proposed algorithm for the identification and quantification of gear tooth spall is assessed by means of a dedicated experiment in both constant and variable regimes. The robustness of the method is further demonstrated by a sensitivity analysis focused on the filter length, being the most critical parameter. Finally, a run-to-failure experiment addressing a

bearing outer-race fault has been examined in a similar fashion. The effectiveness of the early detection and identification of bearing faults has been investigated and a statistical threshold for the assessment of faulty states has proposed as well.

2.2 PROBLEM STATEMENT

This section provides the general formulation of a (SISO) BD problem and a more specific formulation for rotating machine applications.
In general, BD aims to recover - i.e. deconvolve - the input signal $\mathbf{s}_0$ from a noisy observed signal $\mathbf{x}$, viz:

$$\mathbf{s} = \mathbf{x} * \mathbf{h} = (\mathbf{s}_0 * \mathbf{g}) * \mathbf{h} \approx \mathbf{s}_0 \tag{1}$$

where $\mathbf{g}$ is the unknown impulse response function (IRF), $\mathbf{h}$ is the inverse filter (from now assumed to be a FIR filter), $\mathbf{s}$ is the estimated input and $*$ refers to the convolution operation. Note that, from now, bold lowercase letters refer to vectors whereas bold capital letters refer to matrices. A convenient way to express the convolution for discrete signals in matrix form is

$$\mathbf{s} = \mathbf{X}\mathbf{h} \tag{2a}$$

$$\begin{bmatrix} s[N-1] \\ \vdots \\ s[L-1] \end{bmatrix} = \begin{bmatrix} x[N-1] & \cdots & x[0] \\ \vdots & \ddots & \vdots \\ x[L-1] & \cdots & x[L-N-2] \end{bmatrix} \begin{bmatrix} h[0] \\ \vdots \\ h[N-1] \end{bmatrix} \tag{2b}$$

where L and N are the total samples of $\mathbf{s}$ and $\mathbf{h}$, respectively. Such expressions will be widely recalled in the next sections.
According to the scheme proposed in Refs. [38, 39] valid for vibration signals belonging to gearboxes, the observed signal in Eq. (1) can be rearranged as summarized in Fig. 35. The measured signal $\mathbf{x}$ is assumed to be composed of: an impulsive part $\mathbf{s}_0$ due to a localized fault, a pure periodic component $\mathbf{p}$ (e.g. related to the gear mesh) and Gaussian background noise $\mathbf{n}$, such that:

$$\mathbf{x} = \mathbf{s}_0 * \mathbf{g}_s + \mathbf{p} * \mathbf{g}_p + \mathbf{n} * \mathbf{g}_n \tag{3}$$

where $\mathbf{g}_s$, $\mathbf{g}_p$ and $\mathbf{g}_n$ are the IRFs related to $\mathbf{s}_0$, $\mathbf{p}$ and $\mathbf{n}$, respectively. Substituting Eq. (3) into Eq. (1), the mathematical formulation of BD in the context of diagnostics is given by:

$$\mathbf{s} = \left(\mathbf{s}_0 * \mathbf{g}_s + \mathbf{p} * \mathbf{g}_p + \mathbf{n} * \mathbf{g}_n\right) * \mathbf{h} \approx \mathbf{s}_0 \tag{4}$$

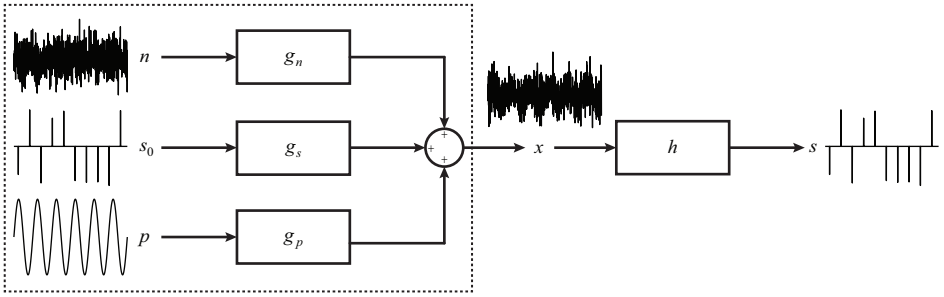

Figure 1: General scheme of blind deconvolution for mechanical system diagnostics.

where, in practice, $\mathbf{s}_0$ represents the excitation force due to an incipient fault. Thus, in this context, BD aims to estimate $\mathbf{h}$ such as to recover $\mathbf{s}_0$ linked to a machine faults minimizing the other contributions, i.e. $\mathbf{p}$ and $\mathbf{n}$.
The assumptions of the mathematical problem in Eq. (4) are: the samples of $\mathbf{s}_0$ are independent identically distributed random variables having a distinctive statistical property (e.g. impulsiveness), $\mathbf{g}$ is a stable Linear Time Invariant system and the stationary Gaussian noise, $\mathbf{n}$, and the periodic contribution, $\mathbf{p}$, are additive and do not share the same characteristics of $\mathbf{s}_0$. As it is, the problem is ill-posed since the IRFs – namely $\mathbf{g}_s$, $\mathbf{g}_p$, $\mathbf{g}_n$ – are not available. However, an estimation of the solution can be achieved considering an arbitrary criterion that imposes an expected solution based on a prior assumption, e.g. assuming a certain statistical property is met by the desired estimated source. In this respect, if the sources are convolved with different IRFs and are characterized by different statistical properties, the estimated inverse filter can highlight the target source reducing at the same time the contributions of the other sources. This happen when the frequency contents of the IRFs are not overlapped.
It should be noted that many BD methods are amplitude invariant, i.e. do not recover the actual source magnitude. However, BD deconvolution methods can provide useful information in terms of waveform, extracting a desired source that exhibits a certain statistical behavior.

2.3 OVERVIEW ABOUT BLIND DECONVOLUTION TECHNIQUES

This section is focused on the description of several BD algorithms. Priority has been given to the general explanation of the most common algorithms used in rotating machine diagnosis, divided by algorithm typology and high-

Table 1: Overview of BD algorithms.

	Method	Criterion	Feature to maximize
MED	iterative	$\frac{\sum_{l=0}^{L-1} \mathbf{s}[l]^4}{\left(\sum_{l=0}^{L-1} \mathbf{s}[l]^2\right)^2}$	impulse
OMEDA	direct	$\max_{k=0,1,\cdots,L-N-1} \left(\frac{\lvert\mathbf{s}[k]\rvert}{\lVert\mathbf{s}\rVert}\right)$	impulse
MCKD	iterative	$\frac{\sum_{l=0}^{L-1} \left(\prod_{m=0}^{M} \mathbf{s}[l-mT_{imp}]\right)^2}{\left(\sum_{l=0}^{L-1} \mathbf{s}[l]^2\right)^{M+1}}$	equispaced impulses
MOMEDA	direct	$\frac{1}{\lVert\mathbf{t}\rVert} \frac{\mathbf{t}^T\mathbf{s}}{\lVert\mathbf{s}\rVert}$	periodic impulses

lighting differences, pros and cons. Table 1 summarizes the salient points addressed.

The first category of BD algorithms is represented by methods that are solved iteratively using approaches such as the OFM or the EVA. In the specialized literature the most used BD methods for rotating machine diagnostics are: MED [38, 28, 44, 51] and MCKD [39, 48]. The second presented category regards the BD algorithms solved directly: OMEDA [42, 40] and its improved version MOMEDA [40].

2.3.1 *Minimum Entropy Deconvolution*

The MED algorithm has been firstly introduced by Wiggins [41] in seismic applications, exploiting the maximization of the kurtosis in order to recover a impulse-like estimation of the source. A criterion based on kurtosis maximiza-

tion represents a very reasonable choice also in machinery diagnostics since kurtosis is widely used as a general purpose indicator for fault identification in bearings and gears.
With reference to Equation (1), the method provides an estimation of $\mathbf{s}_0$ (and $\mathbf{h}$) given $\mathbf{x}$ which maximizes the following criterion, i.e. the sample kurtosis:

$$\kappa_4 = \frac{\sum_{l=N-1}^{L-1} \mathbf{s}[l]^4}{\left(\sum_{l=N-1}^{L-1} \mathbf{s}[l]^2\right)^2}. \tag{5}$$

Note that this definition of sample kurtosis assumes zero-mean signals, as obtained after centering. Moreover, the first considered sample is $N-1$ instead of 0. This choice is demonstrated in Ref. [40] and reduce possible numerical artifacts on the recovered signal due to the deconvolution process. From now, this strategy will be applied to all the blind deconvolution methods.
It should be remarked that MED is based on kurtosis maximization rather than entropy minimization. The definition of the entropy can assume many possible declinations. However, in this context, it is convenient to recall the entropy definition given by the probability theory [52]: the entropy is a measure of the average amount of information needed to specify the state of a random variable. Thus, the probability distributions having peak-like shape would exhibit low entropy values. Since kurtosis is also a measure of the sharpness of a probability distribution, this perspective establishes the link between the entropy and kurtosis. Moreover, if the signal probability distribution is symmetric and slightly non-Gaussian, then the Gram-Charlier expansion of the differential entropy is related to the opposite of the kurtosis (see Appendix A.1).
Inverse filter $\mathbf{h}$ is the results of the following maximization problem:

$$\mathbf{h} = \arg\max_{\mathbf{h}}(\kappa_4) \tag{6}$$

that can be estimated iteratively by the OFM. Analogous results can be achieved also using an eigenvalue (EV) approach exploiting the fourth-order cross cumulant [46]. For the full demonstrations see: Refs. [41, 40] for the OFM and Ref. [46] for the EVA. This criterion does not require any prior information

about the mechanical systems involved; thus it can be considered more general than other criteria that need, for instance, the prior knowledge of the fault period.

Nevertheless, as pointed out in Ref. [40], the main limit of MED is that it tends to extract the most impulsive source rather than a pattern of periodic impulses, that actually is how the local faults of the rotating machines appear in vibration signals. This shortcoming usually occurs when the FIR filter length is too long. This behavior is due to the nature of kurtosis since it theoretically reaches its maximum value for signals containing a unique impulse.

The term "too long" is on purpose ambiguous; in fact, a priori estimation of the proper FIR filter length is not possible even if the FIR filter length is a critical parameter that strongly influences the final results. This limitation does not regard only MED but it is shared by all the blind deconvolution algorithms. Thus, particular attention should be paid also to the selection of the filter length.

2.3.2 *Maximum Correlated Kurtosis Deconvolution*

The MED algorithm has been recently improved by McDonald et al. [39], which presented an iterative blind deconvolution method, called MCKD, based on a novel criterion called correlated kurtosis. The definition of correlated kurtosis reads:

$$CK_M = \frac{\sum_{l=N-1}^{L-1} \left(\prod_{m=0}^{M} \mathbf{s}[l - mT_{imp}] \right)^2}{\left(\sum_{l=N-1}^{L-1} \mathbf{s}[l]^2 \right)^{M+1}} \tag{7}$$

where T_s is the impulse period and M is the number of shifts. Note that the correlated kurtosis is equivalent to the kurtosis for $T_s = 0$ and $M = 1$. This criterion is a measure of signal impulsiveness connected with a given period T_s, taking advantage of two characteristics frequently encountered with machine faults: high kurtosis and repetitive occurrence of the impulses.

Despite correlated kurtosis has been proposed by intuition, it is worth noting that, de facto, is a cyclostationary criterion. A clarifying example is given in case of $M = 1$:

$$CK_1 = \frac{\sum_{l=N-1}^{L-1} \left(\mathbf{s}[l]\mathbf{s}[l - T_{imp}]\right)^2}{\left(\sum_{l=N-1}^{L-1} \mathbf{s}[l]^2\right)^2}. \tag{8}$$

Eq. (8) shows an evident similarity with the definition of kurtosis (see Eq. 5). However, it should be noted that the numerator of Eq. (8) is the discrete autocorrelation of the signal power, $\mathbf{s}^2$, at lag T_{imp}. This quantity is nothing but the signal power contribution which changes cyclically with frequency $\frac{1}{T_{imp}}$. De facto, since the correlated kurtosis is a measure of cyclostationarity according to a given cyclic frequency defined through $\frac{1}{T_s}$, MCKD allows for the estimation of a source exhibiting the maximum cyclostationarity at cyclic frequency $\frac{1}{T_{imp}}$.

The number of shifts M represents a parameter to be carefully set when MCKD is applied to real vibration signals. From experience [39], low values of M may not encourage enough the deconvolution of periodic impulses. Moreover, high values of M (in general more than 8) can compromise the correct source estimation. The previous considerations can be used to provide a informal justification about how correlated kurtosis behaves with respect to M. The presence of strong background noise ($SNR < 0$) affects the estimation of correlated kurtosis in particular for low values of M. For instance, with regard to $M = 1$, the numerator of Eq. (8) is not a consistent estimator of discrete autocorrelation in presence of noise. Furthermore, it is frequent that many rotating machines, even at nominal constant speed, exhibit slight regime fluctuations which reflect in fluctuating values of T_{imp}. This contributes further to a poor estimation of correlated kurtosis, in particular when $M \gg 1$.

2.3.3 *Optimal Minimum Entropy Deconvoluton Adjusted*

The first direct method discussed in this work is the so called OMEDA, that is an improvement of the original algorithm, proposed by Cabrelli [42] and

advanced by McDonald and Zhao [40]. This method is based on the following criterion:

$$\text{D-Norm} = \max_{k=N-1,1,\cdots,L-1} \left(\frac{|\mathbf{s}[k]|}{\|\mathbf{s}\|} \right) \tag{9}$$

where $\|\bullet\|$ is the Euclidean norm. The FIR filter that maximizes Equation (9) is given by one of the columns of

$$\mathbf{H} = \left(\mathbf{X}\mathbf{X}^H \right)^{-1} \mathbf{X} \tag{10}$$

that corresponds to the output, $\mathbf{s}$, having maximum D-Norm. The OMEDA solution can be easily computed by pre-multiplying Equation (10) by $\mathbf{X}^T$. The mathematical steps to obtain Equation (10) can be found in Refs. [42, 40]. According to Refs. [42, 40], it has been proved by means of numerical simulations that the OMEDA returns outputs having simpler structure than the MED solution.

A simpler interpretation of this approach can be given noting that Equation (10) is similar to the solution of a Least Square problem. The product between the right side of Equation (10) and identity matrix $\mathbf{I}$ yields to an equation where the k^{th} column of $\mathbf{H}$ is the Least Square solution of:

$$\mathbf{h}_k = \left(\mathbf{X}\mathbf{X}^H \right)^{-1} \mathbf{X}\mathbf{e}_k \tag{11}$$

where $\mathbf{e}_k$ is the k^{th} column of $\mathbf{I}$. In other words, Equation (11) is the solution of the following minimization problem:

$$\mathbf{h} = \arg\min_{\mathbf{h}} \left(\|\mathbf{X}\mathbf{h} - \mathbf{e}_k\| \right) \tag{12}$$

where $\mathbf{e}_k$ actually is an ideal impulsive signal, i.e. a Dirac impulse having unitary amplitude. Equation (11) is the Least Square solution of the filter coefficients based on a simple sharp target signal. Equation (10) is the extension of this logic, being $\mathbf{H}$ the set of solutions obtained considering shifted Dirac impulses as target signals. This interpretation is in agreement with the formulation of OMEDA, since it is designed to recover the simplest source from a given observation. Indeed, OMEDA scans all the possible Least Square solutions keeping the one returning the highest D-Norm. Finally, this interpretation is particularly convenient since it gives a prompt explanation about the tendency of OMEDA to deconvolve single peaks.

2.3.4 *Multi-point Optimal Minimum Entropy Deconvolution Adjusted*

An improvement of OMEDA has been proposed by McDonald and Zhao [40] by introducing a target vector $\mathbf{t}$ that promotes the deconvolution of a sequence of periodic impulses instead of a single one. The modified version of D-Norm (Equation (9)) is called Multi D-Norm and it reads:

$$\text{Multi D-Norm} = \frac{1}{\|\mathbf{t}\|}\frac{\mathbf{t}^T\mathbf{s}}{\|\mathbf{s}\|}. \tag{13}$$

The corresponding BD algorithm is called MOMEDA. The FIR filter $\mathbf{h}$ that maximizes Equation (13) is:

$$\mathbf{h} = \left(\mathbf{X}\mathbf{X}^H\right)^{-1}\mathbf{X}\mathbf{t} \tag{14}$$

where $\mathbf{t}$ drives the deconvolution by imposing the positions and the weights of the impulses to recover. A valid solution can be obtained by selecting the FIR filter length greater than the fault period. In this way, the correct position of the impulses are automatically adjusted by the filter delay. As for OMEDA, it can actually be checked that maximizing Equation (13) is equivalent to finding the Least Square solution of:

$$\mathbf{h} = \arg\min_{\mathbf{h}} \left(\|\mathbf{X}\mathbf{h} - \mathbf{t}\|\right) \tag{15}$$

i.e. the filter coefficients are estimated in order to minimize the least square error between $\mathbf{s}$ and an ideal Dirac comb, $\mathbf{t}$. Thus, by definition, MOMEDA overcomes the limitation of OMEDA to deconvolve only a single impulse and the restriction of MCKD to deal with short signals. By the way, MOMEDA presents also some drawbacks as the overestimation of pattern of impulses.

2.4 PROPOSED METHOD

In the following section, a BD algorithm based on the Rayleigh quotient is proposed. Firstly, a general criterion based on higher-order statistics is obtained; then, the novel BD criterion based on the cyclostationary maximization is explained and discussed.

2.4.1 *Blind deconvolution driven by kurtosis maximization and extension to higher-order statistics*

Unlike the methods proposed in refs. [41, 46] – which are based on the OFM method and the EVA method, respectively – BD with kurtosis maximization can be reformulated as follows. Let us first recall the definition of the fourth normalized moment, also called kurtosis. The expected mean for vibration signals is zero, therefore the kurtosis of $\mathbf{s}$ (which is zero mean) reads:

$$\kappa_4 = \frac{M_4}{M_2^2} = \frac{\mathbf{s}^H \mathbf{W} \mathbf{s}}{(\mathbf{s}^H \mathbf{s})^2}(L - N + 1) \tag{16}$$

where M_4 and M_2 are the fourth and the second moments, respectively, and the weighting matrix $\mathbf{W}$ is defined as:

$$\mathbf{W} = diag\left(\frac{\mathbf{s}^2}{\mathbf{s}^H \mathbf{s}}\right)(L - N + 1) = \begin{bmatrix} \ddots & & 0 \\ & s[n]^2 & \\ 0 & & \ddots \end{bmatrix} \frac{(L - N + 1)}{\sum_{n=N-1}^{L-1} s[n]^2}. \tag{17}$$

Substituting Equation (2a) in Equation (16), the following expression can be obtained:

$$\kappa_4 = \frac{\mathbf{h}^H \mathbf{X}^H \mathbf{W} \mathbf{X} \mathbf{h}}{\mathbf{h}^H \mathbf{X}^H \mathbf{X} \mathbf{h}} = \frac{\mathbf{h}^H \mathbf{R}_{XWX} \mathbf{h}}{\mathbf{h}^H \mathbf{R}_{XX} \mathbf{h}} \tag{18}$$

where $\mathbf{R}_{XWX}$ and $\mathbf{R}_{XX}$ are the weighted correlation matrix and the correlation matrix, respectively. Coming to the kurtosis maximization, it should be noticed that Equation (18) is a generalized Rayleigh quotient whose maximization with respect to $\mathbf{h}$ is equivalent to the eigenvector associated with the evaluation of the maximum eigenvalue λ of the following generalized eigenvalue (EV) problem [53]:

$$\mathbf{R}_{XWX} \mathbf{h} = \mathbf{R}_{XX} \mathbf{h} \lambda \tag{19}$$

then λ corresponds to maximum κ_4. Since $\mathbf{R}_{XWX}$ and $\mathbf{R}_{XX}$ are real and symmetric by construction and $\mathbf{R}_{XX}$ is also semi-positive definite, it implies that λ must be positive. This property is in agreement with the fact that the kurtosis is always positive by definition. The complete proof about optimization problems by means of the generalized Rayleigh quotient can be found in Appendix

A.2. Furthermore, it should be noted that **W** has to be initialized with a guess; hence, the equivalence between the maximum EV λ and the maximum κ_4 is reached only by means of an iterative algorithm summarized by the following steps:

Step 1: assume a guess of **h**;

Step 2: estimate **W** evaluating Equation (2a) given **X** and guessed **h**;

Step 3: solve Equation (19) finding **h** associated to the maximum EV λ;

Step 4: return to Step 2 using **h** estimated in Step 3 until convergence.

Since BD is based on the hypothesis that the source is a independent identically distributed random variable, a good initialization of **h** is given by a whitening filter, according to Ref. [54]. In practice, the whitening filter can be computed by means of an auto-regressive model filter by using the Yule-Walker equations for the filter coefficients estimation. Moreover, in mechanical applications, the vibration signal spectra can be dominated by sharp peaks related to the gear mesh harmonics or other deterministic sources [29]. Thus, the inverse AR filter strongly attenuates all the predictable components, returning a signal with a flat spectral density, which is the expected shape, on the average, for a signal containing a series of impulses. In order to improve the algorithm speed, the complete evaluation of the generalized EV problem can be avoided taking advantage of the fact that the algorithm needs only the maximum value of λ. For this purpose, dedicated algorithms for the estimation of the greatest EV (e.g. the power method) can be exploited.
At this point, an extension of the proposed algorithm can be written considering an arbitrary p^{th} order normalized moment by properly modifying **W**. Proceeding from the definition of the p^{th} order normalized moment, the following criterion is proposed:

$$\kappa_p = \frac{M_p}{M_2^{p/2}} = \frac{\mathbf{s}^H \mathbf{W} \mathbf{s}}{(\mathbf{s}^H \mathbf{s})^{p/2}} (L-N+1)^{\frac{p}{2}-2} \tag{20}$$

where the related weighting matrix is expressed as

$$\mathbf{W} = diag\left(\frac{\mathbf{s}^{p-2}}{(\mathbf{s}^H \mathbf{s})^{\frac{p}{2}-1}}\right)(L-N+1)^{\frac{p}{2}-2} = \begin{bmatrix} \ddots & & 0 \\ & s[n]^{p-2} & \\ 0 & & \ddots \end{bmatrix} \frac{(L-N+1)^{\frac{p}{2}-2}}{\sum_{n=N-1}^{L-1} s[n]^{p-2}}.$$

(21)

Hence, the BD algorithm via kurtosis maximization (see Equation (18)) can be easily extended for any normalized moment just using the weighted function defined in Equation (21). Note that in Equation (21) only $p > 2$ is relevant in the interests of the detection of impulsive components since $\kappa_{p>2}$ is a measure of the impulsiveness.

2.4.2 *Blind deconvolution driven by cyclostationarity maximization*

Analogously to the algorithm proposed in Section 2.4.1, a novel criterion for BD is proposed hereafter based on the maximization of the cyclostationarity, as measured by the Indicator of Cyclostationarity (ICS). This indicator has been proposed by Raad et al. [35] and its effectiveness on diagnostic purposes has been demonstrated in several applications such as gears [35], bearings [55] and internal combustion engines [56].
First of all, it may be useful to introduce some basic notions about cyclostationarity. From a general standpoint, a cyclostationary process is a process exhibiting a periodic behavior of its statistical properties. It has been demonstrated [34] that the rotating machine vibration signals are well modeled by cyclostationary processes. The real mechanical signals are often a mixture of first-order and second-order cyclostationary processes, called also CS1 and CS2, respectively. The CS1 part, whose mean is periodic, represents the perfectly deterministic part of the signal, which embodies all the periodic components of the signal, and the CS2 part is the purely random signal part, whose autocorrelation function is periodic. On these grounds, it is clear that the cyclostationary approach turns out to be more realistic and general with respect to the approaches (as assumed in the MOMEDA) that consider only the periodic part. Furthermore, the concept of cyclic frequency should be given in order to clarify the further dissertation. In the cyclostationary background, the cyclic frequency can be seen as the carrier frequency related to a certain (hidden) fluctuation of the signal energy, which can be related to physical phenomena as gear faults and bearing, for instance. In this context, the (discrete) cyclic frequency is defined as

$$\alpha = \frac{k}{T} \tag{22}$$

where k is the number of the harmonic and T is the fault period (in samples). Coming back to the proposed criterion, let us recall the general definition of the second-order ICS:

$$ICS_2 = \frac{\sum_{k>0} \left|{c_s}^k\right|^2}{\left|{c_s}^0\right|^2} \tag{23}$$

with

$${c_s}^k = \left\langle |\mathbf{s}|^2, e^{j2\pi\frac{k}{T}n} \right\rangle = \frac{1}{L-N+1} \sum_{n=N-1}^{L-1} |s[n]|^2 e^{-j2\pi\frac{k}{T}n} \tag{24a}$$

$${c_s}^0 = \frac{||\mathbf{s}||^2}{L-N+1}. \tag{24b}$$

Equations (24a) and (24b) may be expressed in a matrix form as follows:

$${c_s}^k = \frac{\mathbf{E}^H |\mathbf{s}|^2}{L-N+1} \tag{25a}$$

$${c_s}^0 = \frac{\mathbf{s}^H \mathbf{s}}{L-N+1} \tag{25b}$$

where

$$|\mathbf{s}|^2 = [|s[N-1]|^2, ..., |s[L-1]|^2]^T \tag{26a}$$

$$\mathbf{E} = \begin{bmatrix} \mathbf{e}_1 & \cdots & \mathbf{e}_k & \cdots & \mathbf{e}_K \end{bmatrix} \tag{26b}$$

$$\mathbf{e}_k = \begin{bmatrix} e^{-j2\pi\frac{k}{T}(N-1)} \\ \vdots \\ e^{-j2\pi\frac{k}{T}(L-1)} \end{bmatrix}. \tag{26c}$$

From Equations (24a) and (24b), Equation (23) may be expressed as:

$$ICS_2 = \frac{|\mathbf{s}|^{2H} \mathbf{E}\mathbf{E}^H |\mathbf{s}|^2}{|\mathbf{s}^H \mathbf{s}|^2}. \tag{27}$$

At this juncture, it may be observed that the signal comprising the periodic components of $|\mathbf{s}|^2$, called $\mathbb{P}\left[|\mathbf{s}|^2\right]$, containing all the cyclic frequencies of interest α can be written as

$$\mathbb{P}\left[\mathbf{s}\right] = \frac{1}{L-N+1} \sum_k e_k \left({e_k}^H |s|^2\right) = \frac{\mathbf{E}\mathbf{E}^H |\mathbf{s}|^2}{L-N+1} \tag{28}$$

Substituting Equation (2a) and Equation (28) into Equation (27) after a simple manipulation returns the final outcome:

$$ICS_2 = \frac{\mathbf{h}^H \mathbf{X}^H \mathbf{W} \mathbf{X} \mathbf{h}}{\mathbf{h}^H \mathbf{X}^H \mathbf{X} \mathbf{h}} = \frac{\mathbf{h}^H \mathbf{R}_{XWX} \mathbf{h}}{\mathbf{h}^H \mathbf{R}_{XX} \mathbf{h}} \tag{29}$$

where the weighting matrix $\mathbf{W}$ reads:

$$\mathbf{W} = diag\left(\frac{\mathbb{P}\left[|\mathbf{s}|^2\right]}{\mathbf{s}^H \mathbf{s}}\right)(L-N+1) = \begin{bmatrix} \ddots & & 0 \\ & \mathbb{P}\left[|\mathbf{s}|^2\right] & \\ 0 & & \ddots \end{bmatrix} \frac{(L-N+1)}{\sum_{n=N-1}^{L-1} |\mathbf{s}|^2}. \tag{30}$$

As done in Subsection 2.4.1, this BD criterion based on ICS_2 can be generalized to the p^{th} order ICS by appropriately modifying Equation (30):

$$\mathbf{W} = \begin{bmatrix} \ddots & & 0 \\ & \mathbb{P}\left[|\mathbf{s}|^p\right] & \\ 0 & & \ddots \end{bmatrix} \frac{(L-N+1)^{\frac{p}{2}}}{\sum_{n=N-1}^{L-1} |\mathbf{s}|^{\frac{p}{2}}}. \tag{31}$$

Equation (29) is the core of the proposed cyclostationary BD method, namely CYCBD. By solving Equation (29) through Equation (30), the proposed method extracts the source exhibiting the maximum CS2 behavior according to the cyclic frequency k.

2.4.2.1 *Extension to the Single-Input Multi-Output systems*

So far, this method has been developed for SISO systems. However, the algorithm can be easily extended to SIMO systems. This version of the algorithm can be exploited in order to improve the final results by performing a simultaneous blind deconvolution of multiple response signals. For the SIMO model, the deconvolution problem can be reformulated considering a number Q of responses $\mathbf{x}_q$. The deconvolution is carried out simultaneously for each $\mathbf{x}_q$ returning the estimation of $\mathbf{s}$, being the sum of the q^{th} contributions computed by the q^{th} inverse filters $\mathbf{h}_q$.
Equation (1a), (29) and (19), that are valid for SISO systems can be modified extending their validity also for SIMO systems. $\mathbf{R}_{XWX}$ and $\mathbf{R}_{XX}$ can be expressed as cross-correlation matrices, being $\mathbf{R}_{qq}$ the auto-correlation matrix of

$\mathbf{x}_q$ and $\mathbf{R}_{qk}$ the cross-correlation matrix between $\mathbf{x}_q$ and $\mathbf{x}_k$ (where $k = 1, \cdots, Q$ and $q \neq k$). Thus, $\mathbf{R}_{XX}$ can is given by:

$$\mathbf{R}_{XX} = \begin{bmatrix} \ddots & & \mathbf{R}_{qk} \\ & \mathbf{R}_{qq} & \\ \mathbf{R}_{kq} & & \ddots \end{bmatrix} \tag{32}$$

where the diagonal blocks are composed of the auto-correlation matrices of $\mathbf{x}_q$ and the off-diagonal blocks are composed of the cross-correlation matrices of $\mathbf{x}_q$ and $\mathbf{x}_k$. The weighted correlation matrix, $\mathbf{R}_{XWX}$, can be defined analogously. Again, the deconvolution problem can be iteratively solved by the generalized eigenvalue problem reported in Equation (19) which returns $\mathbf{h}$, that is the concatenation of vectors of filter coefficients related to the q^{th} response

$$\mathbf{h} = \begin{bmatrix} \mathbf{h}_1 \\ \vdots \\ \mathbf{h}_q \\ \vdots \\ \mathbf{h}_Q \end{bmatrix}, \tag{33}$$

and the final value of maximized criterion λ. From Equation (33), the q^{th} contribution to the source $\mathbf{s}$ can be calculated as:

$$\mathbf{s}_q = \mathbf{X}_q \mathbf{h}_q \tag{34}$$

where $\mathbf{X}_q$ is the Toeplitz matrix estimated as in Equation (1b) related to the q^{th} response $\mathbf{x}_q$. Finally, the overall source, $\mathbf{s}$, is computed by the sum of all the q^{th} sources calculated using Equation (34):

$$\mathbf{s} = \sum_{q=1}^{Q} \mathbf{s}_q. \tag{35}$$

2.4.2.2 *Weighting matrix in the angle domain*

The proposed algorithm may be further enhanced for the diagnostics of rotating machines improving the estimation of the periodic component in Equation

(31). It is a matter of fact that vibration signatures of rotating machines often exhibit periodicity locked in the angle domain rather than in the time domain [19, 34]. Recalling $\mathbb{P}\left[|\mathbf{s}|^p\right]$ in Equation (31), such a term is obtained by extracting the Fourier coefficients related to a certain set of cyclic frequencies and then returning the filtered signal in the time domain; viz:

$$\mathbb{P}\left[|\mathbf{s}|^p\right] = \sum_k c_k e^{j2\pi\frac{kt}{T}} \quad with \quad c_k = \frac{1}{L-N+1}\sum_{n=N-1}^{L-1}|s[n]|^p e^{-\frac{j2\pi kn}{T}}. \tag{36}$$

Exploiting the measured instantaneous speed (if available), the periodic component locked in the angular domain may be extracted avoiding resampling [57] by a change of variable in Equation (36). Therefore, under the assumptions that the considered signal is time/angle dependent, i.e. $\mathbf{s} = \mathbf{s}\left(\theta\left(t\right)\right)$, Equation (31) can be expressed in the time/angle domain as:

$$\mathbb{P}\left[|\mathbf{s}|^p\right] = \sum_k c_k e^{jk\theta} \quad with \quad \begin{cases} c_k = \frac{1}{\Theta}\sum\limits_{n=N-1}^{L-1}|s[n]|^p e^{-jk\theta}\dot{\theta}[n] \\ \Theta = \sum\limits_{n=N-1}^{L-1}\dot{\theta}[n] \end{cases} \tag{37}$$

where Θ is the normalization term.
The cyclostationary BD method based on Equation (37) is hereafter referred as CYCBDang. The cyclic components extracted by using Equation (37) should lead to better results for the diagnostics of rotating machines since it improves the estimation of the cyclostationary signal part also in presence of speed fluctuations.

2.4.2.3 *Further considerations*

It should be observed that the weighting matrix reported in Equation (30) is reminiscent. De facto, $\mathbf{W}$ expressed for the maximum kurtosis BD (see Equation (17)) is very similar to the weighting function obtained in Equation (30). Furthermore, this similarity allows advancing another interesting observation: the maximization of ICS_2 is equivalent to maximize kurtosis of the signal composed by a given set of cyclic frequencies α. From the physical point of view, this criterion drives the deconvolution (based on maximum kurtosis) with respect to only one phenomenon characterized by a specific period.

This property is particularly relevant for the diagnosis of rotating machines. Indeed, as pointed out in Refs. [39, 40], it may be exploited to highlight a specific fault as well as to discriminate the faulty rotating component from the healthy ones. However, the proposed criterion adds something more than the others presented in the specialized literature. On the one hand, MOMEDA deals with the extraction of an impulsive source approaching a Dirac comb, which is deterministic. On the other hand, MCKD exploits a cyclostationary criterion - i.e. the correlated kurtosis - as the CYCBD but owns some limitations (see also Paragraph 2.3.2). The first one is that the MCKD can be used just for short signals involving a very limited number of consecutive impulses [39]. The second one regards the definition of the fault period, which is constant and therefore valid only for systems operating at constant speed while CYCBD can benefit of Equation (37) in order to deals with fluctuating speeds. Eventually, the MCKD looks for the maximization of the kurtosis related to a certain period and it is a matter of fact that the kurtosis may be not the best indicator in some circumstances [58]. Moreover, CYCBD can be adapted to maximize different orders of cyclostationarity. Conceptually, this is a key point since the rotating machines exhibit cyclostationary behaviors of different order depending on the type of fault and of the systems [19]. Thus, CYCBD can be more versatile for the rotating machine diagnosis than the MCKD.

To sum up, it has been demonstrated that BD problem expressed as a generalized Rayleigh quotient represents a versatile approach being easily adapted to arbitrary criteria, such as the maximization of κ_p (see Equation (21)) or ICS_p (see Equation (31)), just by selecting proper weighting matrices.

2.5 APPLICATION TO SYNTHESIZED SIGNALS

Validation of the criterion based on the maximization of ICS_2 using simulated signals is provided in this section. BD via ICS_2 maximization (CYCBD) is performed considering basic synthesized signals and comparing the results among other techniques already published such as: BD via kurtosis maximization (Equation (17)) that can be considered as MED, OMEDA [42, 40], MCKD [39] and MOMEDA [40].

2.5.1 *Description of synthesized signals*

The simulations have been carried out in Matlab environment exploiting also the Matlab scripts available in Ref. [40]. Let us consider different types of signals holding cyclostationary behavior:

1. cyclic impulses with Gaussian distributed amplitudes and additive Gaussian background noise (SNR = -19 dB);
2. cyclic impulses having Gaussian distributed amplitudes with jitter effect (following a Gaussian distribution) and additive Gaussian background noise (SNR = -19 dB);
3. a couple of trains of impulses (with different cyclic frequency sets) having Gaussian distributed amplitude and additive Gaussian background noise (SNR = -19 dB);
4. cyclic impulses with Gaussian distributed amplitudes and additive Gaussian background noise (SNR = -19 dB) with the addition of a single dominant impulse;
5. train of impulses with Gaussian distributed amplitudes having fluctuating cycle and additive Gaussian background noise (SNR = -19 dB);

which, for simplicity, are called $\mathbf{x}_{sim,1}$, $\mathbf{x}_{sim,2}$, $\mathbf{x}_{sim,3}$, $\mathbf{x}_{sim,4}$ and $\mathbf{x}_{sim,5}$, respectively.
These signals are expressed in agreement with the previous general formulation (see Equation (3)), neglecting the periodic component $\mathbf{p}$, viz:

$$\mathbf{x}_{sim} = \sum_{i=1}^{I} \mathbf{s}_{0,i} * \mathbf{g}_{s,i} + \mathbf{n} * \mathbf{g}_n. \tag{38}$$

where index I indicates the number of the impulsive patterns ($I = 1$ for $\mathbf{x}_{sim,1}$, $\mathbf{x}_{sim,2}$ and $\mathbf{x}_{sim,5}$; $I = 2$ for $\mathbf{x}_{sim,3}$ and $\mathbf{x}_{sim,4}$). The parameters used for the synthesized signals are resumed in Table 2 where: f_s is the sampling frequency, T is the time length of the signal, $T_{s,i}$ is the impulse period, $\sigma_{s,i}$ is the standard deviation of the amplitude of the impulses and σ_j is the standard deviation of the jitter. In these simulations, the IRFs $\mathbf{g}_{s,i}$ and $\mathbf{g}_n$ have been modeled as responses of a damped single degree of freedom (SDOF) system to the time

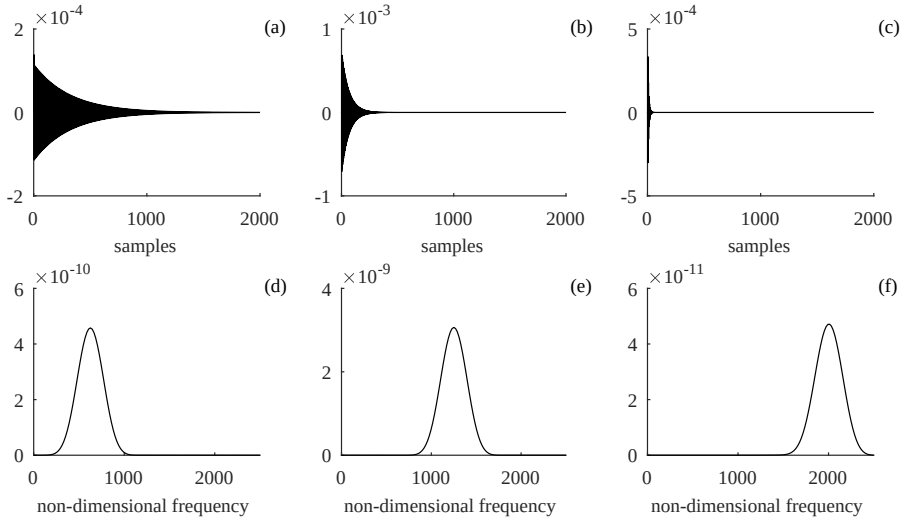

Figure 2: Simulated IRFs modeled as SDOF responses: (a) $\mathbf{g}_{s,1}$ and (d) its PSD, (b) $\mathbf{g}_{s,2}$ and (e) its PSD, (c) $\mathbf{g}_n$ and (f) its PSD.

domain unit impulse [59]. The damping is assumed viscous and sub-critical, as occurs in many real systems. In terms of displacements, the SDOF IRFs are defined as:

$$\mathbf{x}_{SDOF} = Ae^{-\zeta\omega_n t}\sin(\omega_d t) \tag{39}$$

where A is the response magnitude, ζ the damping coefficient, ω_n the resonance (angular) frequency and $\omega_d = \omega_n\sqrt{1-\zeta^2}$. The IRFs $\mathbf{g}_{s,i}$ and $\mathbf{g}_n$, expressed in terms of accelerations, are merely obtained by taking the second derivative with respect to time of Equation (39). Table 3 recaps the IRFs parameters while Figure 2 shows the IRF waveforms and the related power spectral density (PSD) using Welch's estimator (window length: 20 samples, overlap: 75 %). Figures 3, 4, 5, 6 and 7 display simulated signals $\mathbf{x}_{sim,1}$, $\mathbf{x}_{sim,2}$, $\mathbf{x}_{sim,3}$, $\mathbf{x}_{sim,4}$ and $\mathbf{x}_{sim,5}$, respectively, implemented in Matlab environment. Each simulated signal owns a pure cyclostationary source and has been designed with the specific purpose of highlighting the limitations of the considered BD algorithms from different standpoints.

Before examining the results, let us first discuss the general settings used for the different BD techniques in this comparison. As pointed out previously, care should be taken to select the filter length in order to achieve good quality

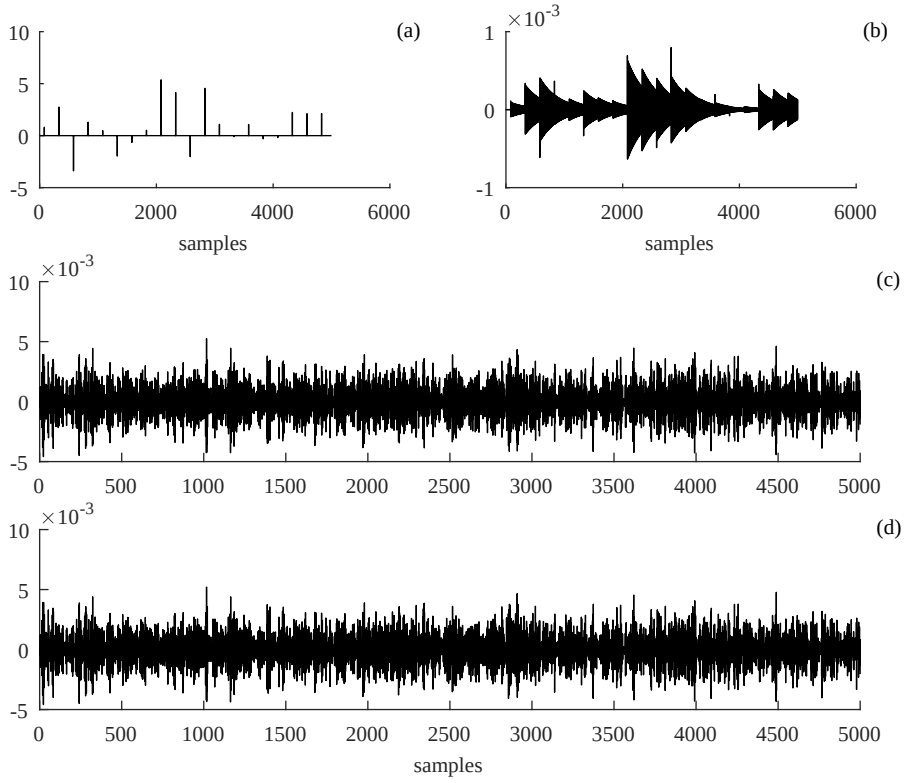

Figure 3: Simulated signal $\mathbf{x}_{sim,1}$: (a) train of equispaced impulses $\mathbf{s}_{0,1}$ having random (Gaussian) amplitudes with cycle $1/T_{s,1}$; (b) $\mathbf{s}_{0,1}$ convolved with the IRF $\mathbf{g}_{s,1}$; (c) Gaussian noise $\mathbf{n}$ convolved with the IRF $\mathbf{g}_n$; (d) overall signal $\mathbf{x}_{sim,1}$ with SNR = -19 dB.

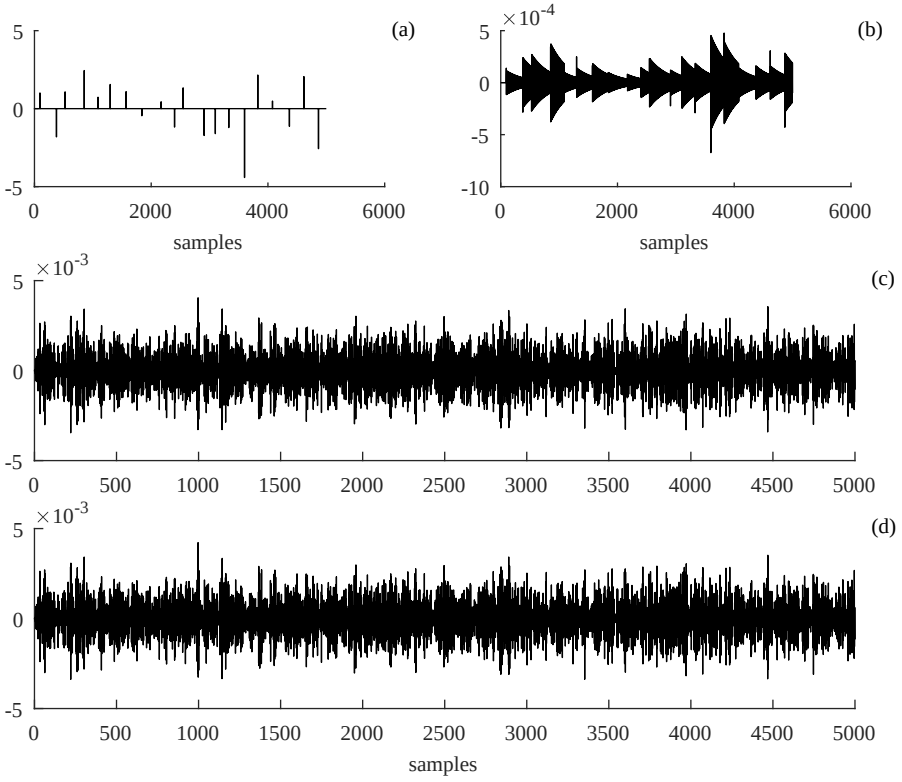

Figure 4: Simulated signal $x_{sim,2}$: (a) train of equispaced impulses $\mathbf{s}_{0,1}$ having random (Gaussian) amplitudes with cycle $1/T_{s,1}$ and jitter (Gaussian distribution); (b) $\mathbf{s}_{0,1}$ convolved with the IRF $\mathbf{g}_{s,1}$; (c) Gaussian noise $\mathbf{n}$ convolved with the IRF $\mathbf{g}_n$; (d) overall signal $\mathbf{x}_{sim,2}$ with SNR = -19 dB.

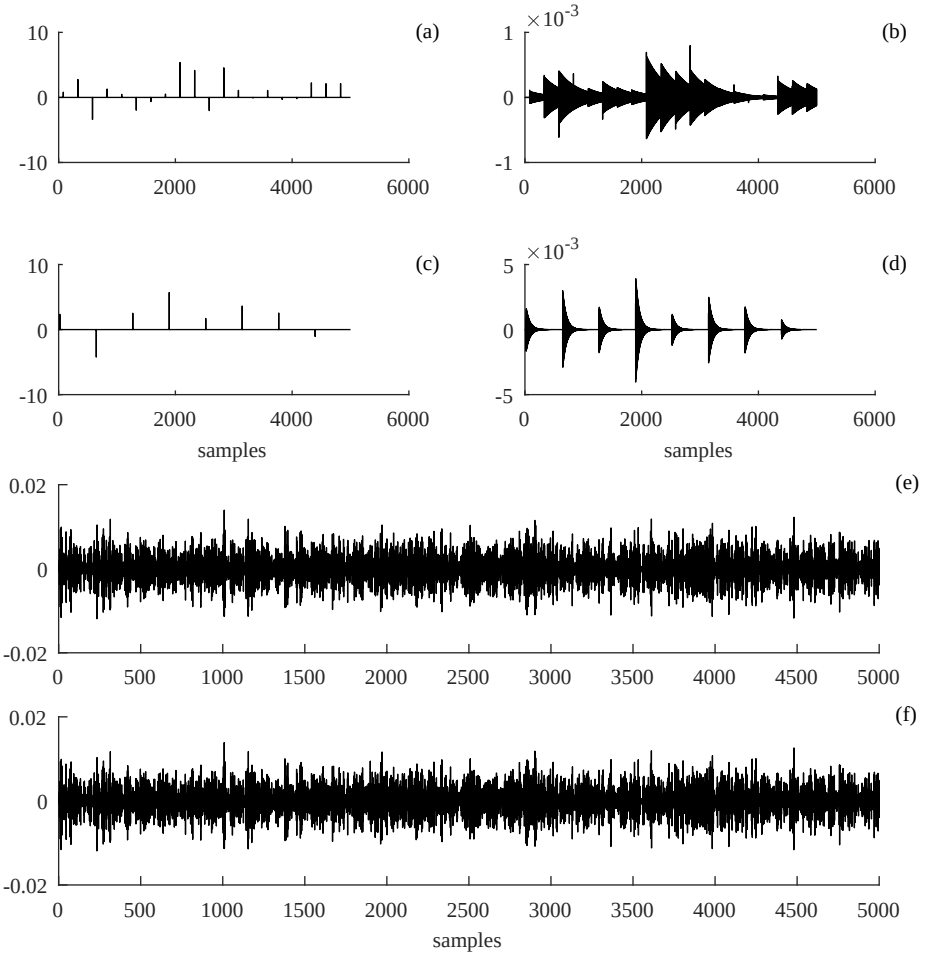

Figure 5: Simulated signal $\mathbf{x}_{sim,3}$: (a) train of equispaced impulses $\mathbf{s}_{0,1}$ having random (Gaussian) amplitudes with cycle $1/T_{s,1}$; (b) $\mathbf{s}_{0,1}$ convolved with IRF $\mathbf{g}_{s,1}$; (c) train of equispaced impulses $\mathbf{s}_{0,2}$ having random (Gaussian) amplitude with cycle $1/T_{s,2}$; (d) $\mathbf{s}_{0,2}$ convolved with IRF $\mathbf{g}_{s,2}$; (e) Gaussian noise $\mathbf{n}$ convolved with the IRF $\mathbf{g}_n$; (f) overall signal $\mathbf{x}_{sim,3}$ with SNR = -19 dB.

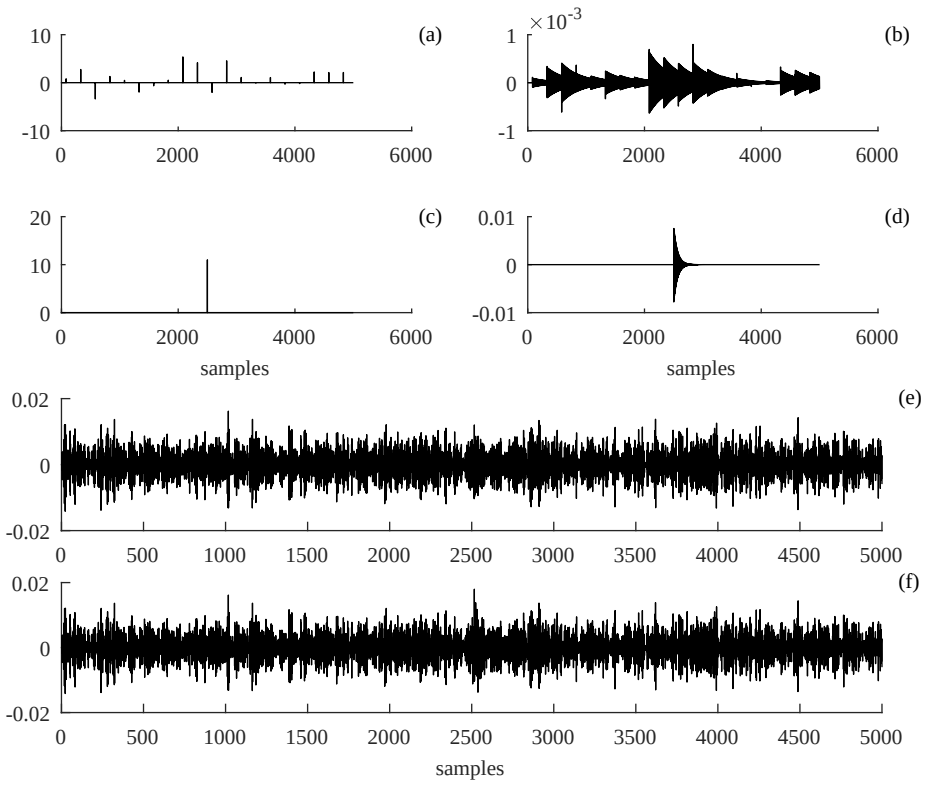

Figure 6: Simulated signal $\mathbf{x}_{sim,4}$: (a) train of equispaced impulses $\mathbf{s}_{0,1}$ having random (Gaussian) amplitudes with cyclic frequency $1/T_{s,1}$; (b) $\mathbf{s}_{0,1}$ convolved with IRF $\mathbf{g}_{s,1}$; (c) the single dominant peak $\mathbf{s}_{0,2}$; (d) $\mathbf{s}_{0,2}$ convolved with IRF $\mathbf{g}_{s,2}$; (e) Gaussian noise $\mathbf{n}$ convolved with IRF $\mathbf{g}_n$; (f) overall signal $\mathbf{x}_{sim,4}$ with SNR = -19 dB.

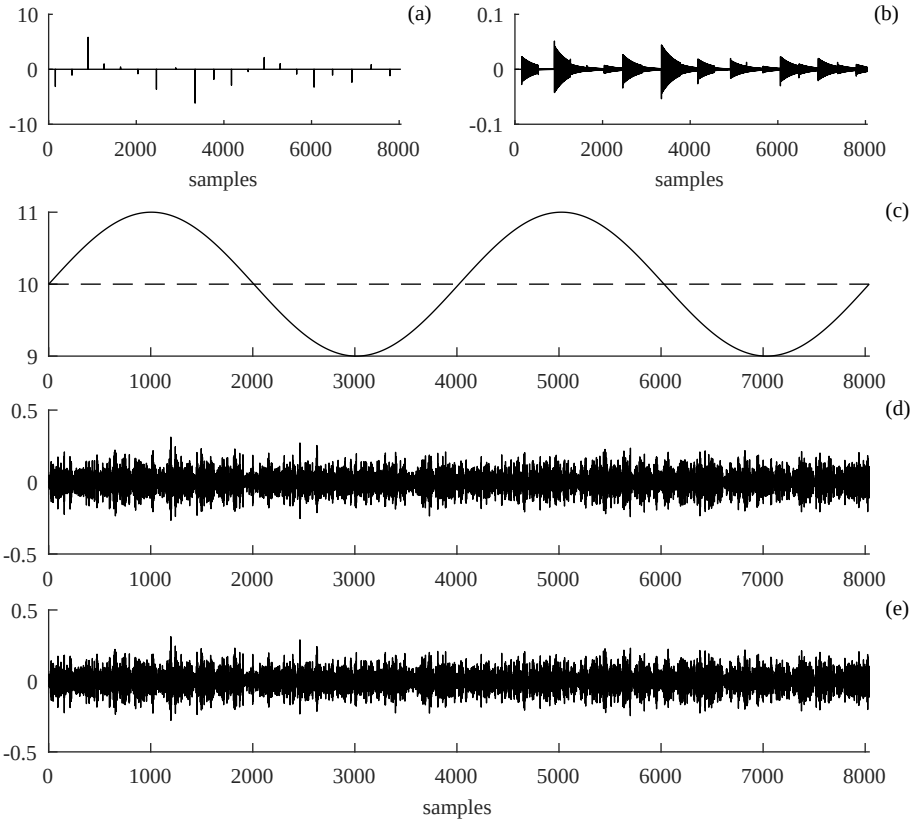

Figure 7: Simulated signal $\mathbf{x}_{sim,5}$: (a) train of equispaced impulses $\mathbf{s}_{0,1}$ having random (Gaussian) amplitudes with variable cycle $1/T_{s,1}$; (b) $\mathbf{s}_{0,1}$ convolved with IRF $\mathbf{g}_{s,1}$; (c) cyclic frequency values fluctuating around the mean value (dotted line); (d) Gaussian noise $\mathbf{n}$ convolved with IRF $\mathbf{g}_n$; (f) overall signal $\mathbf{x}_{sim,5}$ with SNR = -19 dB.

Table 2: Parameters used for the synthesized signals.

	$\mathbf{x}_{sim,1}$	$\mathbf{x}_{sim,2}$	$\mathbf{x}_{sim,3}$	$\mathbf{x}_{sim,4}$	$\mathbf{x}_{sim,5}$
$f_s\ (Hz)$	1000	1000	1000	1000	1000
$T\ (s)$	5	5	5	5	5
$T_{s,1}\ (s)$	0.250	0.250	0.250	0.250	0.250
$T_{s,2}\ (s)$	-	-	0.625	-	$-$
$\sigma_{s,1}$	1.500	1.500	1.500	1.500	1.500
$\sigma_{s,2}$	-	-	3.500	-	-
σ_j	-	0.025	-	-	-
$SNR\ (s)$	-19	-19	-19	-19	-19

Table 3: Parameters used for the computation of the IRFs.

	$\mathbf{g}_{s,1}$	$\mathbf{g}_{s,2}$	$\mathbf{g}_n$
A	$1.963\,10^{-10}$	$3.591\,10^{-10}$	$1.258\,10^{-10}$
ζ	0.004	0.01	0.05
$\omega_n\ (rad/s)$	19.894	39.788	63.662

results using BD algorithms: depending on the criterion, different strategies should be adopted. This aspect is argued in detail in Refs. [39, 40]. Excepting $\mathbf{x}_{sim,5}$, the same filter length has been kept for MED, OMEDA, MCKD and CYCBD (specifically 40 samples) while for MOMEDA the adopted filter length is 300 samples. Regarding $\mathbf{x}_{sim,5}$, the filter lengths used for MCKD, MOMEDA and CYCBDang are 100, 400 and 250 samples, respectively.

2.5.2 *Results and discussion*

Figure 8 summarizes the outputs obtained for different BD algorithms considering $\mathbf{x}_{sim,1}$. Note that source signal s_0 is buried under strong background noise ($SNR = -19\ dB$) and all the output signals are normalized by their respective maximum value. This normalization is allowed since BD is unable to recover the actual source amplitude. From the qualitative standpoint, the best result is achieved by MED, MCKD and CYCBD that provide a satisfy-

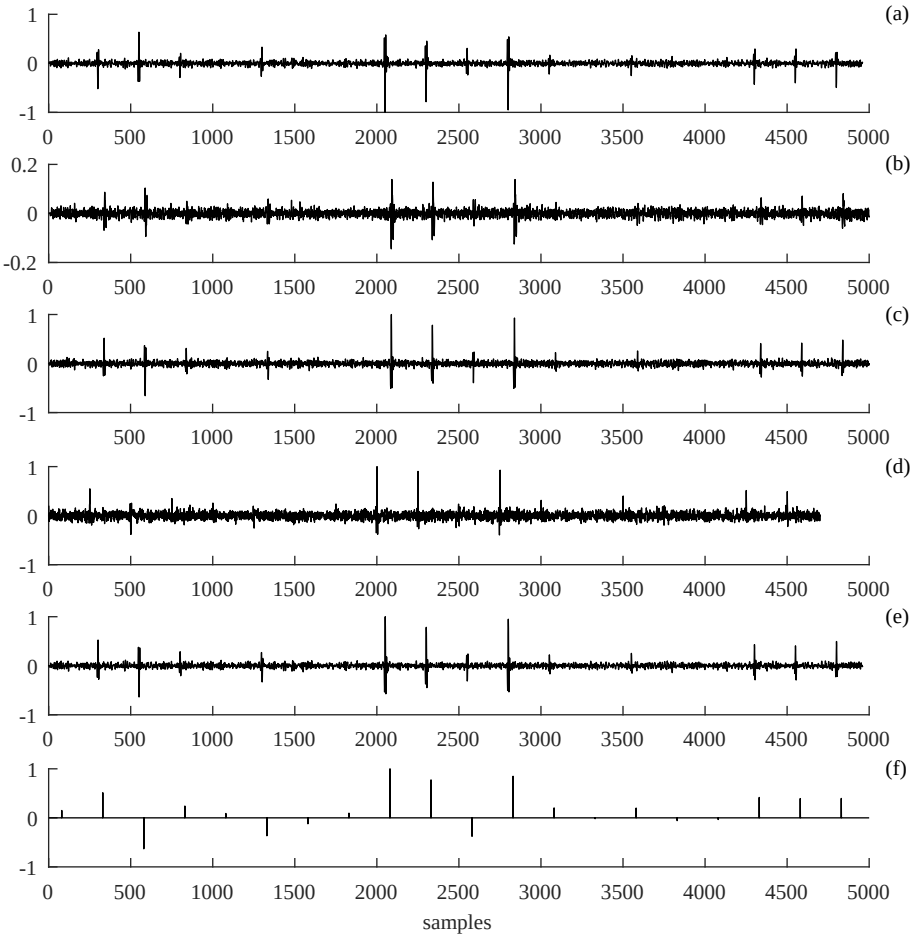

Figure 8: Comparison of the BD results regarding $\mathbf{x}_{sim,1}$: (a) MED, (b) OMEDA, (c) MCKD, (d) MOMEDA, (e) CYCBD and (f) the target source.

ing representation of the source signal. The impulses are extracted with their correct rate of repetition as well as their relative magnitudes. The MCKD performance is expected since it is based on a cyclostationary criterion. However, the correlated kurtosis is very sensitive to slight changes of the fundamental fault cycle. Hence, the jitter effect or even very slight changes on the impulse repetition rate should affect the MCKD results, as demonstrated by further examples. Unfortunately, the smallest impulses are difficult, even impossible, to be detected since they are overwhelmed by the low level background noise that is still present in the recovered signal. MOMEDA and OMEDA are able to properly extract just the prominent peaks, since they present a remarkable background noise kept by the recovered signal.

From these results, it is clear that the outputs of MED and CYCBD appear very similar. This outcome is not surprising since it has been demonstrated in Section 2.4 that there is a strong mathematical similarity between these two criteria. However, CYCBD owns the capability to recover signals characterized by certain cyclic frequencies and this feature may be exploited for diagnostics purpose as investigated in the following section.

In the same fashion, the results regarding $\mathbf{x}_{sim,2}$ are summarized in Figure 9. In this case, the random part of the signal is higher than in the previous example because of the jitter, which follows a Gaussian distribution. The presence of the jitter strongly worsens the MCKD output since the repetition of the impulses is no longer at constant rate. Again, MOMEDA returns to be not effective for the recover of cyclostationary sources since it assumes a periodic source to extract.

So far, no remarkable differences have been found between MED and CYCBD considering $\mathbf{x}_{sim,1}$ and $\mathbf{x}_{sim,2}$. The examples represented by $\mathbf{x}_{sim,3}$ and $\mathbf{x}_{sim,4}$ emphasize the differences between these algorithms. The simulated signal $\mathbf{x}_{sim,3}$ has been obtained by adding a second pattern of impulses with a different cyclic frequency. This signal may be useful in order to inspect the capability of CYCBD to discriminate different types of fault, depending on their periodicity. The expectation is that MED will recover the source exhibiting the lower number of impulses, i.e. the impulses with period $T_{s,2}$, since the lower the number of impulses, the higher the value of the kurtosis. This behavior should be followed also by OMEDA. Assuming that the source of interest is the one having period $T_{s,1}$, the results shown in Figure 10 agrees with the previous prediction. Indeed, MED (diagram (a) in Figure 10) recovers the source

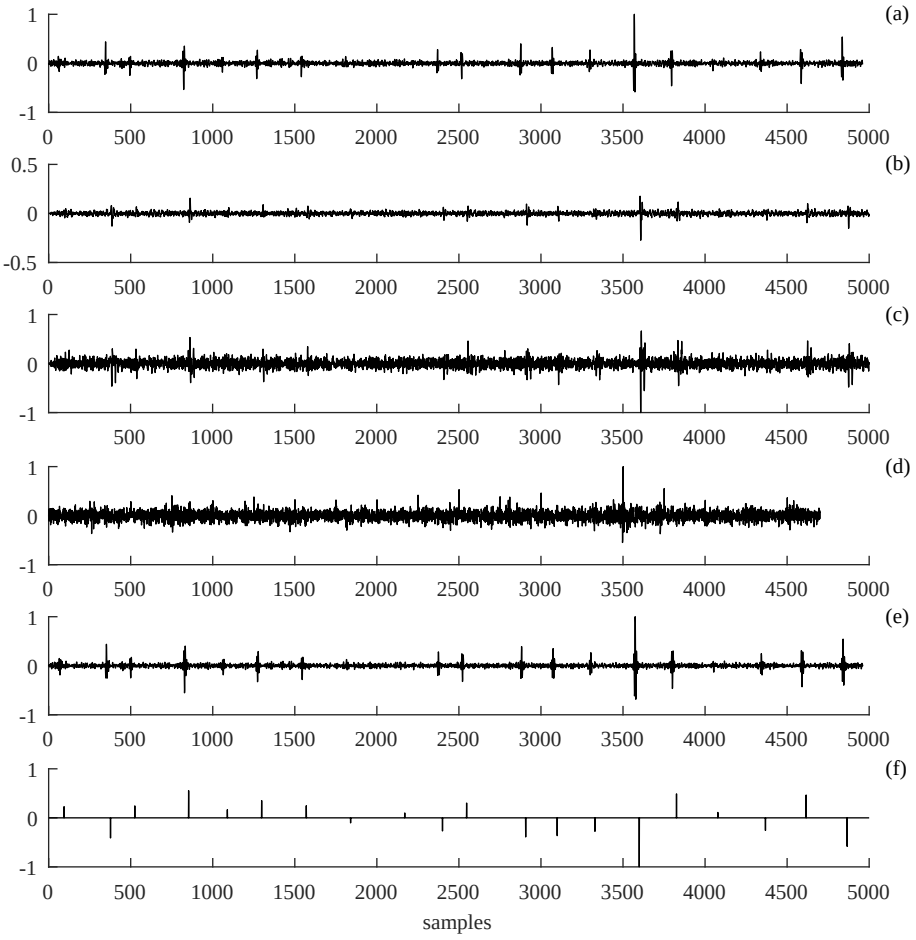

Figure 9: Comparison of the BD results regarding $\mathbf{x}_{sim,2}$: (a) MED, (b) OMEDA, (c) MCKD, (d) MOMEDA, (e) CYCBD and (f) the target source.

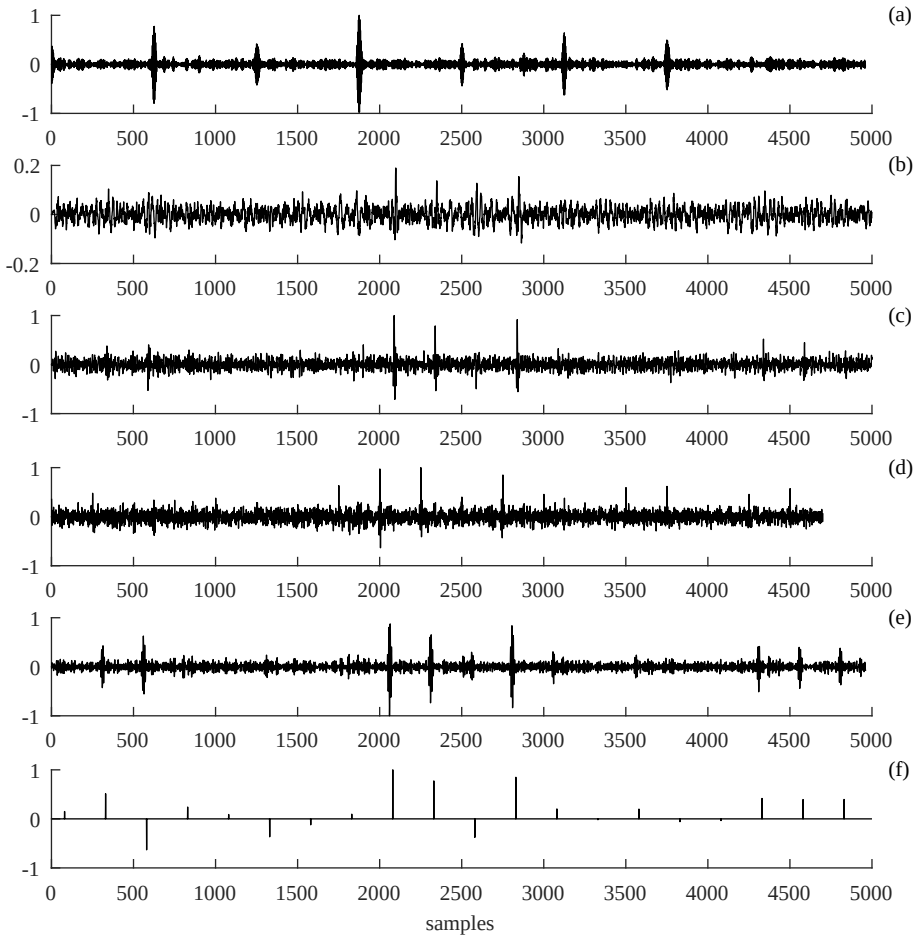

Figure 10: Comparison of the BD results regarding $x_{sim,3}$ focusing on fault period $T_{s,1}$: (a) MED, (b) OMEDA, (c) MCKD, (d) MOMEDA, (e) CYCBD and (f) the target source.

having period $T_{s,2}$ whereas CYCBD is the only one able to recover correctly the desired impulsive source. Moreover, note that MOMEDA is not biased by the presence of another impulsive pattern, but the provided estimation appears very noisy and the recovered peaks are barely observable; analogously, MCKD returns similar results. OMEDA completely fails the source recovering. Figure 11 collects the results obtained with the same data of Figure 10, but focusing on the target source having period $T_{s,2}$. As expected, CYCBD and the other BD techniques that depend on the selected fault period, i.e. MCKD and MOMEDA, can properly extract the target signal (diagram (f) in Figure 11). Note that, in this case, all the recovered signals are globally better than those collected in Figure 10. This behavior can be explained by the fact that, since the two mixed impulsive patterns have similar amplitudes (see diagram (a) and (c) in Figure 5), the maximized criteria tend to be more effective for the pattern, exhibiting the minor amount of impulses in the full time span. The simulated signal $\mathbf{x}_{sim,4}$ (see Figure 6) addresses the case of a train of impulses with Gaussian distributed amplitude with a single dominant impulse. Likewise to $\mathbf{x}_{sim,3}$, MED as well as OMEDA deconvolve the single dominant peak instead of the train of impulses, as reported in Figure 12. Moreover, also MCKD fails to provide the desired results.

Care should be paid to signals that exhibit more than one impulsive source. In fact, all the BD techniques addressed in this research are valid under the hypothesis of the presence of a single impulsive pattern to deconvolve; in other words, they basically refer to Single-Input-Single-Output systems. Hence, the proposed attempt to extract multiple sources only demonstrates that, under certain conditions, CYCBD - and to a lesser extent MCKD and MOMEDA - can overcome this intrinsic limit. But the results shown in Figures 10 and 11 can not be considered as a definitive proof of the effectiveness of CYCBD on signal separation considering multiple sources.

Finally, $\mathbf{x}_{sim,5}$ concerns the case of a train of impulses that are equispaced in the angle domain but they have a variable cyclic frequency in the time domain. In practice, this could be the case of bearing faults or gear faults under variable operating conditions. As reported in Figure 7(c), the cyclic frequency oscillates sinusoidally with a mean value of 10 Hz and an amplitude of ± 1 Hz. Figure 13 summarizes the results of the last numerical example and does not display the results of MED and OMEDA since the goal is to underline the limitations of MCKD and MOMEDA regarding non-equispaced impulses. In this

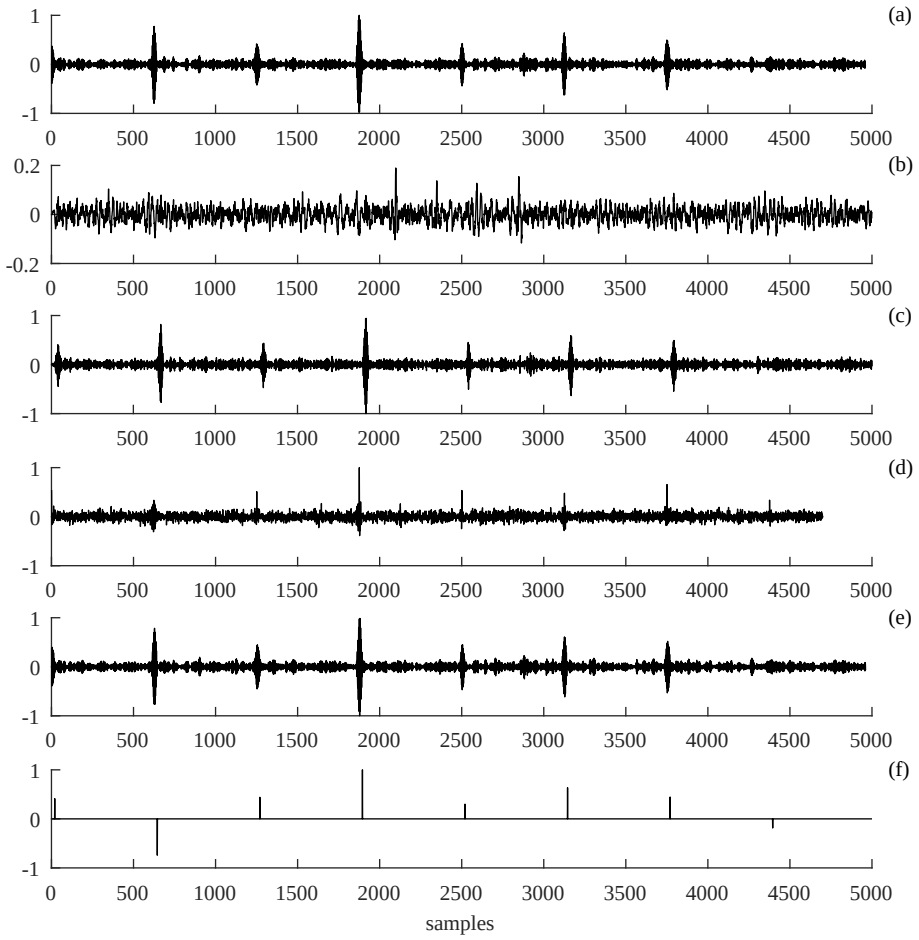

Figure 11: Comparison of the BD results regarding $\mathbf{x}_{sim,3}$ focusing on fault period $T_{s,2}$: (a) MED, (b) OMEDA, (c) MCKD, (d) MOMEDA, (e) CYCBD and (f) the target source.

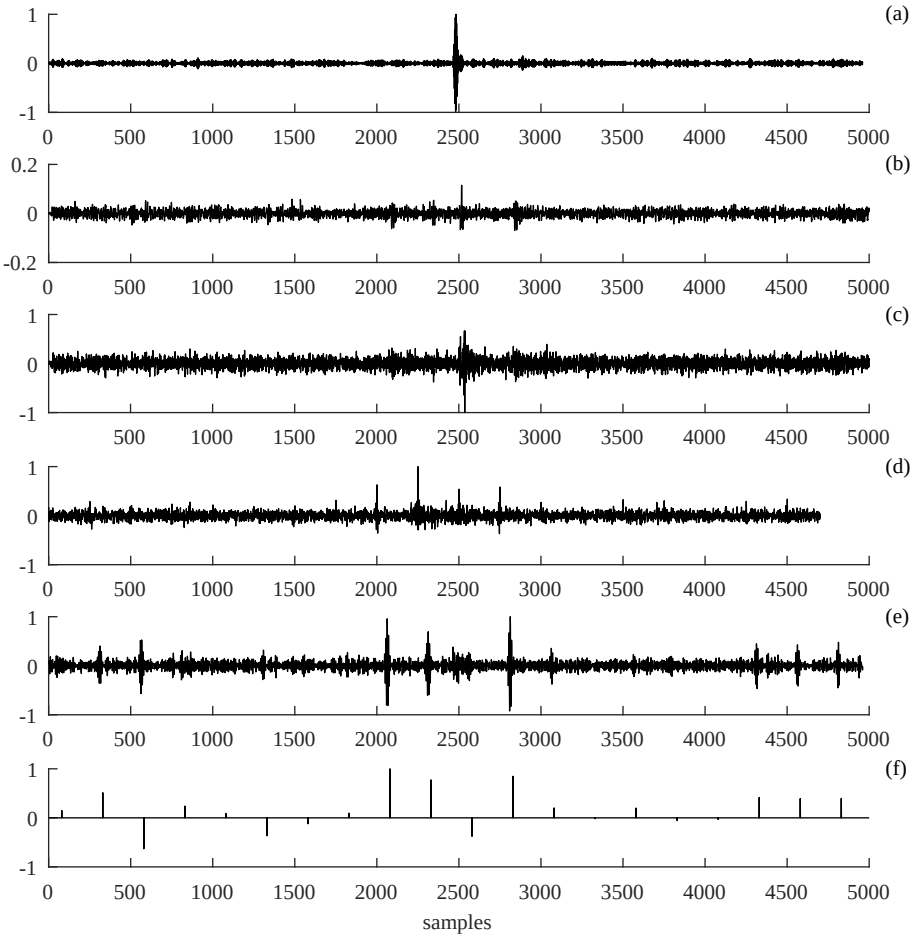

Figure 12: Overall comparison of the BD results regarding $\mathbf{x}_{sim,4}$: (a) MED, (b) OMEDA, (c) MCKD, (d) MOMEDA, (e) CYCBD and (f) the target source.

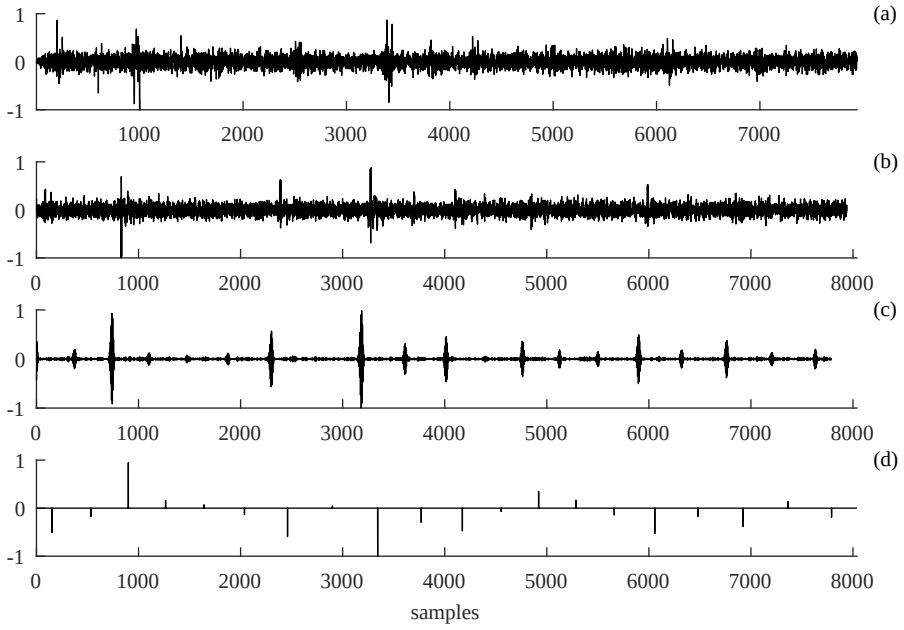

Figure 13: Overall comparison of the results regarding $\mathbf{x}_{sim,5}$: (a) MCKD, (b) MOMEDA, (c) CYCBDang and (d) the target source.

case, the CYCBDang is driven by the tacho reference while MCKD and MOMEDA are performed by using the average impulse period, which is 10 *Hz*. It can be easily noticed that CYCBDang recovers the original source with good accuracy in terms of relative amplitude as well as impulse spacing. However, both MCKD and MOMEDA are not capable to recover the original source providing a noisy output.
This section has remarked the advantages of CYCBD for the analysis of cyclostationary signals in comparison with BD algorithms already published in the literature by using dedicated examples. In general, CYCBD returns better results with respect to the other BD algorithms when the source is purely cyclostationary. The simulated results have highlighted the superiority of CYCBD with respect to MOMEDA, which is expected since MOMEDA fits with periodic sources. Moreover, MCKD is overcome too even if correlated kurtosis is a cyclostationary criterion. This is probably due to the definition of correlated kurtosis. Indeed, as remarked in Section 2.3.2, correlated kurtosis can become nil for long impulse trains as well as impulses not perfectly equispaced. However, this preliminary benchmark has been performed considering ad hoc simulated signals with marked cyclostationary behavior. Thus, further verifications are carried out in the next section considering real signals.

2.6 APPLICATION TO REAL SIGNALS: DIAGNOSIS OF A GEAR TOOTH SPALL

The first example deals with the detection of a gear tooth spall. First, a qualitative comparison of the results of several BD algorithm is presented; second, a procedure for gearbox diagnostics for the identification and quantification of seeded gear spalls based on BD technique is proposed and discussed.

2.6.1 *Experimental setup*

The first experimental verification of the proposed algorithm has been assessed by means of a dedicated test rig, shown in Figure 14, located at the Engineering Department of the University of Ferrara. Detailed information about this test rig can be found in Ref. [60].
The investigated gearbox is composed of two stages of helical gears: the first one having 18 and 71 teeth and the second one 12 and 55 teeth. Four different sizes of gear tooth spall have been realized via milling process in the

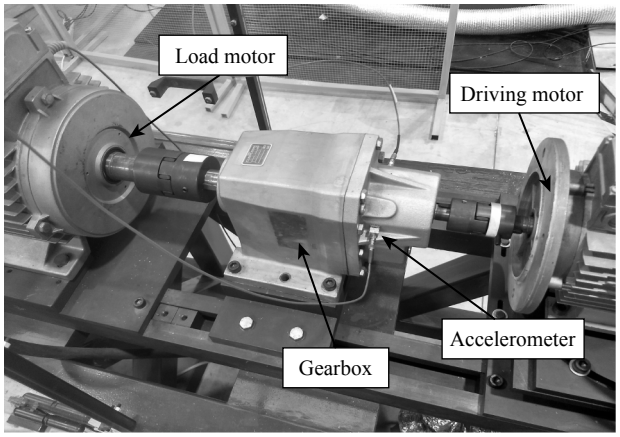

Figure 14: Experimental setup.

71 teeth wheel (first stage) in order to verify the sensitivity of the proposed criterion (see Figure 15). Table 4 collects the details of the artificial defects sorted according to the percentage ratio between the spall size and the whole tooth face. More information about the reproduction of the gear tooth spall by milling process can be found in Ref. [61]. All the steady condition tests have been carried out considering the following nominal conditions: input shaft speed of 3600 rpm and nominal load of 48.8 Nm.

It should be noted that the test condition just described is particularly unfavorable for the spall detection. Firstly, gear tooth spall is harder to detect in helical gears than in spur gears since the contact in helical gear is smoother. This feature, in general, favors the reduction of impulsive components due to the contact among teeth. Secondly, considering that the higher the load, the better the contact among gear teeth, the test load is significantly lower than the nominal load of the gearbox in actual working condition.

A variable speed test has been also carried out in order to validate experimentally the CYCBDang algorithm. In this case, the test has been performed in run-up condition between 30 Hz and 34 Hz referenced to the input shaft rotation frequency, with a load of 45.8 Nm.

The vibration signals in the radial direction have been collected by means of B&K piezoelectric accelerometer placed on the bearing support of the first stage pinion with sampling frequency 10.2 kHz for a total time duration of

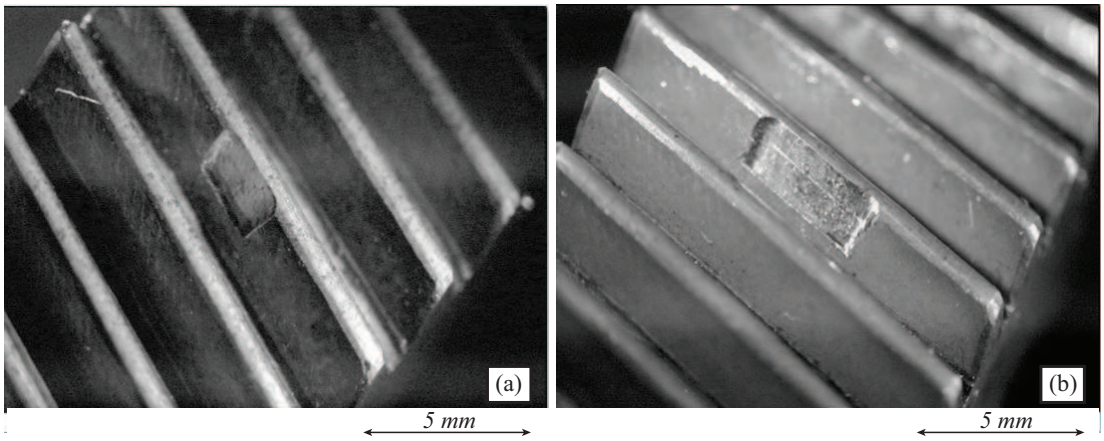

Figure 15: Detail of artificial gear tooth spall: (a) Sp12.5 and (b) Sp25.

Table 4: Description of the gear tooth spalls considered in the experimental campaign [62].

ID	Fault description
Sp12.5	2 *mm* along the tooth profile, 0.6 *mm* depth, 2 *mm* across the tooth face (12.5 % of the tooth face width)
Sp25	2 *mm* along the tooth profile, 0.6 *mm* depth, 4 *mm* across the tooth face (25 % of the tooth face width)
Sp50	2*mm* along the tooth profile, 0.6 *mm* depth, 7.8 *mm* across the tooth face (50 % of the tooth face width)
Sp100	2 *mm* along the tooth profile, 0.6 *mm* depth, 15.5 *mm* across the tooth face (100 % of the tooth face width)

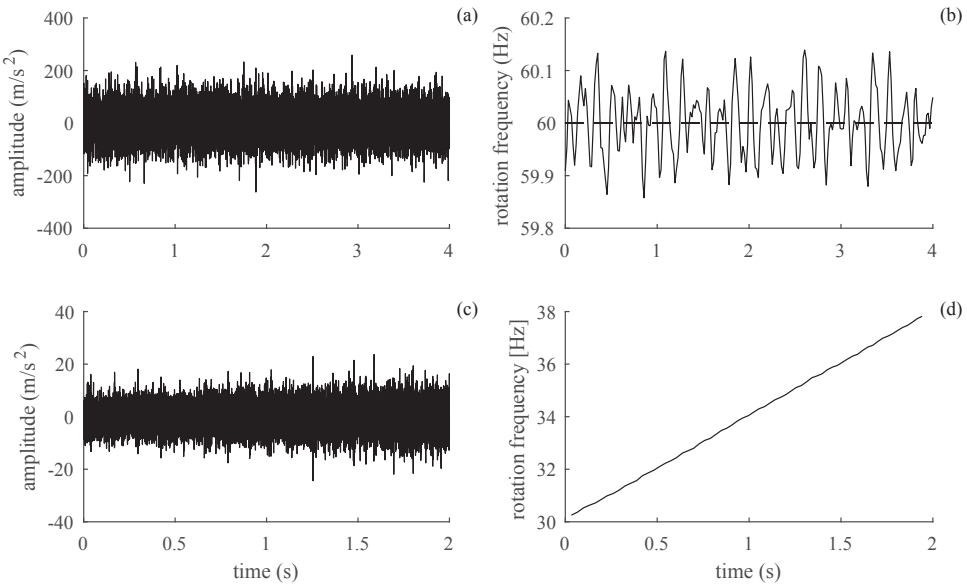

Figure 16: Measured vibration signals in the Sp100 case at (a) constant speed and (c) variable speed with their speed profiles (b,d).

4 s. The measurement campaign has been conducted using LMS SCADAS 310 controlled by LMS Test.Lab. An example of the acquired vibration signals and their speed profiles is reported in Figure 16.

2.6.2 *Discussion of the results: constant regime tests*

The results presented in this section have been carried out considering the following filter lengths: 50 samples for MED and MOMEDA, 40 samples for MCKD (with 5 shifts), 800 samples for MOMEDA and 700 for CYCBD. The CYCBDang has not been considered since the benefits of using this algorithms should be negligible in a constant speed case. All the recovered signals have been normalized by their respective absolute maximum value in order to facilitate their comparison. Furthermore, the MCKD has been performed using the whole signal in order to highlight its intrinsic limitation to deal with long signal and with non-constant speed [39].
Figures 17, 18, 19 and 20 summarize the results related to cases Sp12.5, Sp25, Sp50 and Sp100, respectively. The first observation is that MED correctly re-

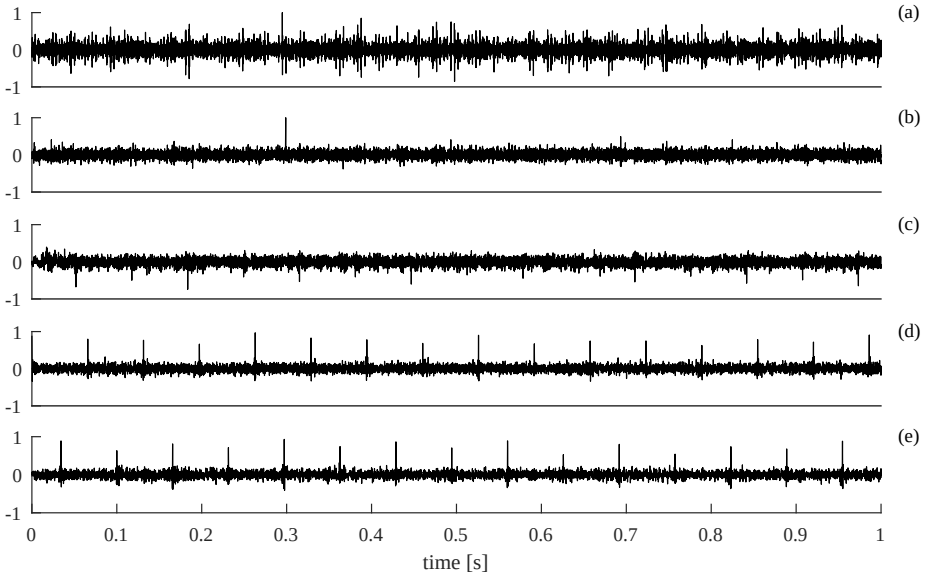

Figure 17: Comparison of the results regarding 12.5 % spalling (Sp12.5) : (a) MED, (b) OMEDA, (c) MCKD, (d) MOMEDA and (e) CYCBD.

covers the fault train only in case Sp100 (see Figure 20), i.e. where the defect should be more evident, whereas OMEDA appears ineffective in all the considered cases. The tendency of OMEDA to be recover a single large impulse is highlighted in Figure 17(b) and to a lesser extent in Figure 18(b). As expected, the challenging test conditions highlighted the significant limitations of MED and OMEDA when applied to mechanical vibration signals.

Now, let us discuss the results related to BD algorithms designed for rotating machine diagnostics (MED and MOMEDA) compared to the proposed ones. The MCKD returns satisfactory results just in cases Sp100 and Sp50 but in the remaining cases the algorithm does not recover correctly the train if impulses. These results can be explained by the fact that, as reported in Figure 16, the instantaneous speed is not perfectly constant. Considering that the definition of correlated kurtosis (see Equation (7)) is based on the correlation of signal segments having a fixed lag mT_{imp}, which correspond to a constant fault period, the MCKD could fail on the extraction of very slight impulsive sources buried in background noise and mechanical interferences. The other BD algorithms examined in this comparison - namely MOMEDA and CYCBD - are able to

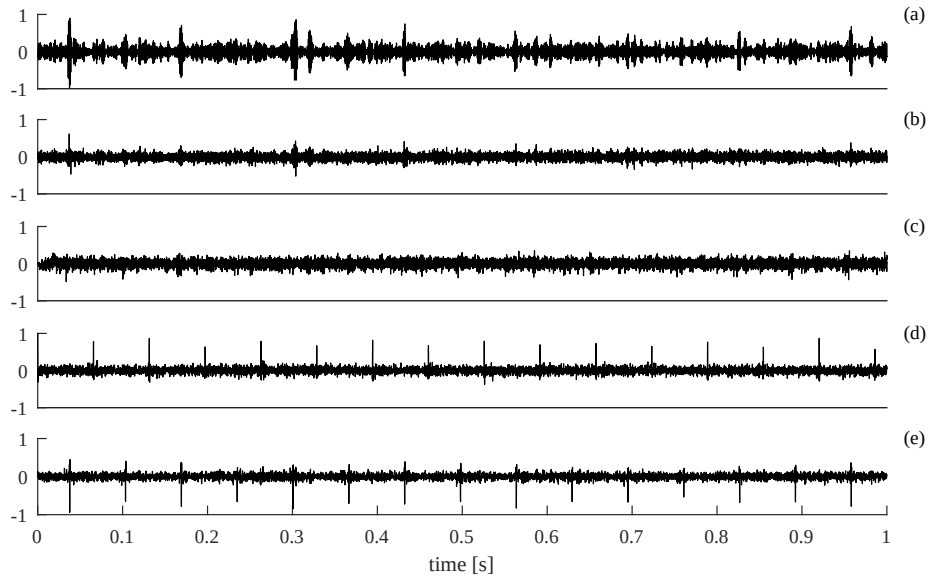

Figure 18: Comparison of the results regarding 25 % spalling (Sp25): (a) MED, (b) OMEDA, (c) MCKD, (d) MOMEDA and (e) CYCBD.

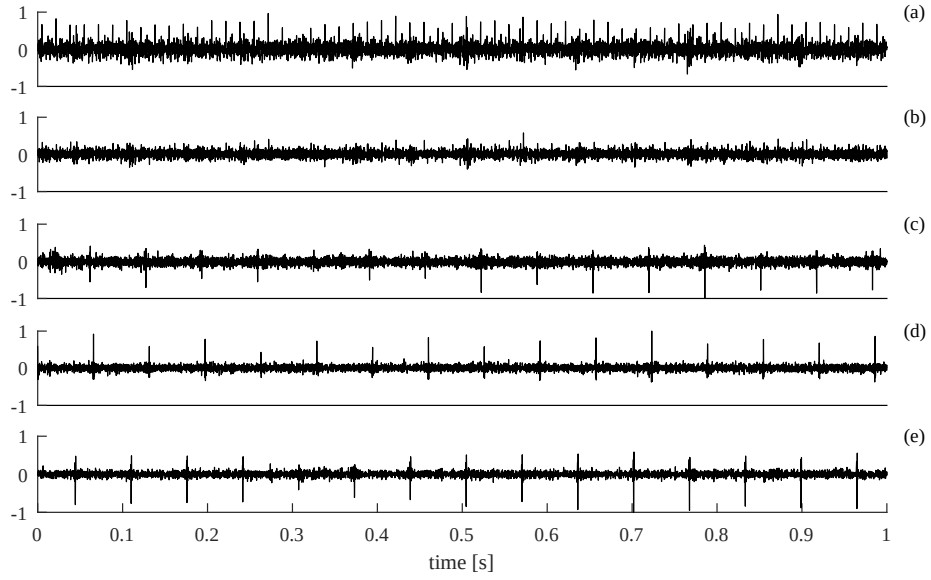

Figure 19: Comparison of the results regarding 50 % spalling (Sp50): (a) MED, (b) OMEDA, (c) MCKD, (d) MOMEDA and (e) CYCBD.

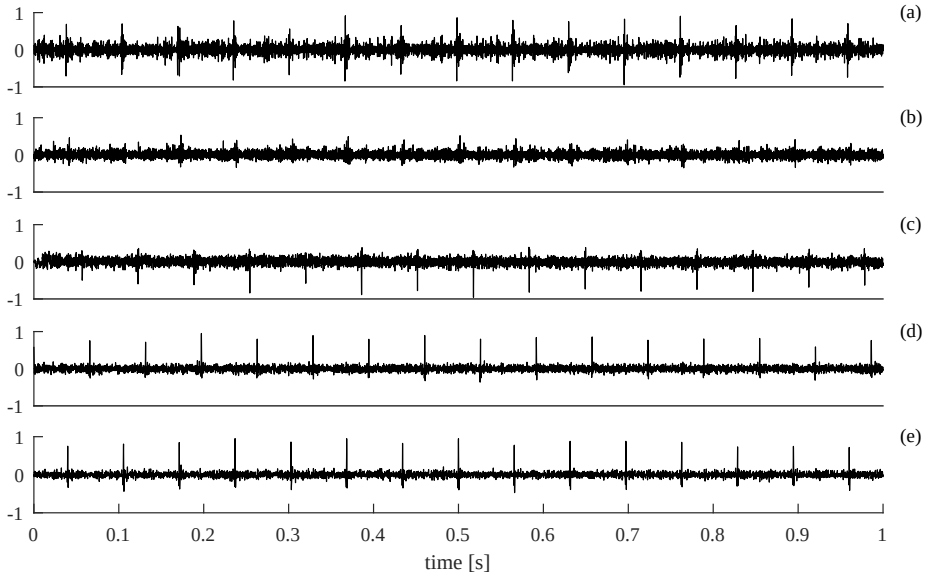

Figure 20: Comparison of the results regarding 100 % spalling (Sp100): (a) MED, (b) OMEDA, (c) MCKD, (d) MOMEDA and (e) CYCBD.

properly deconvolve the sequence of impulses due to the gear tooth spall. De facto, this preliminary result is not surprising since the gear tooth spall can be modeled as a composition of CS1 signal and CS2 signal [35, 20]. On these grounds, even if the criterion of MOMEDA is based on the extraction of a periodic signal rather than a cyclostationary one, the MOMEDA results are as good as the CYCBD results. Therefore, this first comparison highlights the superiority of the proposed CYCBD algorithm with respect to MED, OMEDA and MCKD for the gear tooth spall identification.
Finally, this preliminary study has shown that:

- MED and MOMEDA cannot deal with small gear tooth spalls with small loaded gears;
- MCKD returns better results than MED and OMEDA but only for Sp50 and Sp100 cases;
- MOMEDA and CYCBD have comparable outputs.

This investigation has shown also that the maximized criterion of the CYCBD is sensitive to the spall size. This feature will be exploited later for the design

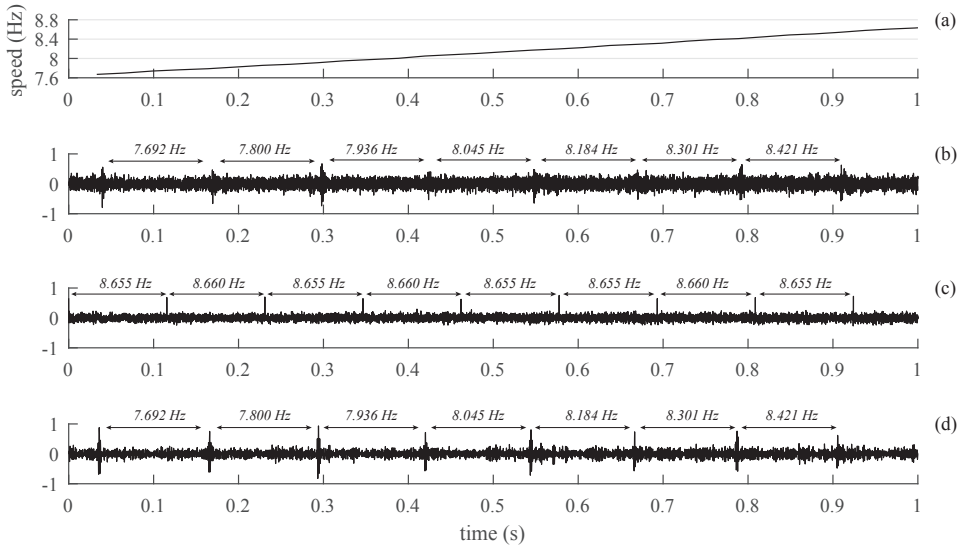

Figure 21: BD results of the run-up test regarding Sp100: (a) instantaneous speed of the intermediate shaft, (b) MCKD output, (c) MOMEDA output and (d) CYCBDang output.

of a diagnostic procedure for gear tooth spalls as well as for pointing out the differences between CYCBD and MOMEDA.

2.6.3 *Discussion of the results: run-up test*

The run-up experiment has been performed in order to confirm the observation made on the simulated case with variable speed, with specific reference to the simulated signal $x_{sim,5}$ and Figure 13. The goal of this validation is to verify the limits of MCKD and MOMEDA to deal with train of impulses having a variable period with respect to CYCBDang. Thus, just the Sp100 have been considered. As done before, MCKD and MOMEDA are referenced to a mean impulse period while CYCBDang is driven by the tachometric signal.
The experimental results of the run-up are shown in Figure 21 and discussed hereafter. For the sake of clarity, only 1 s is shown. In this case MED as well as OMEDA have been neglected since they are not sensitive to the periodicity of the impulse train. The results have been carried out by using a filter length of

50 samples for all the BD methods. It is clear that the best results is returned by CYCBDang and MOMEDA. In fact, the impulses extracted by using the MCKD are buried under strong background noise. For this reason, some impulse is barely visible. It should be noted that the time intervals, which are actually expressed in frequency in Figure 21, are almost constant for the MOMEDA results. The spacing of the impulses is in agreement with the prior periodicity selected (i.e. the average rotation frequency of the intermediate shaft), which is (8.656 Hz). However, the rotation frequency is linearly increasing, that is in contrast with the constant spacing of the extracted impulses.
Finally, this experiment has shown that MCKD returns a very noisy result even if the spacing between the impulses is correct and MOMEDA extracts a train of impulses without a physical meaning but reflecting the periodicity of the Dirac comb $\mathbf{t}$ (see Equation (15)). Instead, CYCBDang returns a clear extraction of the impulses with the proper occurrence rate.

2.6.4 *A diagnostic procedure for the gear tooth spall identification*

The strong points of CYCBD previously highlighted may be exploited in order to design a diagnostic procedure for the identification (and the quantification) of gear tooth spall for gearboxes operating at constant speed. Also if the results presented in the previous subsection are pretty easy to be interpreted, it's a matter of fact that the diagnostics of machines by means of vibration analysis is directing to be less dependent on the user interpretation by using of simple indicators that objectively quantify the state of the machine. For this purpose, a methodology can be advanced that gives a simpler interpretation of the data returning information about both the presence and the severity of the gear tooth spall.
In a similar manner to Refs. [39, 40], the final value of the maximized criterion may be exploited considering the percentage difference between the healthy case and the faulty one. Thus, calling such a percentage difference as F, it reads:

$$F = \frac{C - C_{ref}}{C_{ref}} 100 \tag{40}$$

where C and C_{ref} are the maximized criterion values (see Equations (7), (13) and (23)) for the faulty case and the healthy one, respectively. This indicator

can be used in order to estimate both the size and the position of the gear tooth spall. From the physical standpoint, a positive deviation of F indicates the possible presence of a defect; analogously, a negative deviation as well as very low positive F may be interpreted as the absence of a defect. Furthermore, the value of F can used to determine the severity of the fault since the greater F, the greater the spall size.

Let us apply the proposed indicator for the diagnostics of the gearbox under investigation. This gearbox is composed of two stages that correspond to 3 rotating axes having different rotation frequencies. Performing BD algorithms using the incorrect fault periodicity should lead to negative value of F for all the considered spall sizes. On the contrary, when the proper fault period is taken into account, F should exhibit positive values, increasing with the spall size. Before discussing the results, it should be noted that the cyclic frequency sets used in CYCBD must be computed avoiding overlapped frequencies among the sets in order to guarantee the uniqueness of the information carried by each frequency set.

The final results on the use of indicator F are summarized in Figure 22, considering MCKD (a), MOMEDA (b) and CYCBD (c). MED and OMEDA have been left out on purpose since they are not able to distinguish repetitive impulses having different periods. Moreover, the CYCBD results has been obtained by using a filter length of 200 samples. As demonstrated later, the filter length has a limited influence on the CYCBD results. As mentioned previously, three fault periods have been taken into account, namely the rotation frequencies of the input shaft (first column of Figure 22), of the intermediate shaft (second column of Figure 22) and output shaft (third column of Figure 22). Remember that the seeded fault in the 71 teeth gear is synchronized with the period of the intermediate shaft. Hence, negative values of F should be expected regarding to the periods of the input and the output shafts whereas F must be positive for the intermediate shaft just because it corresponds to the fault period.

The data related to the intermediate shaft period (Figure 22) highlight that MCKD and MOMEDA fail on the full detection of the gear tooth spall. In fact, negative F values occur despite the presence of the defect. Furthermore, unsatisfying results are also achieved considering the period of the input shaft and of the intermediate one, since non-negligible positive values of F are present. However, this experimental evidence is not an absolute proof of the ineffectiveness of such methods. Indeed, it should be remarked that the considered

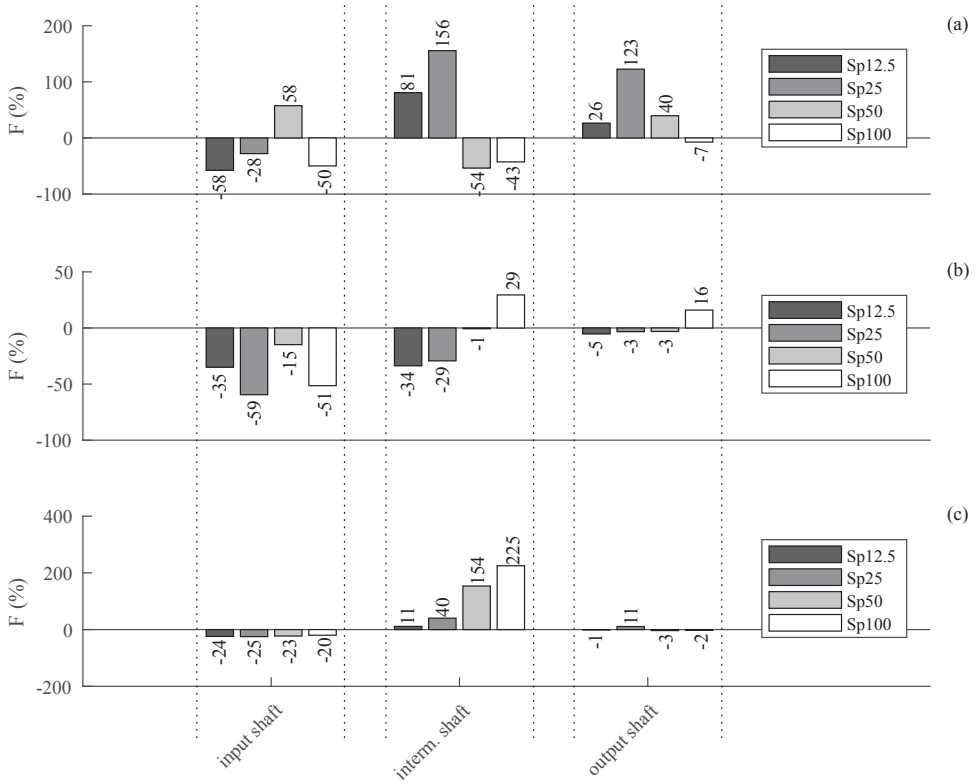

Figure 22: Chart collecting the values of F (Equation (40)) for (a) MCKD, (b) MOMEDA and (c) CYCBD. The percentage values are displayed on the top of each bar.

test condition is particularly hard to detect due to the low load and the gear type (helical). The results perhaps could be improved finding a more convenient filter length - and M shifts for MCKD - by trial-and-error. However, as demonstrated in the following subsection, CYCBD results are robust with respect to the selected filter length.

On the other hand, interesting results are achieved by CYCBD. The gear tooth spall is correctly identified in all the considered cases, since positive values of F are achieved in all the considered cases. In addition, the severity of the fault is also well represented because F increases according to the size of the seeded fault. This result is particularly relevant because it indicates that CYCBD, de facto, is sensitive to the dimension of the fault, which can be of great value in order to monitor the evolution of the defects.

The results of CYCBD for the input shaft are satisfying since they are all negative, indicating that the 18 teeth gear is healthy. Regarding the output shaft, low positive values similar to the Sp12.5 case are present. This result can be interpreted as the presence of a small defect in the 55 teeth gear. However, the proposed method globally gives adequate results considering the slight size of the fault in case Sp12.5 and the unfavorable test conditions due to the small load. Indeed, in more favorable cases (spur gears, higher load..) this method should be even more effective.

2.6.5 *Sensitivity analysis*

Despite the promising results obtained in the previous subsection, a sensitivity analysis must be carried out in order to assess the effect of different filter lengths on the final results. It is a matter of fact that blind deconvolution techniques achieve different results depending on the considered filter length. Thus, this aspect is investigated in more detail below. In this sensitivity analysis, CYCBD has been performed with FIR filter length, N, varying from 10 samples to 800 samples taking into account the cyclic frequency set related to the fault period. Greater values of N are not considered because of the high computational efforts which is unbearable for real time application and, in general, for industrial purposes. The effects of various values of N have been tested in terms of maximized ICS_2, values of F and number of iterations.

Figure 23(a) collects the values of ICS_2 whereas F values are displayed in Figure 23(b). ICS_2 values estimated with the proposed algorithm are in agree-

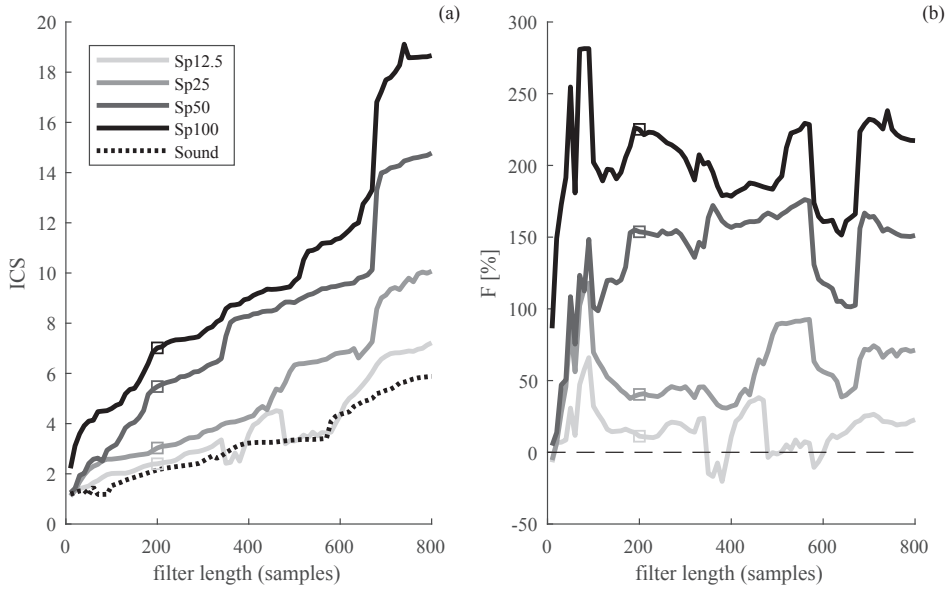

Figure 23: Sensitivity analysis of CYCBD referenced to (a) the ICS_2 values and (b) the F values. The square marks indicate the number of samples used in Figure 22.

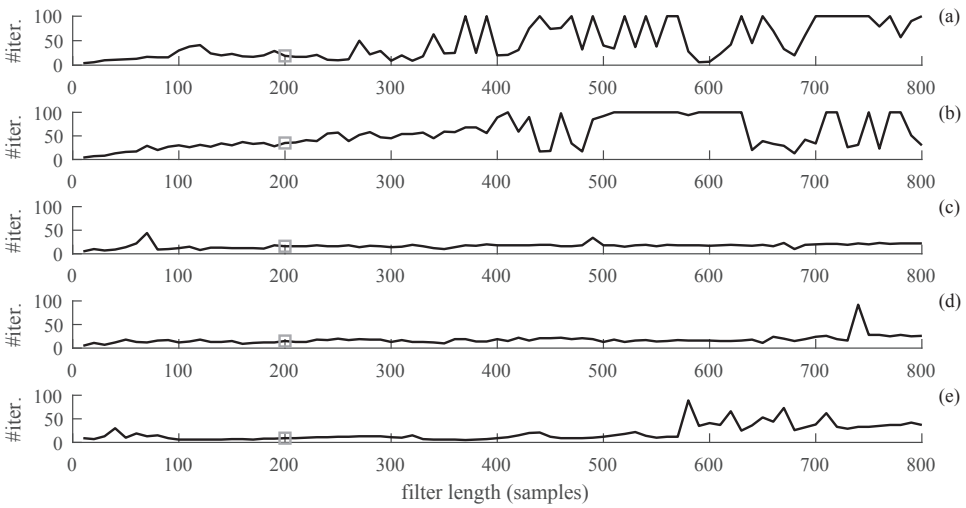

Figure 24: Sensitivity analysis of CYCBD concerning the number of iterations in the cases: (a) Sp12.5, (b) Sp25, (c) Sp50, (d) Sp100 and (e) healthy. The gray square marks indicate the number of samples used in Figure 22.

ment with the related fault size, i.e. the greater the fault, the greater the ICS_2. Furthermore, the value of the final estimated ICS_2 seems directly related to the filter length. However, longer filter lengths should be taken into account in order to clarify this relationship. This investigation is not performed in this work because of the extreme computational effort involved. A sudden increment of ICS_2 values is observed between 670 samples and 680 samples. This effect occurs very likely because in that region of the diagram the filter length approaches the length of the fault period (approximately 673 samples). Interesting remarks can be made observing the values of F collected in diagram (b) of Figure 23. This diagram clearly shows that the proposed methodology is globally consistent considering a wide range of N. The effect of a unlucky choice of N seems limited to a slight range of values and concerns only the identification of case Sp12.5. Hence, the detection of the smallest defect (Sp12.5) is not always guaranteed.

The number of iterations as a function of the filter length shown in Figure 24 can be considered as an indicator of the quality of the deconvolved signal. In fact, a high number of iterations implies a slow convergence rate and consequently a slow algorithm. Two stoppage criteria have been adopted in

the proposed algorithm: the first one regards the percentage difference of two consecutive final values of the maximized criterion; the second one regards the maximum number of iterations, which is activated if the condition of the first one is not met. Hence, the observation of how the number of iterations changes according to the variation of N may lead to pivotal consideration about the proper selection of the filter length. Figure 24 indicates that a large number of iterations is globally needed for the smaller spall sizes, i.e. Sp12.5 and Sp25. The other cases do not highlight particular convergence issues. Hence, taking into account the convergence rate and the computational effort, Figure 24 suggest to limit N to 200 samples.

Thus, according to both Figures 23 and 24, in the considered experimental case N should not be greater than 200 samples (corresponding to the 0.5 % of the total signal length). In fact, in this range, satisfying results can be achieved avoiding slow convergence rate associated with strong computational effort. Furthermore, Figure 23 is a consistent proof of the robustness of the method considering different size faults.

2.7 APPLICATION TO REAL SIGNALS: RUN-TO-FAILURE BEARING TEST

The second example addresses the early bearing fault detection and identification considering a run-to-failure experiment. The capability of the CYCBD to monitor the fault development is investigated and discussed.

2.7.1 *Experimental setup*

The vibration signals used in this example are part of the dataset provided by the Center for Intelligent Maintenance Systems (IMS) of the University of Cincinnati [63]. The IMS dataset provides three endurance tests having different lengths and outcomes. The first dataset has been discarded because several recording interruptions occurred and two bearing faults concurrently developed in two different bearings [64]. Note that BD algorithms are designed for recovering only one source from one or more responses. Moreover, Ref. [64] pointed out that actually the third dataset does not exhibit any fault signature. Thus, the third dataset has been discarded too. On these grounds, the following investigation is referenced only to the second dataset.

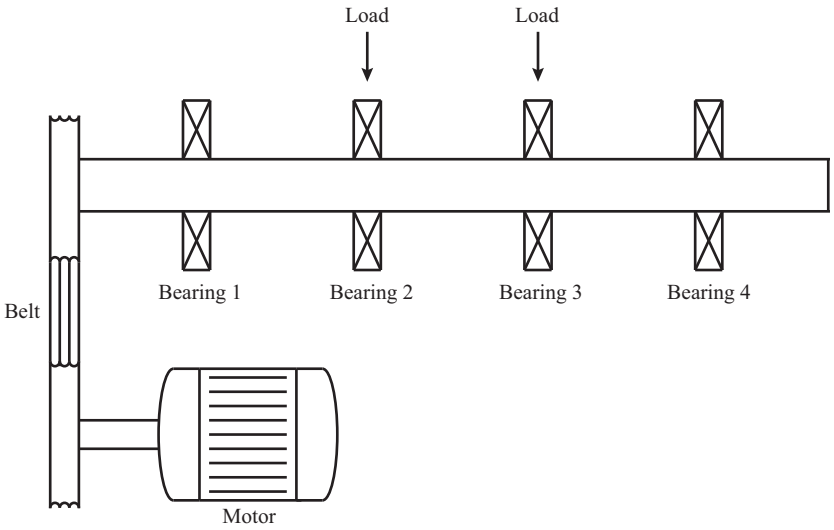

Figure 25: Schematic of the IMS test rig.

According to the scheme shown in Figure 25, the test rig is composed of four bearings type Rexnord ZA-2115 installed in the same shaft. This test has been performed with a fixed shaft speed of 2000 rpm and a load of 27.7 kN applied to Bearings 2 and 3. Each bearing is monitored by two accelerometers PCB type $253B33$ mounted in radial direction. It should be noted that only one sensor for each bearing is available for this test. The vibration signals have been continuously acquired with a sampling frequency of 20.48 kHz, collecting 1 second of samples each 10 minutes. The test has been stopped after 7 days, which correspond to 16.4 minutes of actual acquisition, revealing an outer race fault occurred in Bearing 1 (no photos are available). Further detail about the experimental apparatus can be found in Refs. [63, 65] whereas the whole dataset is openly available online[1].

2.7.2 *General data inspection*

The IMF dataset has been widely analyzed using different approaches and goals. This dataset has been designed and created in order to provide an experimental framework for prognostic investigations. These tests are par-

1 `http://ti.arc.nasa.gov/tech/dash/pcoe/prognostic-data-repository` Last consulted on 11/10/2017

ticularly valuable for two main reasons: first, bearing faults naturally occur without external intervention; second, the test length allows for the natural development and degradation of faults. These test conditions are particularly interesting since natural faults in dedicated test benches are surely closer to a real scenario than an artificial fault.

For instance, the work of Gousseau et al. [64] exploited the Squared Envelope Spectrum [17] (SES) and the Spectral Coherence [33] in order to detect the bearing faults through visual inspection of time/frequency or frequency/cycle representations. The major part of research works involving this dataset deals with the prediction of the remaining useful life and the early stage bearing fault identification by means of techniques (as machine learning techniques) barely linkable to physical phenomena.

A global time/frequency representation of the vibration signal is given by the Short Time Fourier Transform (STFT) shown in Figure 26. The STFT has been performed on segments of 1 s without overlap, since the signal has not been acquired continuously. For this representation, the raw vibration signal has been pre-whitened by means of AR filters in order to attenuate the deterministic part of the signal highlighting the random part related to the bearing fault, i.e. enhancing the visibility of the all Pass Frequency Outer race (BPFO) harmonics. In this respect, several research works [29, 17, 66, 67] demonstrated that AR models can be used for reducing the periodic contributions in vibration signals, highlighting the random part – i.e. second-order cyclostationary – related to a bearing fault.

As pointed out in a previous research work on IMF dataset #2 [64], the time/frequency representation highlights that some components corresponding to sole BPFO harmonics rise up just before day four. Concurrently, the fundamental BPFO harmonics is present from the beginning. The growth of these components strongly suggest the development of a defect on the outer race. This behavior is particularly visible in the frequency range $0 - 4.5\ kHz$.

A more quantitative data analysis can be conducted by means of time domain feature analysis. As suggested in Ref. [68], Figure 27 collects two common statistical indicators estimated by using the raw vibration signals: Root Mean Square (RMS) and kurtosis. Also in this case, both the diagrams in Figure 27 suggest a deviation from the healthy state. RMS and kurtosis trends globally reflect the considerations made after inspecting the time/frequency representation in Figure 26. RMS appears more sensitive than kurtosis since a visible

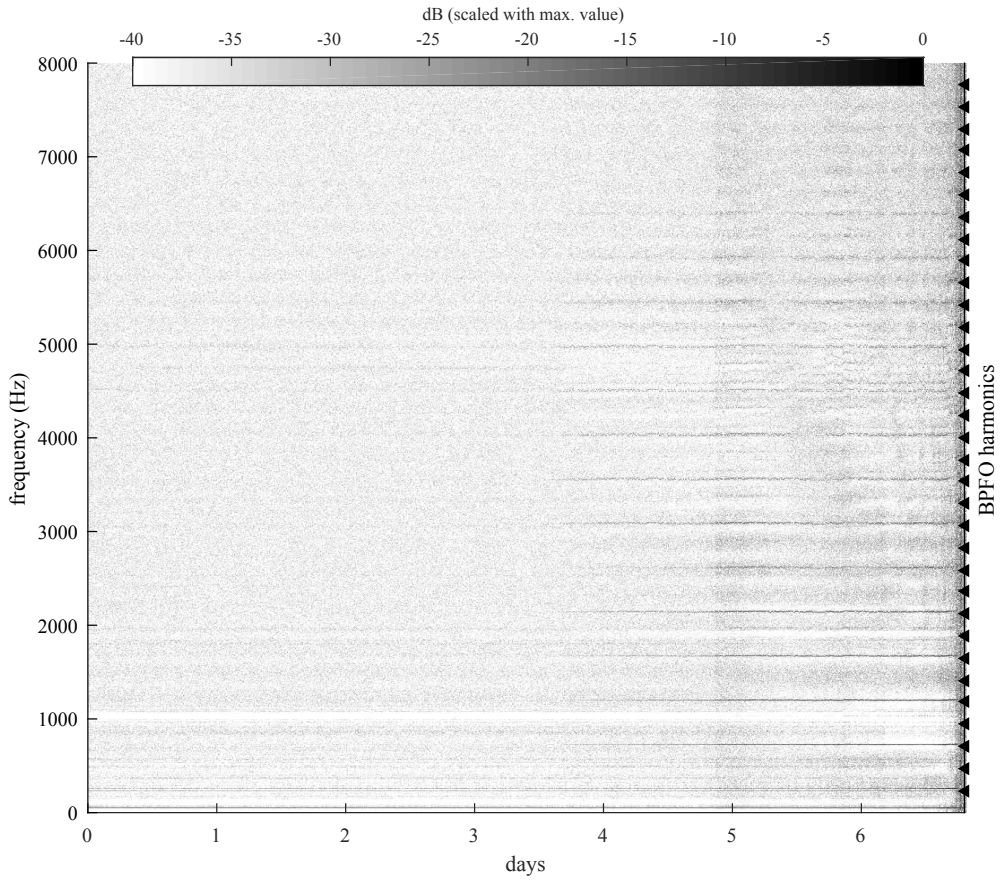

Figure 26: Short Time Fourier Transform (STFT) representation of the pre-whitened vibration signal normalized with respect to the global maximum value.

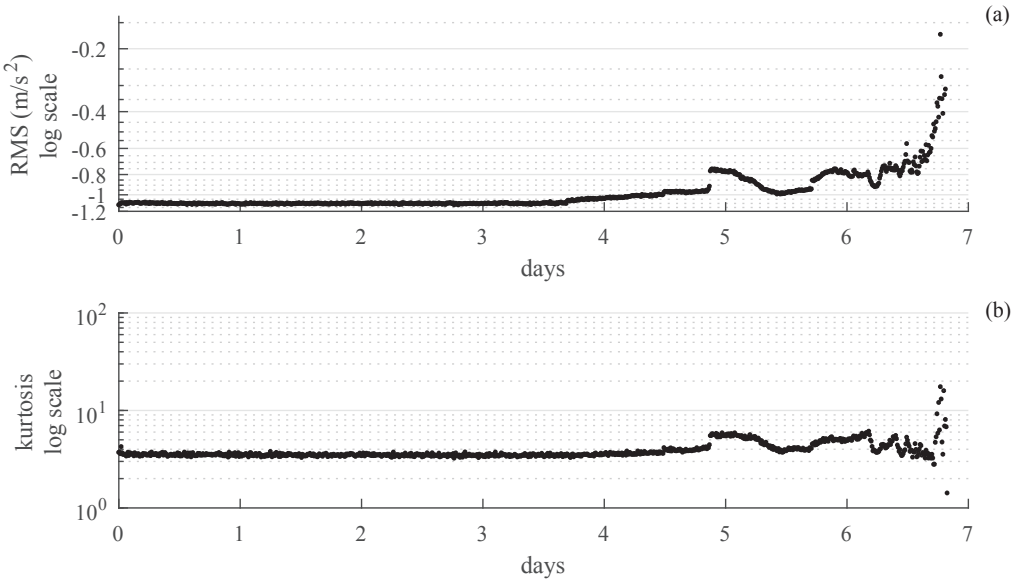

Figure 27: Values of (a) RMS and (b) kurtosis computed from the raw vibration signals.

deviation of the values can be seen after approximately 3.5 days (according to Ref. [64]) while the kurtosis values show a visible deviation only after four days. Even if these indicators have quiet good performance on the early fault detection, they do not give any information about the fault typology being just global statistical descriptors.

These considerations represent a starting point for further analyses using BD algorithms. In fact, on the one hand, time/frequency approaches provide a good fault identification capability and a mediocre predisposition to pass/-fail decision strategies. On the other hand, scalar indicators fit naturally into pass/fail decision methods but often are too general to effectively identify bearing faults. In light of these results and in the wake of Ref. [64], CYCBD can be used as a cyclostationary indicator being able to early detect and concurrently identify bearing faults. Moreover, since CYCBD is based on a cyclostationary criterion, this approach guarantees a strong link with all physical phenomena involved in the mechanical signature framework, as opposed to machine learning approaches that are purely data-driven and lack of physical interpretations.

2.7.3 *Early fault diagnosis by blind deconvolution analysis*

On the basis of the previous discussion and according to Section 2.6, the results can be analyzed observing the behavior of maximized BD criteria with respect to time. To this purpose, CYCBD output (i.e. the ICS_2 final value) can be used as an indicator capable to identify also the kind of the fault as opposed to RMS and kurtosis, for instance. In this respect, two different frequencies of interest, the BPFO and the Ball Pass Frequency Inner race (BPFI), are considered. As done previously in Section 2.6, the effectiveness of CYCBD, using both the SISO and SIMO formulations, is verified and compared with MCKD and MOMEDA. Both BPFO and BPFI have been estimated through the enhanced enevelope spectrum computed with spectral correlation proposed in Ref. [33]. Briefly, this procedure consists on selecting the BPFO and BPFI corresponding to the envelope maximum value within a frequency range centered in the theoretical BPFO and BPFI estimated by using the average rotating speed and the bearing geometrical characteristics.

Considering this kind of data representation, a threshold can be designed in order to establish both fault type and first fault manifestations. In a general context, a threshold based on the presence of outliers, i.e. observations that are distant from a given distribution pattern, is a reasonable choice. Frequently, outliers indicate the presence of some kind of anomaly due, for instance, to regime changes or faults. Hence, the idea is to define a threshold from observations related to a supposed healthy state (e.g. samples acquired during the test beginning) and check if the following observations are outliers or are coherent with the initial pattern distribution.

Among all the possible methods, a consistent rule of thumb for identifying suspected outliers is the Tukey's method that has been already successfully used for pass/fail decision tests by using vibration-based scalar indicators in other research works [56, 69]. The Tukey's method is quiet general and does not require prior distribution knowledge. The only limitation is that Tukey's method could lose effectiveness for data having non-symmetric probability distribution. Moreover, for bearing fault monitoring applications, another necessary condition is that the system operates in stationary conditions because all the vibration signature changes should be associated to faults rather than regime variations. According to Ref. [70], this method exploits the interquartile range (IQR), namely the distance between first and third quartile, in order

to define two classes of outliers: "outside" and "far out". The first class refers to mild outliers (i.e. data not so far from the reference distribution) and it is defined as 1.5 times the IQR distance. The second one refers to extreme outliers (i.e. data significantly distant from the reference distribution) and it is defined as 3 times the IQR distance. In this application, the threshold is represented by the latter class just for the upper limit since it is expected that the considered indicators rise when a fault occurs.

The comparison of BD methods is performed in terms of bearing fault identification and early detection dedicated diagrams from Figure 28 to Figure 33. In these diagrams, dark gray data points refer to the maximized BD criterion that works as a scalar indicator referring to a specific type of bearing fault (outer race fault or inner race fault in this case). The threshold has been estimated by using the Tukey's method on the data acquired in the first day of test, under the hypothesis that all the bearings are healthy in that time interval. Note that time window related to the healthy condition has been highlighted in light gray.

Moreover, it is expected a certain dispersion of the indicator even when the bearings are healthy. This is due to unpredictable phenomena such as measurement uncertainty and other events unrelated to bearing faults. Such phenomena could produce also outlier data points that can be misinterpreted. Consequently, it is convenient to smooth the data points in order to estimate a consistent average trend that simplify the data verification with respect to a given threshold. The data smoothing has been performed by the moving average method, which can be easily implemented by convolving a given time series with a fixed rectangular window of 50 samples.

Figure 28 collects the ICS_2 final values estimated by SISO CYCBD for the sensor on Bearing 1 with a FIR filter length of 80 samples. Figure 28 highlights that, considering the BPFO, a clear increasing trend can be detected after 3.8 days, with three consecutive local sudden deviations in correspondence to day 5, 6 and 6.5. This global fluctuations of the indicator trend, also observed in Figure 27, are likely due to propagation phenomena of the bearing fault. As reported in Ref. [71], after the defect appearance, the propagation mechanism of bearing faults is composed by consecutive propagation and smoothing effects. The diagram related to the BPFI shows a slighter increasing trend due to the presence of a certain number of values above the threshold. This happen especially when also the ICS_2 values referenced to the BPFO significantly

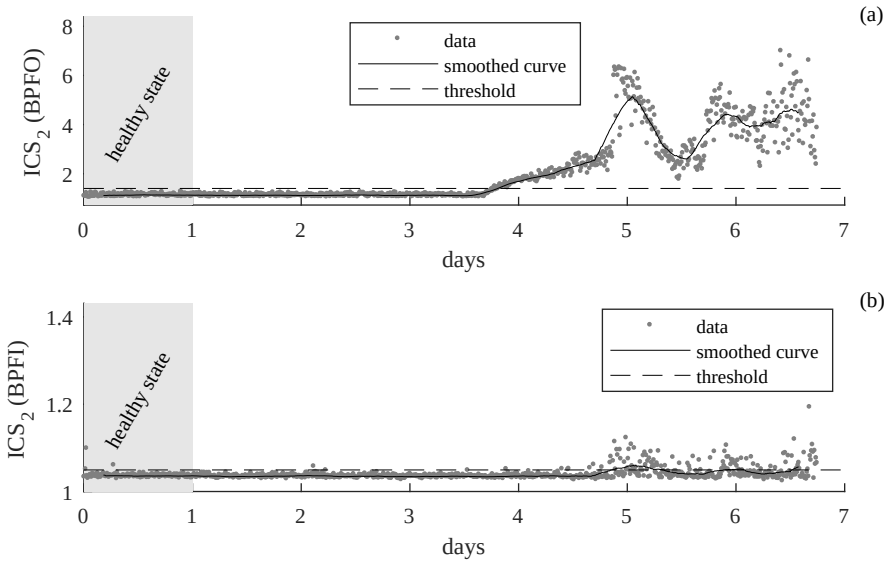

Figure 28: ICS_2 final values of CYCBD (SISO) for the sensor on Bearing 1 referenced to (a) the BPFO and (b) the BPFI.

deviate. This behavior is in agreement with the physical interpretation of the fault development, since a marked growing trend of the indicator related to the outer race fault is expected. By the way, the presence of some data points beyond the threshold in the BPFI case could make the interpretation of the data difficult.

The SIMO approach may improve the results because the weighting matrix estimation is enhanced when several responses are considered. Since the quality of the CYCBD output is strictly related to the accuracy of the extracted cyclic components, a good estimation of the weighting matrix leads to a better source estimation. In this particular case, the low frequency resolution of the measurements (1 *Hz*) is not ideal for bearing diagnostics due to leakage effects and consequent bad estimation of ICS, that is the CYCBD criterion. Thus, the SIMO approach can be used to counter-balance this limitation by exploiting the presence of multiple sensors on the test bench. Four transducers have been used in this experimental campaign, therefore SIMO CYCBD has been performed considering different combinations of sensors. Figure 29 accounts the sensors placed on Bearings 1 and 2, Figure 30 accounts the sen-

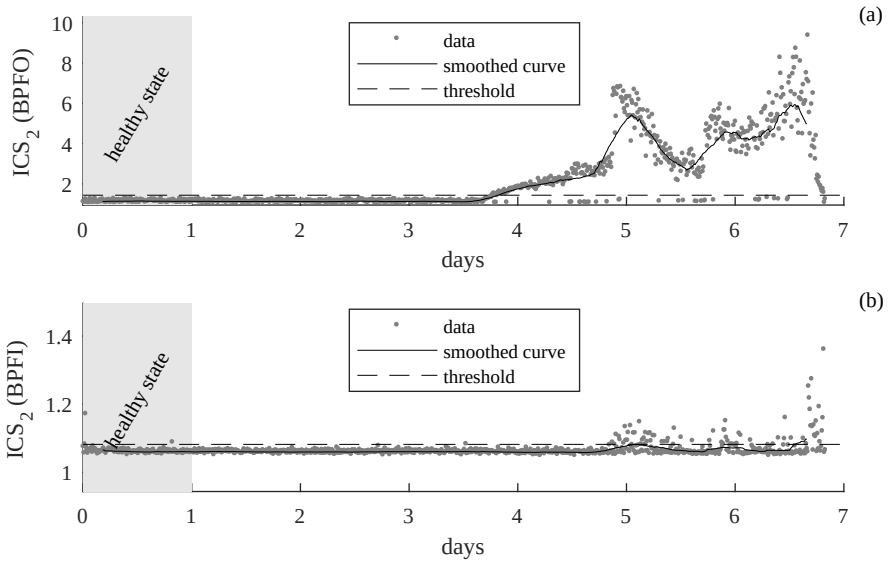

Figure 29: ICS_2 final values of CYCBD (SIMO) referenced to (a) the BPFO and (b) the BPFI taking into account the sensors on Bearingd 1 and 2.

sors placed on Bearings 1, 2 and 3 and Figure 31 accounts all the available accelerometers. It can be observed that the result quality has been strongly improved by performing the SIMO CYCBD. In this case, the outer race fault results are not significantly improved since becomes visible after 3.8 days, as highlighted also by SISO CYCBD results. However the diagrams related to the inner race fault are generally enhanced. In fact, the ICS_2 values referenced to the inner race fault shows decreasing number of outliers as the number of considered sensors increases. This leads to a reduced chance to detect false positives since the smoothed trend never across the threshold, in particular in Figures 30 and 31.

Furthermore, it should be noted that when accelerometers far from the excitation (i.e. the outer-race fault in Bearing 1) are involved, data points below the threshold may appear in the diagrams concerning BPFO. This can be explained because the effectiveness of SIMO CYCBD can decrease considering accelerometers very far from the source implying to a strong reduction of the SNR, even if the system is very stiff. The best results regarding the SIMO CYCBD algorithm is achieved with three accelerometers (see Figure 30) but also

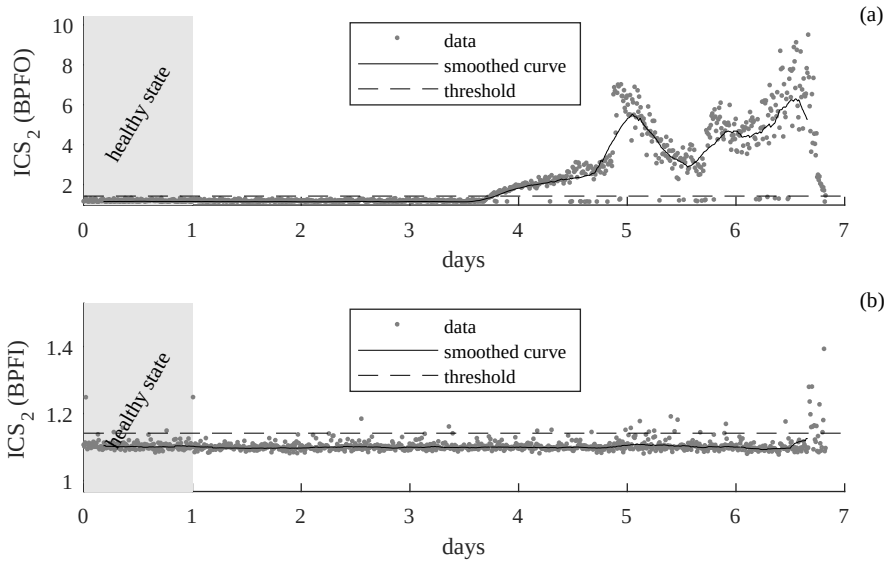

Figure 30: ICS_2 final values of CYCBD (SIMO) referenced to (a) the BPFO and (b) the BPFI taking into account the sensors on Bearings 1, 2 and 3.

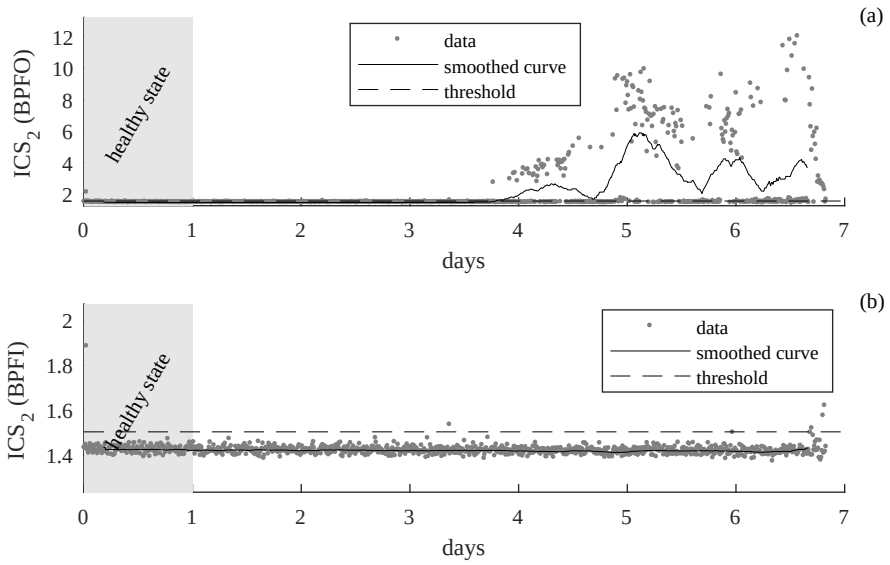

Figure 31: ICS_2 final values of CYCBD (SIMO) referenced to (a) the BPFO and (b) the BPFI taking into account all the available sensors (on Bearings 1 to 4).

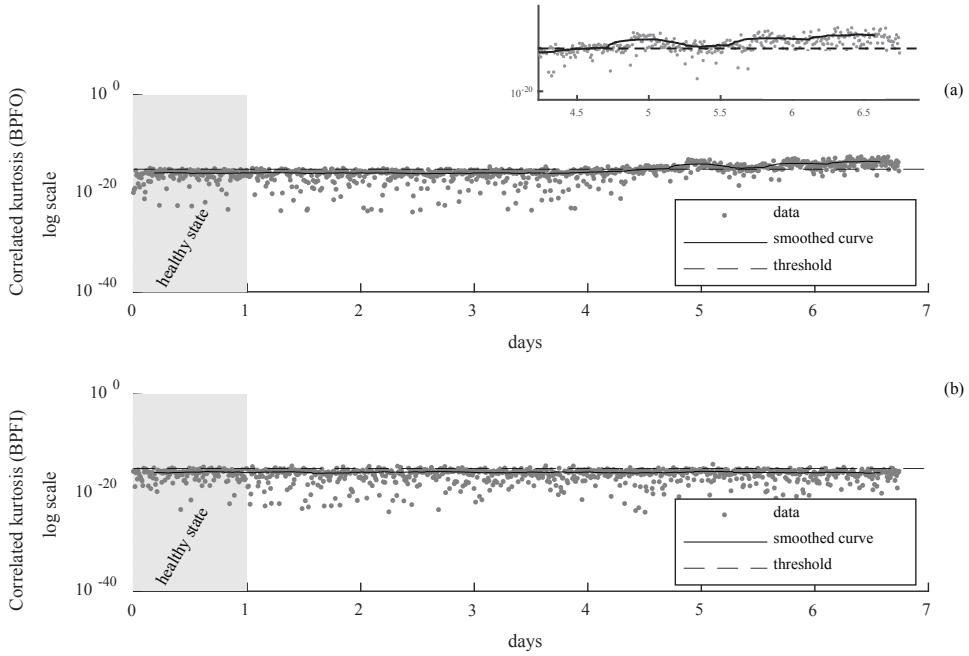

Figure 32: Correlated kurtosis final values of MCKD referenced to (a) the BPFO and (b) the BPFI.

the other cases return a satisfying result. Therefore, this experimental test has shown that SISO CYCBD is effective but the results can be further enhanced by the SIMO approach at the cost of higher computational effort.

As done before, the results obtained by MCKD and MOMEDA are reported in Figures 32 and 33, respectively. For the sake of clarity, the correlated kurtosis values in Figure 32 are expressed in logarithmic scale. For the MCKD, the filter length has been set to 120 samples using 7 shifts. Moreover, only 2000 samples of each records have been taken into account, according to the suggestion in Ref. [39]. The results obtained with MCKD referenced to the BPFO are worse than the SIMO CYCBD in terms of early fault detection and of data dispersion. However, with some limitations, the MCKD allows for the bearing fault identification. Indeed, the fault typology is correctly detected, as well as the increasing trend of the BPFO indicator. However, the threshold is crossed after 4.5 days that is approximately one day later with respect to CYCBD results. The effectiveness of MCKD can be explained by observing Figure 26.

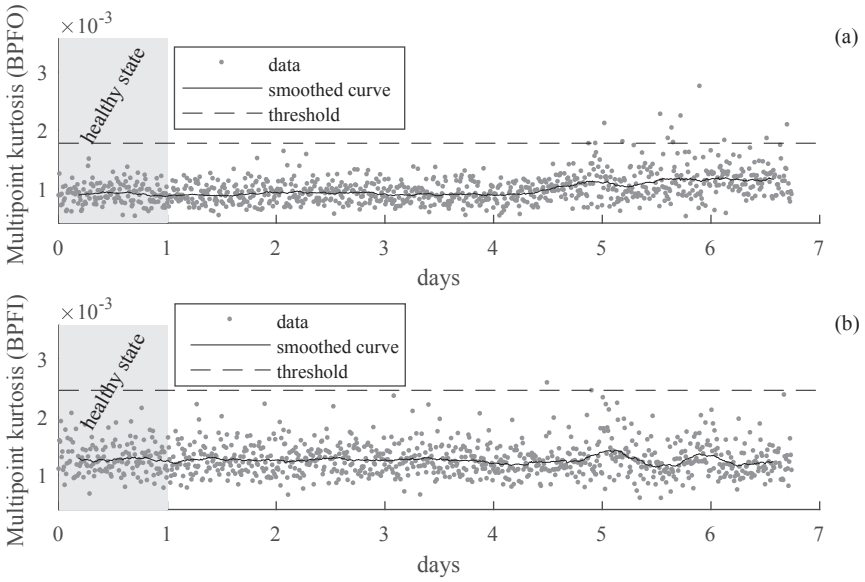

Figure 33: Multipoint kurtosis final values of MOMEDA referenced to (a) the BPFO and (b) the BPFI.

It should be noted that MCKD is based on the fundamental periodicity of the fault rather than a set of frequencies as in the CYCBD method. Since the STFT in Figure 26 shows a prominent component at the fundamental BPFO, this may be the reason of the effectiveness of MCKD. Indeed, in other circumstances where the first BPFO harmonics are not visible, MCKD may return unsatisfactory results because the algorithm tries to recover impulses strictly related to a given period rather than a set of (multiple) periods. Thus, after these observations, CYCBD results should be preferred.

Considering now MOMEDA results in Figure 33, the filter length has been set to 120 samples as in the MCKD. In this case the indicator of MOMEDA (i.e. multipoint kurtosis [40]) gives unsatisfactory results. In fact, some data point from day 5 to the last day are above the threshold but the smoothed curves, which represents the data trend, is always below the threshold. Actually, this is not surprising since the bearing faults are well modeled as second-order cyclostationary signals [19] but MOMEDA is sensitive to periodic signals. Even if the BPFO highlights a weak increasing trend, the data dispersion is too

high to be reliable. In fact, the fitted curve remains below the threshold in the whole dataset.
Finally, this experimental case has shown the effectiveness of CYCBD in order to identify the outer race fault considering the natural advancement of the bearing fault. This is all the more accurate as BD is performed considering several sensors placed on the test rig.

2.8 SUMMARIZING COMMENTS

In this chapter, a novel BD algorithm has been introduced involving higher-statistics criteria and a second-order cyclostationary criterion (called CYCBD). The proposed method has been firstly deduced for SISO systems, then it has been extended for SIMO systems and time/angle dependent signals. An extensive benchmarking with other BD methods has been discussed considering both experimental and real vibration signals. Simulated signals and real ones have been involved in such comparisons.
Briefly, this research activity led to the following achievements:

- an alternative BD algorithm has been proposed, which is constituted of an iterative EV decomposition algorithm based on maximizing (or minimizing) a generalized Rayleigh quotient;
- the advantages of CYCBD have been highlighted in 5 different synthetic signals. CYCBD proved to be superior to the other BD methods regarding the extraction of cyclostationary sources in stationary and non-stationary regimes. Moreover it is not affected (in certain limits) by the presence of other cyclostationary sources or single dominant impulses;
- as regards gear spall tooth identification, a diagnostic protocol based on CYCBD has been developed and tested. The CYCBD results exceed the results of other BD methods considering constant regime tests and run-up tests;
- concerning a run-to-failure bearing test, CYCBD proved to be the most effective BD method. In this scenario, a diagnostic methodology based on for the identification of outer race faults has been proposed also.

This chapter owns several aspects of originality. The main one is the formulation of a BD criterion based on second-order cyclostationary maximization by

means of a generalized Rayleigh quotient that has been extended for SIMO systems and time/angle dependent signals. Furthermore, the cyclostationary framework in BD algorithms has been explicitly faced for the first time in the vibration-based rotating machine diagnosis, highlighting once again the pivotal role of cyclostationarity for mechanical fault diagnosis. All the theoretical considerations have been supported by extended experimental studies involving both a gear tooth spall and an outer-race bearing fault.

3

FAULT IDENTIFICATION FOR SYNCHRONOUS GEARS BY EMD-BASED ALGORITHMS

3.1 INTRODUCTION

Multi-stage gearboxes are employed in a wide range of mechanical systems representing a fundamental component for the correct functioning of the entire machine. Since they are often subjected to faults due to heavy working conditions, manufacturing errors or harsh operational environment, gear fault identification is of prime importance in the industrial scenario.
Many complex transmissions have gears that can be easily inspected and possibly substituted, while others may require a remarkable amount of time for their maintenance. For instance, the maintenance cost of a pinion embodied with the shaft (gear shaft) is generally higher than a gear mounted with splined bore [72]. For this purpose, the combination of non-destructive techniques and the knowledge of the exact fault position simplify the maintenance process, avoiding burdensome global visual inspections.
This chapter faces the development of an automatic procedure for gear fault diagnosis based on the vibration analysis by means of EMD-algorithms. After this introductory section, the rest of the chapter is organized as follows: Section 3.2 addresses the theoretical background, the method is then described in Section 3.3 while Section 3.4 and Section 3.5 are devoted to the validation by means of simulated signals and experimental signals, respectively.

3.1.1 *Gear fault diagnosis by vibration analysis*

The vibration analysis proves to be an effective non-destructive technique for gear fault diagnosis [9]. Nowadays, the specialized literature offers a number

of consolidate methodologies. The cyclostationary theory, pioneered in the telecommunication field by Gardner [73] and developed in the mechanical field mainly by Antoni [11, 34], is probably one of the most powerful approach since the vibrations produced by mechanical systems are well represented by cyclostationary processes [19]. The SC [33, 34, 74] and its normalized version (the spectral coherence), the separation of the signal into a deterministic part and a pure (second order) cyclostationary part [20] and dedicated cyclostationary indices as the ICS [35] and the DCS (Degrees of Cyclostationarity) [20, 75] are some effective applications of the cyclostationary framework on the mechanical field with remarkable implications on the industrial scenario.

On these grounds, many connections have been established with other signal processing techniques that have long been used in the diagnosis of rotating machines, such as the the TSA [21], the envelope analysis and the spectral kurtosis. The TSA, de facto, is a common estimator of the CS1 part in the angle domain. Randall et al. [36] demonstrated that the envelope analysis is nothing but the integral of the SC over the frequency axis. Eventually, the kurtosis evaluated over a certain frequency band is the sum of all the peaks of the normalized SES [37]. Thus, the cyclostationarity gave also a novel theoretical framework to several signal processing techniques.

The state of the art about localized gear fault identification includes also many other effective strategies. For instance, the abrupt changes (i.e. transients) in the vibration signature due to the local gear fault have been widely investigated by means of time-frequency representations like the spectrogram [76], the Continuous Wavelet Transform [25], the Wigner-Ville distribution [77] and, more recently, the Hilbert-Huang Transform (HHT) [26]. Other common methodologies for the gear fault diagnosis are: the power cepstrum analysis, originally used for the suppression of echoes [78] and anon in gear diagnostics [23, 79]; the Kurtogram [30, 80] proposed by Antoni [81] for the selection of the optimum frequency based on the maximum Spectral Kurtosis [82]; the blind deconvolution algorithms [39, 40], extensively explained in Chapter 2; condition indicators estimated in the time and in the frequency domain [22] and auto-regressive models [66].

3.1.2 *Gear fault diagnosis using EMD algorithms*

Among all the aforementioned approaches, the Empirical Mode Decomposition (EMD) algorithm can be used for the diagnosis of local gear fault being effective for the analysis of signals exhibiting non-stationary and non-linear behavior. The EMD has been originally designed as the first step of the HHT that is used for the extraction of mono-component signals for the estimation of the instantaneous frequency through the Hilbert transform.

The HHT was introduced by Huang et al. [83] and is a self-adaptive time-frequency analysis technique. The HHT is constituted by two separate steps: the first one is the EMD, which decomposes the original signal into a set of (simple) oscillatory modes, also called Intrinsic Mode Functions (IMF); the second one is the Hilbert Spectral Analysis (HSA), which estimates the instantaneous frequency by means of the Hilbert transform. Despite the EMD has been designed as a pre-processing tool of the HSA, it has been successfully applied in combination with other signal processing techniques.

The EMD is a signal decomposition algorithm based on the local time scales of the signal rather than on a pre-determined kernel. The point of strength of the EMD is, indeed, that the signal decomposition is directly driven by the nature of the input data without prior assumptions. From this point of view, the EMD approach is different with respect to other signal processing techniques. For instance, the results of the Continuous Wavelet Transform (which actually is a time-scale representation) or the smoothed Wigner-Ville distributions strongly depend on the mother Wavelet and the kernel function, respectively; moreover the original Wigner-Ville distribution exhibits interferences, commonly called cross-terms, when the signal has non-linear frequency modulations or multiple components (in opposition to the definition of mono-component signal) [84]. Since the representation of non-stationary signals as well as non-linear phenomena should require an adaptive basis [85], the EMD overcomes this issue being completely data-driven and fully defined as the output of an iterative algorithm.

Despite the advantages of the EMD over the other methods, it exhibits also some limitations. The main issue regards the lack of a theoretical foundation. Indeed, as its name would suggest, the EMD is empirical in the sense that it has been designed thanks to the intuition rather than a rigorous framework.

Thus, although the attempts to formulate a mathematical framework of the method [86, 87], this aspect is still an open question. Moreover, the EMD is affected by other secondary drawbacks: the end effect problem [88] and the mode mixing problem [89]. Further explanations will be given in the next subsections. Many efforts have been made in both directions in order to reduce such limitations of the EMD algorithm.

The EMD has been successfully used in a number of different research fields (economy, speech recognition, chemistry, biology, medicine, etc.) but only in the last decade it has been exploited in the mechanical field with particular reference to the diagnosis of gear faults such as gear cracks [90, 91], broken teeth [26, 92] and wear [93].

The algorithm improvement has been object of several studies, leading to improved versions of the original algorithm. The EEMD (Ensemble Empirical Mode Decomposition) [94], the CEEMD (Complementary Ensemble Empirical Mode Decomposition) [95] and the CEEMDAN (Complete Ensemble Empirical Mode Decomposition with Adaptive Noise) [96] are among the most popular improved EMD algorithms proposed in the literature.

In the gear fault diagnosis, Lin and Chen [97] exploited the EEMD for the extraction of multiple fault information from the vibration signals measured on gearboxes, a diagnostic method for wind turbine planetary gearboxes based on the EEMD has been proposed by Feng et al. [98] and the CEEMD combined with permutation entropy has been used for the identification and the severity recognition of gear faults by Zhao et al. [99]. On the other hand, a very limited number of research works can be found in the literature about the gear fault diagnosis by means of CEEMDAN [100, 101, 102]. A complete literature review about EMD algorithms for the diagnosis of rotating machines can be found in [103]. In this literature review, Lei collects over one hundred of papers about rotating machine diagnosis involving EMD algorithms. This literature review highlights that researchers have largely exploited EMD algorithms for the diagnosis of rotating machines. Moreover, the major part of these consists of investigations by means of EMD and EEMD while, as mentioned before, an inadequate number of works pertains the CEEMDAN being actually very recent.

3.1.3 *Problem statement*

The methodologies listed in Section 3.1.1 are designed to be effective not only with vibration signals acquired in dedicated test benches but also considering real applications, which generally includes the presence of strong background noise and interferences of different nature.

However, considering multi-stages gearbox, the localization of a gear fault occurring in a wheel located in the intermediate shaft can be a difficult task due to the superposition of the vibration signature of synchronous wheels as well as the presence of other vibration sources and interferences. Indeed, all these methodologies exploit the period of the repetitive transients caused by the gear fault in order to recognize the fault position. Such information allow to identify the stage where the faulty gear is mounted rather than the faulty gear itself. Thus, when the fault occurs in an intermediate shaft (i.e. a shaft having two or more wheels) these methods do not provide sufficient information for a precise fault identification.

For instance, it's possible to detect the fault by using blind deconvolution methods (see Figure 20) in the vibration signal used for the experimental validation in Section 2.6 in the case of a full spalled tooth. Moreover, Figure 34 collects the results of some other signal processing techniques previously described in the state of the art. The raw vibration signal in Figure 34(a) does not exhibit any evident information about the presence of the spalled tooth. However, the TSA computed using the intermediate shaft as reference (Figure 34(b)) shows an abrupt amplitude change due to the local gear fault. Analogously, the SC (Figure 34(c)) as well as the enhanced SES (Figure 34(d)) indicate the presence of a cyclostationary component at the cyclic frequency of the intermediate shaft frequency, which is typically caused by a gear fault. The same conclusions can be drawn considering the SES obtained after performing a band-pass filter selected using the kurtogram results (Figure 34(f)) . The results clearly shows that with these methods is not possible to detect which is the faulty gear but only to which shaft the faulty gear belongs.

On this basis, a EMD-based methodology for the diagnosis of multi-stage gearboxes is proposed with particular focus to the gear fault identification in intermediate shafts containing a couple of (synchronous) wheels where one of them is faulty. For this goal, a selection criterion of the estimated oscillatory modes has been advanced, in order to separate the TSA vibration signal

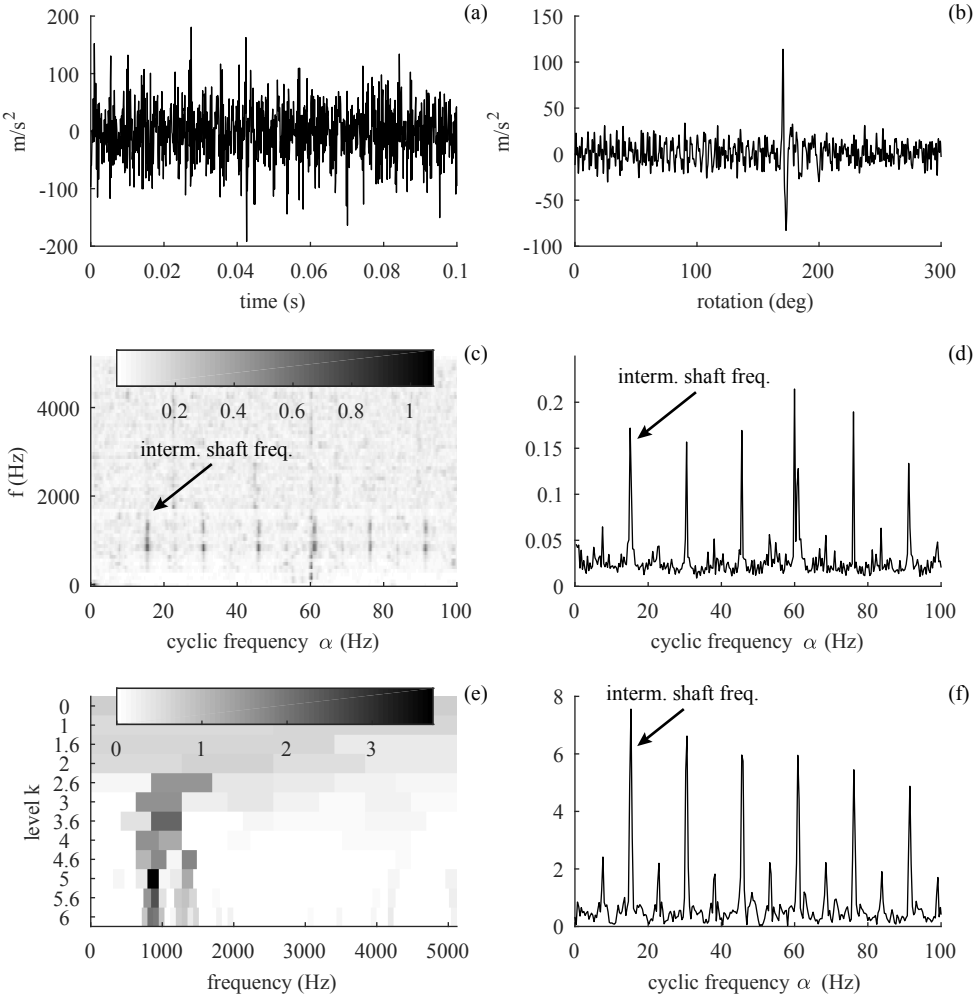

Figure 34: Signal processing techniques applied to a full spalled tooth vibration signal: (a) raw vibration signal, (b) TSA related to the intermediate shaft, (c) smoothed spectral coherence and [33], (d) enhanced SES, (e) fast kurtogram [81] and (f) SES of the filtered signal in the optimal band selected by the fast kurtogram (carrier frequency $880Hz$ and k level 5).

into two representative vibration signals referenced to the synchronous gears. Three EMD algorithms are taken into account (EMD, EEMD and CEEMDAN) in order to verify how the signal separation is influenced by the different decomposition methods.
Upon obtaining the separated signals, which represent the vibration signature of the single gears, the fault identification can be achieved by means of condition indicators by comparison. A number of indices devoted to the gear fault diagnosis can be found in the literature and a complete review can be found in Ref. [22]. It has been widely recognized that, among such parameters, the kurtosis and the CF (crest factor) are quite general indicators, being sensitive to local changes in the vibration signature due to gear tooth defect. Nevertheless, this research proposes also two novel condition indicators based on the vibratory changes occurring in each circular pitch, hence purposely designed for gearbox diagnosis.

3.2 THEORETICAL BACKGROUND

In this section, the main signal processing tools necessary for the comprehension of the proposed methodology are concisely introduced. Only the fundamental concepts are described avoiding unnecessary theoretical explanations.

3.2.1 *First-order cyclostationarity and the Time Synchronous Average*

The vibration signals acquired on gearboxes can be modeled as wide-sense cyclostationary signals, where the term "cyclostationary" refers to a special family of non-stationary signals characterized by hidden periodicities in their structure. This fact has been analytically demonstrated by Mark [12] and, later, explicitly connected to the cyclostationary framework by Capdessus [104, 20] first, then by Antoni [19]. A general definition of CS1 processes is given in Ref. [34] and recalls the definition given by Gardner in Ref. [73]: *a signal is said to exhibit first-order cyclostationarity if there exists a cascade of linear transformations that produces a periodic component*. From another point of view, a stochastic process is said to be CS1 if its expected value is periodic with period T.
An approach for the estimation of the CS1 part of the signal is the time-domain averaging [27, 105]. The averaged signal is obtained by cutting the whole signal into a set of segments where each one corresponds to one gear

revolution. This method is effective if the rotation frequency, and therefore the length of each segment, is constant. Hence the time averaging computed considering a prior period of interest T allows for estimating all the periodic contributions with that fundamental period. Note that, under the hypothesis of cycloergodicity (which is equivalent to the ergodicity for stationary signals), the expected value (i.e. the averaging process) can be computed by the ensemble averaging.
However, the rotating machine vibration signals, are not perfectly periodic in the time domain, even in steady state conditions. This means, for example, that the assumption that the gear mesh component should be modeled by a perfect sinusoid corresponding to a precise Fourier coefficient is no more valid. This behavior is typically due to the slight speed fluctuation caused by the not perfectly constant loads and torques/forces involved. Hence, the averaging process in the time domain may cut out precious information since such components are not perfectly periodic in time.
Thus, a step forward for the estimation of the CS1 part of the signal is the TSA [34]. The TSA is the same of the time-domain averaging but performed in the angle domain. The variable change from the time to the angle domain can be accomplished by directly sampling the vibration signal with a tacho reference or by computing the angular resampling [21].
The TSA becomes very effective for the machine diagnosis when it is applied into the angle domain because many parameters are locked in the angle variable rather than in the time one, such as the loads, the torques and the kinematics variables of the system. For these reasons, the TSA is conveniently performed into the angle domain in order to maintain the cyclostationary properties of the signal. In a general view, the angular resampling allows the application of the cyclostationary framework to the rotating machine vibration signals relaxing the restriction to be in a perfect steady state condition, which is seldom met in real application. For a deeper discussion about this topic, excellent references can be found in [19, 34, 20]
Let $x(\theta)$ be the vibration signal synchronized with rotation θ of a certain rotating mechanical component taken as reference. Considering a periodicity of $\Theta = 2\pi$ and an integer number N of revolutions, the length of $x(\theta)$ is $N\Theta$. Thus, the time synchronous average, $x_{TSA}(\theta)$, of $x(\theta)$ can be defined as:

$$x_{TSA}(\theta) = \frac{1}{N}\sum_{n=0}^{N-1} x(\theta + n\Theta) \;\; with \;\; 0 \leq \theta < 2\pi \tag{41}$$

The change of variable from time to angle implies that the frequency variable will change accordingly. The new frequency variable is called "order" and it is defined as the ratio between the actual frequency and the rotation frequency of the component. Taking into account a proper number of averages, the main result of the TSA is the strong attenuation of all the not periodic components with respect to the reference and the improvement of the SNR (Signal-to-Noise Ratio). Furthermore, the fact that the TSA is performed in the angle domain strongly reduces the effects of slight speed variations masking the effects of possible gear faults.

Thus, the TSA allows for extracting the periodic contributions tied to a rotating component of interest from the raw vibration signature with a contextual noise reduction, which is of great value in order to distinguish components having different periods as in the case of multi-stage gearboxes.

3.2.2 *The Empirical Mode Decomposition*

The EMD [83] is the first step of the HHT that is a time-frequency representation where amplitudes and frequencies are instantaneous quantities. A signal which exhibits a well-behaved instantaneous frequency is also called mono-component signal, as reported in Ref. [106]. However, many real signals are multi-component and may not admit the Hilber transform. In this scenario, the EMD is basically a self-adaptive pre-processing tool for decomposing a signal in a set of oscillatory modes, that are called commonly intrinsic mode functions (IMFs). According to Ref. [83], each IMF has to meet two fundamental properties: i) the number of zero-crossing points and of extrema have to be equal or differ by one; ii) at any point the mean value of the envelope evaluated by the local maxima and by the local minima have to be zero. By virtue of these properties, the last component extracted by the EMD is a monotonic signal, called residue. As reported in [83], these properties should guarantee that each IMF is actually mono-component, i.e. they do not exhibits negative frequencies, and thus the Hilbert transform is admitted. These IMFs are supposed to be mono-components, i.e. they does not exhibits negative frequencies, and the instantaneous frequency and instantaneous amplitude can be correctly estimated.

For the sake of brevity, the essential steps of the EMD algorithm are described in Figure 35, but a more comprehensive explanation about this algorithm can

be found in [83]. The envelope process and the sifting process are the key points of the algorithm in Figure 35. The sifting process is a recursive procedure which ensures that the estimated modes satisfy the characteristic properties of the IMF. The sifting process ends when a certain stopping criterion is met. Several stopping criteria can be found in the literature, as reported in Ref. [107]. The original stop criterion of the sifting process proposed in Ref. [83] is the Cauchy-type convergence criterion (SD in short), it involves the estimation of the standard deviation of two consecutive IMFs. In this thesis, the mean fluctuation thresholds method proposed by Rilling [108] has been adopted. This stopping criterion aims to *guarantee globally small fluctuations in the mean while takes into account locally large excursions*.

The envelope process regards the evaluation of envelopes of the maxima and the minima of the signal. The cubic spline interpolation, which is generally used, is preferred over other interpolation methods, such as the linear and the polynomial, since they are more sensitive to over-decomposition problems (mode mixing).

Hence, the main drawbacks of the EMD mainly linked to the sifting process and the envelope estimation are the mode mixing and the end effect. The mode mixing concerns the combination of signals with several widely different scale, while the end effect is the distortion at the extremity of the signal. These shortcomings can undermine the physical meaning of the estimated IMFs and many investigation have been made in order to reduce these issues. The board effect is mainly due to the envelope of a finite length signal. This negative effect can be strongly reduced by mirroring the extrema at both the sides [108]. On the other hand, the mode mixing problem is a more serious issue and it has been addressed in many works [94, 95, 96] leading to the development of several improved versions of the EMD algorithm.

3.2.3 *The Ensemble Empirical Mode Decomposition*

The EEMD (Ensemble Empirical Mode Decomposition) [109] is a noise-assisted data analysis method based on the EMD algorithm. The main steps of the EEMD algorithm are summarized in Figure 36. Unlike the EMD, which could estimate IMFs affected by mode mixing, the EEMD calculates the so-called true modes or IMF^* representing a more reliable decomposition of the signal.

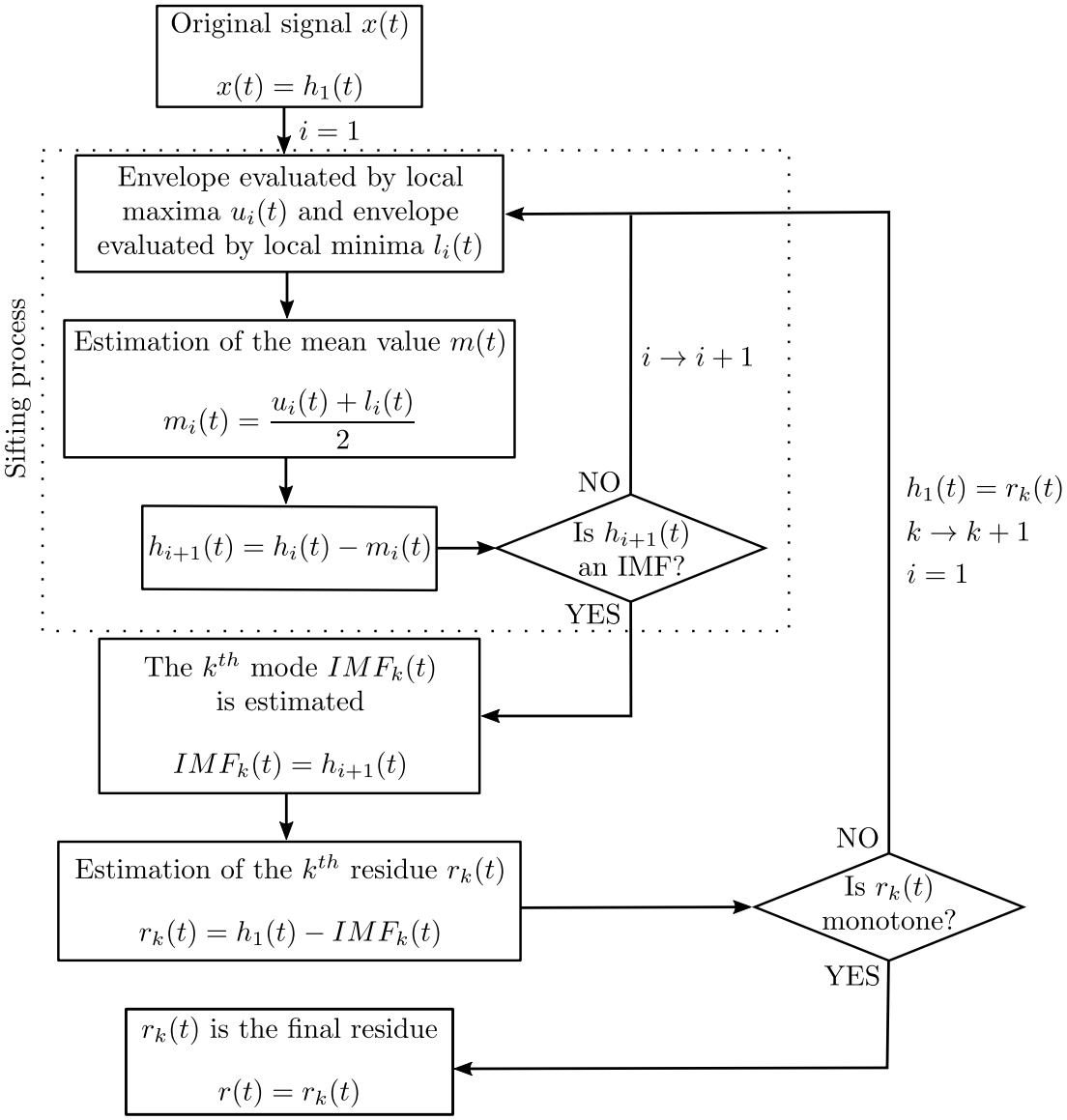

Figure 35: Flow chart of the EMD algorithm.

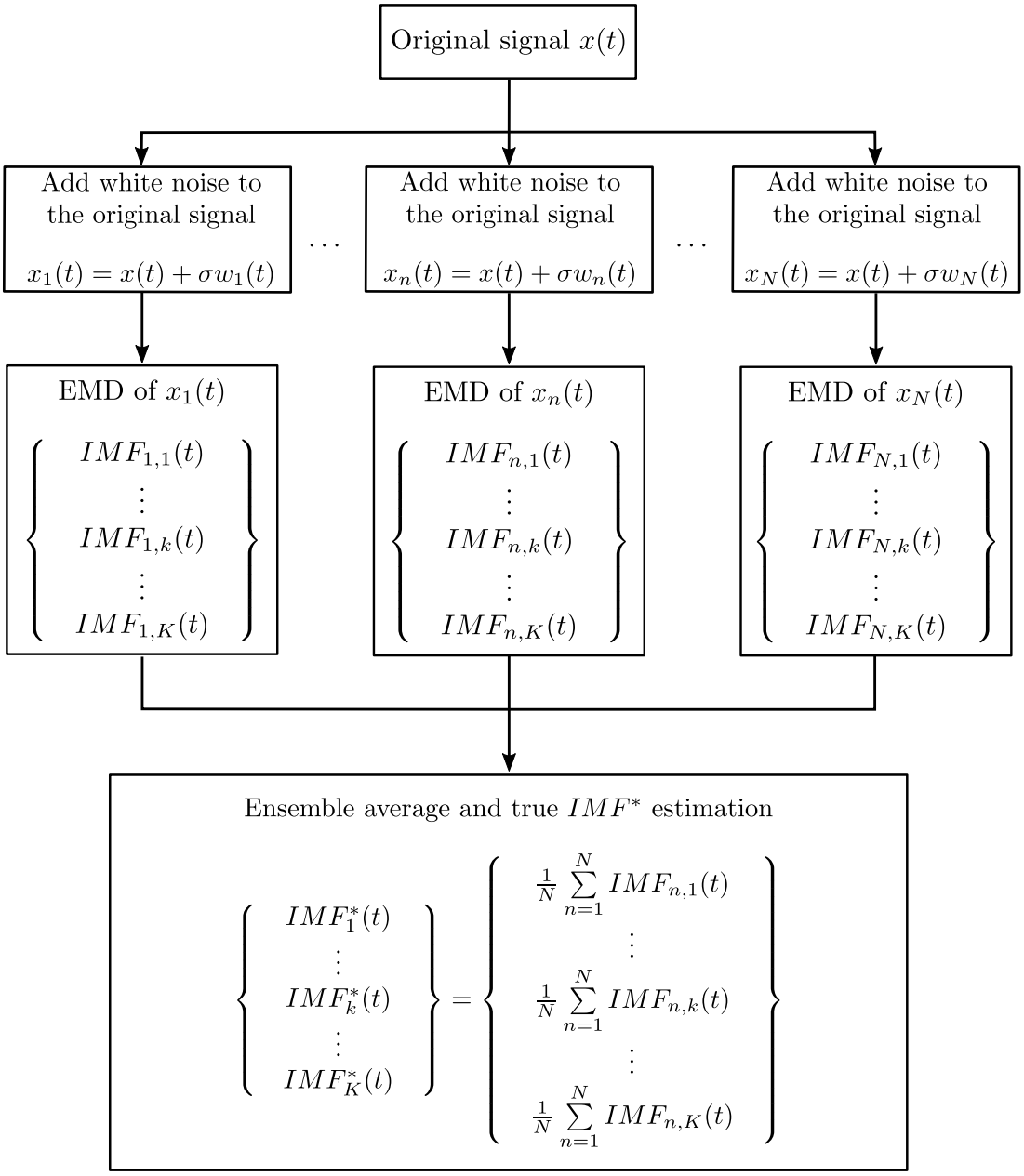

Figure 36: Flow chart of the EEMD algorithm with N trials and K modes per trial.

Departing from original signal $x(t)$, a new set of N signals (where N represents the number of trials or realizations) is created by adding different zero-mean white Gaussian noise $w(t)$ of finite standard deviation σ. The added noise bring two main benefits: the EMD acts as a dyadic filter when applied to pure white noise [87], the small perturbations introduced by the white noise force the algorithm to scan all the possible solutions (in terms of mode decomposition). Then, the EMD is performed for each signal x_n obtaining N (noisy) mode sets composed by K modes each. At the end, the true IMF set composed by a number K of true modes IMF^* is evaluated by ensemble averaging each k^{th} IMF set previously obtained. Thanks to the cancellation statistical property of the additive white Gaussian noise, the ensemble averaging strongly reduces the noise level of each mode. The final results are called "true IMF" just because they represent the persistent part of each IMF set that has not been erased by the ensemble averaging.

Differently from the EMD, the EEMD depends on two arbitrary parameters: the number of trials and the standard deviation of the added white noise. The number of trials must be large enough in order to guarantee a satisfactory suppression of the added noise. The link between these parameters, as reported in Ref. [94], is given by the following relationship:

$$\varepsilon = \frac{\sigma}{\sqrt{N}} \tag{42}$$

where N is the number of trials, σ is the standard deviation of the added noise and ε is the error standard deviation defined as the difference between the original signal and the corresponding IMFs. This relationship implies that the larger the noise standard deviation, the larger the number of trials.

These parameters are pivotal in order to obtain satisfying results. Commonly [94, 110], a few hundreds of averages and a noise standard deviation between 0.1 and 0.4 are enough but some research works [111, 112] use a noise standard deviation proportional to the standard deviation of the original signal. Moreover, it has been demonstrated [83] that the selection of σ depends on the application since high values of σ are suitable for data dominated by low-frequency signals and vice versa. Thus, the selection both the number of trials and the noise standard deviation is still an open question depending on the input data and the experience.

3.2.4 *The Complete Ensemble Empirical Mode Decomposition with Adaptive Noise*

The Complete Ensemble Empirical Mode Decomposition with Adaptive Noise (CEEMDAN) represents a step further with respect to EEMD and it has been proposed for the first time by Torres et al. [96] and improved by the same authors in Ref. [113].
As shown in Figure 36, the EEMD calculates the true modes by averaging a certain number of noisy IMF sets, which have been evaluated independently each other. Each $IMF_{n,k}$ is determined by considering the residue of the corresponding previous mode, $IMF_{n,k-1}$, therefore a (small) reconstruction error is introduced using this approach.
The CEEMDAN algorithm has been proposed with the precise goal to deal with the reconstruction error by computing the modes sequentially. The estimation of each true mode is achieved by the CEEMDAN algorithm by taking into account the contribution of the residue evaluated from the previous true mode. Therefore, the CEEMDAN guarantees the exact correspondence between the original signal and the set of decomposed signals, which is not ensured by the EEMD [113]:

$$x(t) = \sum_{n=k}^{K} IMF_k{}^*(t) + r(t). \tag{43}$$

The flowchart of the algorithm is presented in Figure 37 where operator $E_k(\bullet)$ refers to the extraction of the k^{th} mode by using the EMD algorithm, according to Ref. [113]. In reference to Figure 37, at each iteration, the k^{th} true mode is estimated from the previous residue calculated by the $k-1^{th}$ mode perturbed by the additive noise. The added white Gaussian noise for the estimation of the k^{th} IMF actually is the k^{th} mode obtained performing the EMD to the white noise itself.
It is worth noting that σ_k means that the standard deviation of the added noise can be changed at each iteration. According to the studies reported in Refs. [94, 110], the varying amplitude of the added noise can improve the performance of the signal decomposition when low amplitude noise is considered for the first stages and large amplitude noise for the late stages. A more exhaustive explanation of the CEEMDAN algorithm can be found in the following research works [96, 110, 113].
Finally, this approach guarantees the following benefits:

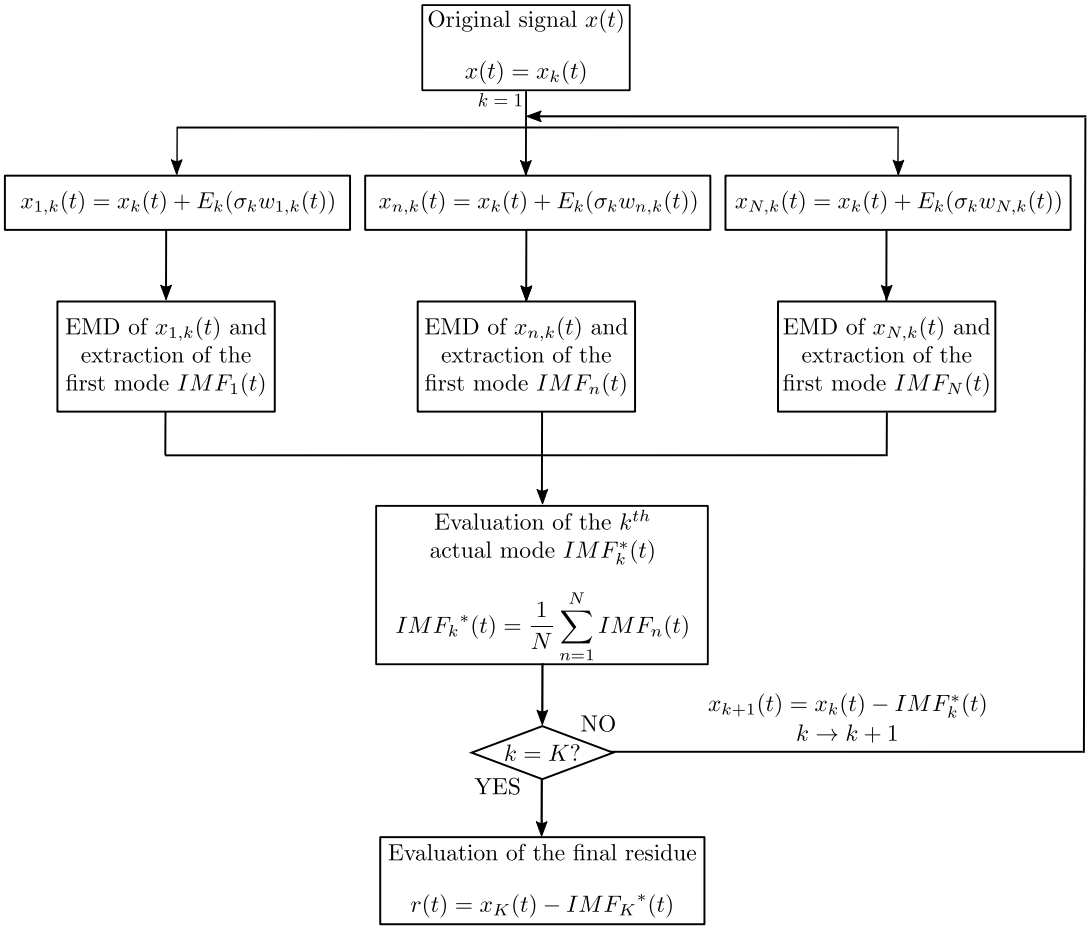

Figure 37: Flow chart of the CEEMDAN algorithm.

- the original signal can be reconstructed by adding all the estimated IMFs (completeness property);

- a smaller number of sifting iterations are needed with respect to the EEMD, which implies less computational effort [110];

- the noise standard deviation can be changed at each stage.

3.2.5 *Gear fault identification by condition indicators*

The presence of gear faults leads to changes in the vibration signature measured on the gearboxes. A number of researches can be found in the literature about the development of parameters for the quantification of the vibration signature modification [35, 22, 66]. These parameters are generally called Condition Indicators (CIs).

In this study, the following standard CIs have been considered: kurtosis, Crest Factor (CF) and FM0. The kurtosis is the fourth-order standardized moment of a probability distribution, the CF is the ratio of the peak value to the RMS value and the FM0 is the ratio of the peak-to-peak value to the sum of the gear mesh harmonics amplitudes. These parameters are particularly effective for the identification of local changes in the vibration signature, as in the case of localized gear faults.

Furthermore, two new CIs are proposed based on the vibration signal RMS values evaluated for each tooth: Crest Pitch Factor (CPF) and the Normalized Skewness Variance Product (NSVP). For their computation, the TSA, i.e. x_{TSA}, is split into a number of parts equal to the number of teeth; then, the RMS value is estimated for each part. Let ${RMS_p}^i$ be the RMS value of the i^{th} tooth, ${RMS_p}^i$ is defined as follows:

$$ {RMS_p}^i = RMS\left[x_{TSA}\left(\theta + \frac{2\pi}{z}(i-1)\right)\right] \quad with\ 0 \leq \theta < \frac{2\pi}{z} \tag{44} $$

where $\frac{2\pi}{z}$ is the angular pitch, z is the number of teeth and $RMS[\bullet]$ is the Root Mean Square of a given data series. The whole set of ${RMS_p}^i$ is:

$$\{RMS_p\} = \left\{ \begin{array}{c} {RMS_p}^1 \\ \vdots \\ {RMS_p}^i \\ \vdots \\ {RMS_p}^z \end{array} \right\} \tag{45}$$

For a gear having localized faults, a local deviation from the mean value of RMS_p is expected. The first CI, called CPF, it is defined as the ratio of the maximum value of RMS_p with respect to the RMS_p ensemble mean value:

$$CPF = \frac{max[RMS_p]}{\mathbb{E}[RMS_p]} \tag{46}$$

where $\mathbb{E}[\bullet]$ is the expectation operator. Now, let us consider the difference among adjacent RMS_p^i values:

$$\{RMS_{pd}\} = \left\{ \begin{array}{c} {RMS_p}^2 - {RMS_p}^1 \\ \vdots \\ {RMS_p}^i - {RMS_p}^{i-1} \\ \vdots \\ {RMS_p}^z - {RMS_p}^{z-1} \end{array} \right\} \tag{47}$$

Intuitively, RMS_{pd} values should be close to zero for healthy gears since the variation between two consecutive RMS pitch values is slight. On the other hand, RMS_{pd} exhibits non-zero values when local changes of the vibration signature occur, since the vibration signature of a healthy meshing tooth is very different from a faulty one. On the basis of these considerations, a second indicator, called NSVP, is defined as the product between skewness and variance of the RMS_{pd} divided by the peak-to-peak value of RMS_{pd}:

$$NSVP = \frac{var[RMS_{pd}]skew[RMS_{pd}]}{pp[RMS_{pd}]} \tag{48}$$

where $var[\bullet]$ is the variance of a given data series, $skew[\bullet]$ is the skewness of a given data series and $pp[\bullet]$ is the peak-to-peak value.

3.3 RATIONALE AND PROPOSED METHOD

In theory, the vibration signal of a gearbox operating at steady-state condition appears as a composition of harmonics having as fundamental frequencies the meshing frequencies. The localized gear faults can appear in the vibration signals as impulsive components and local modulations of amplitude and/or phase [10]. These local modulations are visible in the spectrum as side-bands centered on the meshing frequencies. A pure impulsive component depends on the period of occurrence (the shaft period) and on the IRF of the system. Thus, in the case of an intermediate shaft, a pure impulsive component depends on parameters that are not strictly related to one single wheel mounted on that shaft. The local modulations of amplitude and phase are a function of meshing frequency and the rotation frequency of the faulty wheel. These modulations reflect on the spectrum as sidebands around the gearmesh frequency. Hence, considering two gears with different (and not multiple) number of teeth and mounted on an intermediate shaft, the analysis of the sideband families due to local modulations should lead to the identification of the faulty gear since these sideband families are related to a specific wheel.

When the TSA is performed according to a certain shaft period, it is possible to set apart only the tones that are synchronous with the shaft of interest. However, the TSA cannot separate a pure impulsive component due to a localized fault of two or more gears mounted on the same shaft, as they exhibit the same orders. Hence, in order to identify the faulty gear, the basic idea of this work is to exploit the local changes of meshing vibration due to the amplitude and phase modulations rather than the pure impulsive component. In the TSA, the meshing harmonics of two or more gears with not multiple number of teeth are separated, but the families of sidebands of different meshing harmonics can be partially overlapped. Thus, it can be difficult to separate the local modulations contributions due to different gears. Moreover, it is difficult to establish a priori which harmonics are clearly affected by modulation effects as well. On these grounds, a signal separation method based on EMD algorithm is described hereafter in order to overcome to this problem, which is fairly common in practical applications with a significant implication concerning the reduction of maintenance costs and time.

Let us consider the two-stage gearbox shown in Figure 38, composed by four spur gears (namely I, II, III and IV) operating at steady-state conditions. Fur-

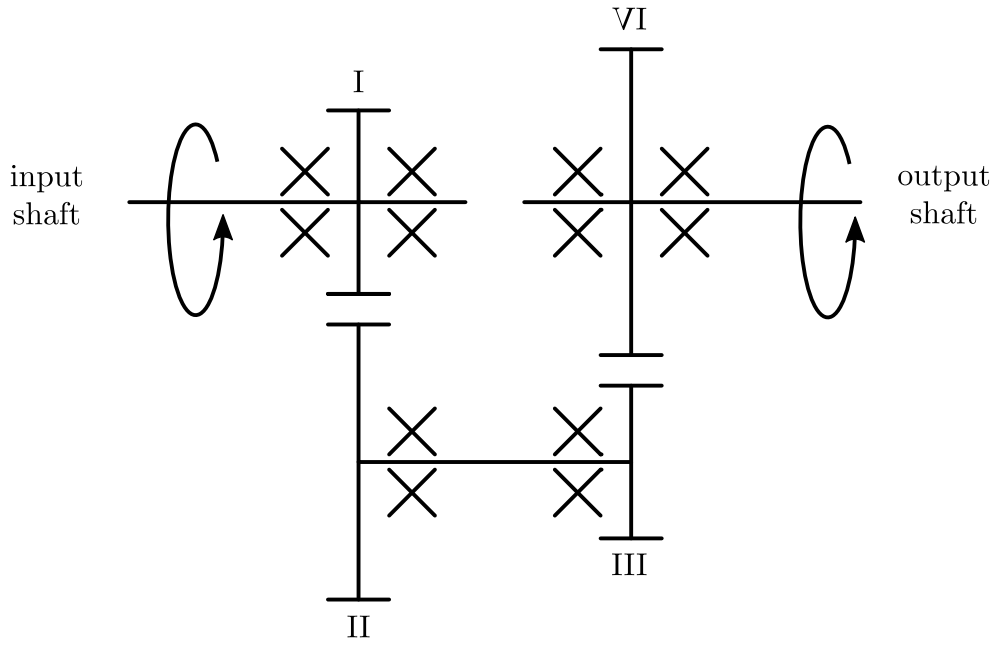

Figure 38: Schematic of a two-stage gearbox.

thermore, let us suppose the presence of a localized fault on wheel II. Thus, taking advantage from the EMD-based decomposition, two representative vibration signatures characterizing the meshing vibration of gear II and gear III, respectively, can be built taking into account the physically meaningful IMFs. The physically meaningful IMFs are intended as those IMFs that describe the gearmesh vibration signature of the gear of interest. Therefore, the representing signal of the gear will be the sum of these modes (if they are more than one). Figure 39 describes the proposed methodology (summarized in 4 fundamental steps) for the generic two-stage gearbox in Figure 38.

Under the assumption that the gear fault on the intermediate shaft is evident on the TSA, the first step involves the low-pass filtering since several high frequency signal components unrelated with the gear mesh vibration signature can persist also after the TSA. In addition, the proposed signal processing procedure focuses on the local modulation of amplitude and phase, hence a

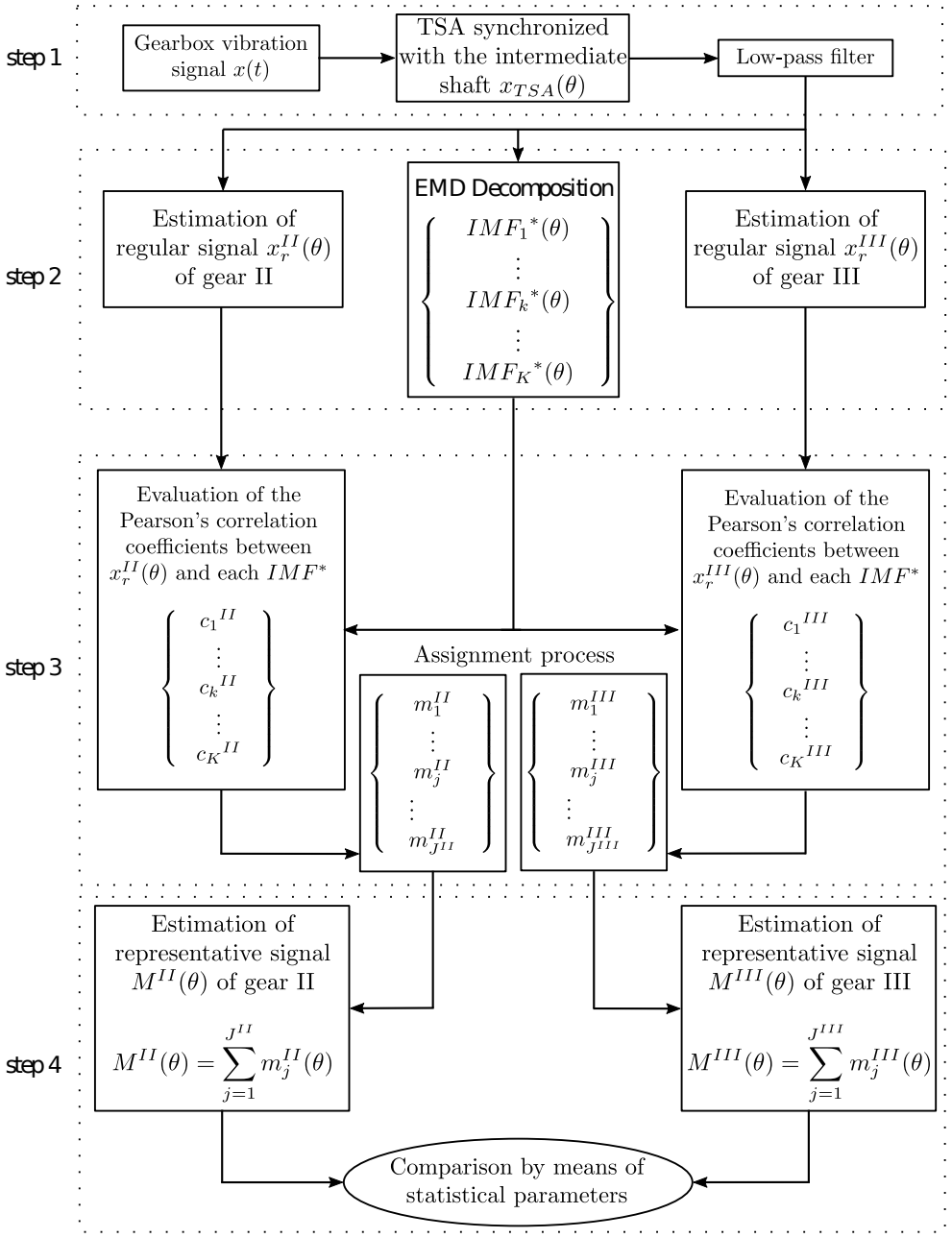

Figure 39: Flow-chart of the proposed methodology.

low-pass filter is desirable in order to cut off the high frequency signal components that should belong to the impulsive events. Therefore, the signal is

conditioned with a low-pass filter with a cut-off order (the signal belongs to the angle domain) equal to 3 times the gear mesh order of the greater gear. Bearing in mind that the filtering process could reduce also some significant components, it is anyway reasonable to assume that the gear mesh vibration signature is properly described taking into account the first 3 meshing gear harmonics (and their side-bands).

The second step consists in the decomposition of the signal and the estimation of the regular signals of gears II and III. EMD, EEMD and CEEMDAN have been considered, in order to investigate the effects on the use of different EMD algorithms for the signal decomposition. In this work, 500 trials and a fixed white noise standard deviation of 0.2 have been adopted, as suggested in [113, 109]. Furthermore, it has to be remarked that the procedure has been developed in Matlab environment exploiting the EMD algorithms available online[1,2]. Instead, the regular signal is defined as the sum of the gear mesh harmonics from the TSA signal. In this application the fundamental gear mesh order and the first two harmonics are taken into account. The meaning of the estimation of the regular signals will be clarified hereafter.

The third step is the core of the proposed methodology. A major issue on the use of the Empirical Mode Decomposition is the physical interpretation of the IMFs. In fact, there are not established procedures for the identification of the meaningful modes for gear applications. Otherwise, the aim of this work is to generate from the calculated IMF set, two signals representing the gear mesh vibration signals of gear II and gear III, distinctly. Therefore, it is not just important to identify the physically meaningful modes but also to determine if the mode describes the gear mesh vibration signature of gear II, gear III or neither of these. The selection criterion of the physically meaningful modes developed in this work is based on the PCC (Pearson's Correlation Coefficient) between the regular signals and the IMFs. The PCC is an indicator of the linear correlation between two variables (signals) and conceptually is similar to the normalized cross-correlation between two signals with zero lag [114].

1 http://perso.ens-lyon.fr/patrick.flandrin/emd.html
2 http://bioingenieria.edu.ar/grupos/ldnlys/metorres/re_inter.htm

PCC value c evaluated for discrete dataset x and y of n samples (e.g. discrete vibration signals), is defined as follows:

$$PCC = \frac{\sum_{i=1}^{n} (x_i - \overline{x})(y_i - \overline{y})}{\sqrt{\sum_{i=1}^{n} (x_i - \overline{x})^2 \sum_{i=1}^{n} (y_i - \overline{y})^2}} \tag{49}$$

where $\overline{x}$ and $\overline{y}$ are the mean value of x and y respectively. The PCC can takes values between -1 and 1, where positive values mean a direct correlation while negative ones mean inverse correlation. For our purpose, $PCC \geq 0.7$ means a strong linear correlation, $0.3 \leq PCC < 0.7$ means moderate correlation, $0.1 \leq PCC < 0.3$ means weak correlation and $PCC = 0$ means no correlation. In this work the PCC has been exploited as the merit index for the mode selection in order to allocate each IMF to gear II, gear III or neither of these. Referring to Figure 39, the assignment process regards the mode selection procedure for building the representative signals of gear II and gear III, namely $M^{II}(\theta)$ and $M^{III}(\theta)$ respectively. The selection criterion that evaluates the physical significance of the modes is based on these properties:

1. if $PCC \geq 0.3$ (which means at least moderate correlation), the mode is assigned to the representative signal set;
2. if no IMF fulfills the previous properties, the mode having the maximum value of PCC is representative of the gear.

Therefore, referring to Figure 39, the representative vibration signal of gear II, $M^{II}(\theta)$, is composed by all the modes (called $m_j^{II}(\theta)$) satisfying one of these properties and the same occurs for $M^{III}(\theta)$. The PCCs are evaluated by the regular signal (e.g. an ideal healthy mesh gear vibration) and the IMFs. Since the modes are estimated from the faulty gear vibration signal, a moderate correlation with the regular signal is expected. Thus, property 1 aims to include all the modes showing a moderate correlation with the regular signal having, however, a significant relationship with the gear vibration signature from the physical standpoint. The second property is introduced in order to include at least one IMF also if property 1 is not met.
Lastly, in the fourth step the estimation of $M^{II}(\theta)$ and $M^{III}(\theta)$ of gear II and gear III, respectively, are carried out by means of the sum of the selected

modes $m_j^{II}(\theta)$ and $m_j^{III}(\theta)$ evaluated in the third step. After a visual inspection of the representative signals, the objective comparison between $M^{II}(\theta)$ and $M^{III}(\theta)$ is achieved by means of different CIs. For this purpose, in order to identify localized gear faults, several CIs can be used for the evaluation of the vibration signal peakiness, which is correlated with the severity of the localized fault. In this study, the following standard CIs have been considered: kurtosis and Crest Factor (CF) [66, 22]. Furthermore, the effectiveness of the proposed CIs, i.e. CPF and NSVP, has been tested for the simulated vibration signals and the real case studies.

3.4 VALIDATION BY SIMULATED SIGNALS

3.4.1 *Vibration signal model*

Several works [10, 14, 115] regarding the time domain vibration signal modeling of gear faults can be found in the literature. Since the proposed method departs from the TSA, a vibration signal model of the TSA referenced to a gearbox is proposed hereafter. The TSA of a healthy gearbox, x, with respect to angle θ is mainly composed by harmonics with fundamental order corresponding to the number of teeth of the gear of interest. For a complete revolution, $x(\theta)$ can be expressed as follows:

$$x(\theta) = \sum_{n=1}^{N} X_n \cos\left(nz\theta + \phi_n\right) \tag{50}$$

where N is the number of harmonics, X_n is the amplitude of the n^{th} harmonics, ϕ_n is the phase of the n^{th} harmonics and z is the number of teeth of the gear. Let us consider the two-stage healthy gearbox shown in Figure 38. In a complete revolution, the angle domain meshing vibration $x(\theta)$ related to the intermediate shaft may be expressed as:

$$x(\theta) = \sum_{n=1}^{N} X_{II,n} \cos(nz_{II}\theta + \phi_{II,n}) + \sum_{n=1}^{N} X_{III,n} \cos(nz_{III}\theta + \phi_{III,n}) \tag{51}$$

where N is the number of harmonics, $X_{II,n}$ is the amplitude of the n^{th} harmonics of gear II, $\phi_{II,n}$ is the phase of the n^{th} harmonics of gear II, z_{II} is the number of teeth of gear II, $X_{III,n}$ is the amplitude of the n^{th} harmonics of gear

III, $\phi_{III,n}$ is the phase of the n^{th} harmonics of gear III and z_{III} is the number of teeth of gear III. Equation (51) states that the meshing vibration signal $x(\theta)$ is composed by the meshing vibration related to gear II and the gearmesh vibration related to gear III since both gears II and III rotate synchronously. The presence of a localized gear fault causes a change in the vibration signal model that involves a local amplitude modulation, a local phase modulation and an impulsive component. Hence, assuming a localized faults in gear II, Equation (51) can be rewritten as:

$$\begin{aligned} x_{sim,II}(\theta) &= x^{II}(\theta) + x^{III}(\theta) + d(\theta) = \\ &\sum_{n=1}^{N} X_{II,n}\left[1 + a_{II,n}(\theta)\right]\cos\left[nz_{II}\theta + \phi_{II,n} + b_{II,n}(\theta)\right] + \\ &\sum_{n=1}^{N} X_{III,n}\cos(nz_{III}\theta + \phi_{III,n}) + d(\theta) \end{aligned} \tag{52}$$

where $a_{II,n}$ is the local amplitude modulation function due to localized fault in gear II, $b_{II,n}$ is the local phase modulation function due to localized fault in gear II and d is the impulsive component due to localized fault in gear II. The local amplitude function $a_{II,n}$ and phase modulation function $b_{II,n}$ used in section 3.4.1 are described as a Gaussian shape window centered at angle θ_0 as follows:

$$a_n(\theta) = A_n e^{-\frac{(\theta-\theta_0)}{\sigma_a^2}} \tag{53}$$

$$b_n(\theta) = B_n e^{-\frac{(\theta-\theta_0)}{\sigma_b^2}} \tag{54}$$

where A_n and B_n are the intensity of the local modulations while σ_a and σ_b are the window widths. In addition, $d(\theta)$ (see Equation (52)) is the damped impulse response accounting for the impulsive component due to the faulted tooth engagement in the angle domain. This component is defined as an ideal impulse convoluted by an arbitrary IRF, h, of a SDOF system:

$$d(\theta) = s(\theta) * h(\theta) \tag{55}$$

where s is the impulse due to the fault occurrence. Figure 40 illustrates the spectrum of h in the order domain obtained by imposing a damping coefficient of 0.17% and a natural frequency corresponding to the 1023^{rd} order.

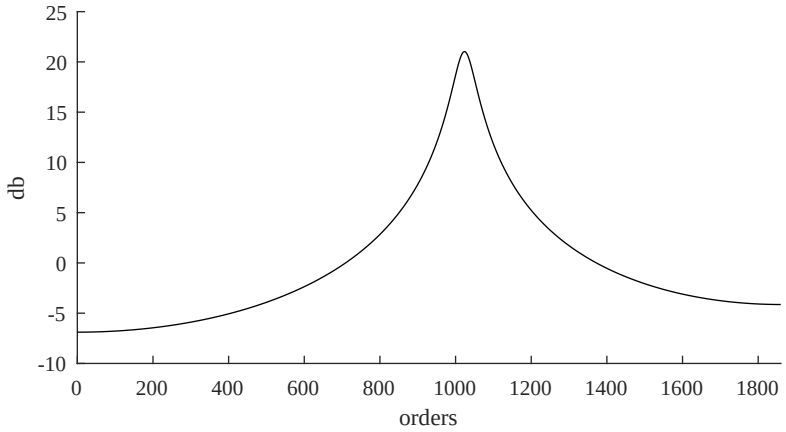

Figure 40: Spectrum of h.

From the physical standpoint, the IRF of a mechanical system makes sense only in the time domain. However, under certain hypotheses, an IRF keeps its physical meaning also in the angle domain. This direct link between the order domain and the frequency domain is allowed only in steady-state regimes and when the transfer path between source and receiver (i.e. a transducer) do not change with respect to time. The first assumption is met because this chapter considers only steady-state regimes. The second hypothesis is met as well: in gears it is reasonable to assume that a faulty tooth is engaged always in the same location and therefore the transfer path is time-invariant.

Analogously, the gear mesh vibration model can be written in the case of a localized fault in gear III:

$$\begin{aligned} x_{sim,III}(\theta) &= x^{II}(\theta) + x^{III}(\theta) + d(\theta) = \\ &\sum_{n=1}^{N} X_{II,n} \cos\left(n z_{II} \theta + \phi_{II,n}\right) + \\ &\sum_{n=1}^{N} X_{III,n} \left[1 + a_{III,n}(\theta)\right] \cos\left[n z_{III} \theta + \phi_{III,n} + b_{III,n}(\theta)\right] + d(\theta) \end{aligned} \tag{56}$$

Referring to the gearbox depicted in Figure 38, Equations (52) and (56) represent the gearmesh vibration models used for the preliminary verification of the methodology.

3.4.2 *Results and discussion*

Two different simulated signals called $x_{sim,II}(\theta)$ and $x_{sim,III}(\theta)$ have been considered: the first simulated signal is described in section 3.4.1 and refers to the case of a localized defect in gear II; the second one is described in section 3.4.1 and refers to the case of a localized defect in gear III. The parameters used for the Matlab implementation of $x_{sim,II}(\theta)$ and $x_{sim,III}(\theta)$ are reported in detail in Table 5, while Figure 41 shows the simulated signals. In the first case the localized fault has been simulated on the 45^{th} tooth of gear II whereas in the second case the localized fault has been simulated on the 6^{th} tooth of gear III, which correspond to an angle rotation of about $174\,deg$ and $180\,deg$, respectively.

As mentioned in Section 3.4.1, the overall simulated signal is a superposition of the vibration signature in the angle domain of the two gears, where the healthy gear is represented by pure tones and the faulty gear is composed by pure tones having local amplitude and phase modulation with the contribution of an impulsive component. De facto, such signals represent a synthesized version of the TSA computed with respect to the intermediate shaft and, according to the properties of the TSA, the contribution of the background noise has been neglected. Considering the proposed diagnostic protocol, Step 1 can be skipped with this vibration signal model since the starting signal is already the TSA of the signal.

The method has been performed using EMD, EEMD and CEEMDAN in order to investigate the effect of different EMD algorithms on the effectiveness of the signal decomposition. In agreement with the settings suggested in the literature, 500 averages and white noise standard deviation of 0.02 has been used for the EEMD and CEEMDAN. The results of the signal decomposition of $x_{sim,II}(\theta)$ and $x_{sim,III}(\theta)$ is reported in Figures 42 and 43, respectively. The residue signal, which is a monotonic function, is not displayed since it is not useful for the goal of this work. It should be noted that EMD returns a limited number of modes (4 excluding the residue) whereas the total number of tones present on the simulated signal is 6 since it's equal to the total number of gearmesh harmonics accounted. This behavior can be interpreted as poor quality of the signal decomposition using EMD with respect to EEMD and CEEMDAN.

Table 5: Simulated signal parameters.

	$x_{sim,II}(\theta)$	$x_{sim,III}(\theta)$
z	93	12
N	3	3
X_1	6.000	6.000
X_2	3.639	3.639
X_3	2.207	2.207
A_1	1.075	1.075
A_2	3.668	3.668
A_3	-4.518	-4.518
B_1	0.862	0.862
B_2	0.319	0.319
B_3	-1.308	-1.308
σ_a	0.011	0.087
σ_b	0.011	0.087
$\theta_0\,(rad)$	3.040	3.142

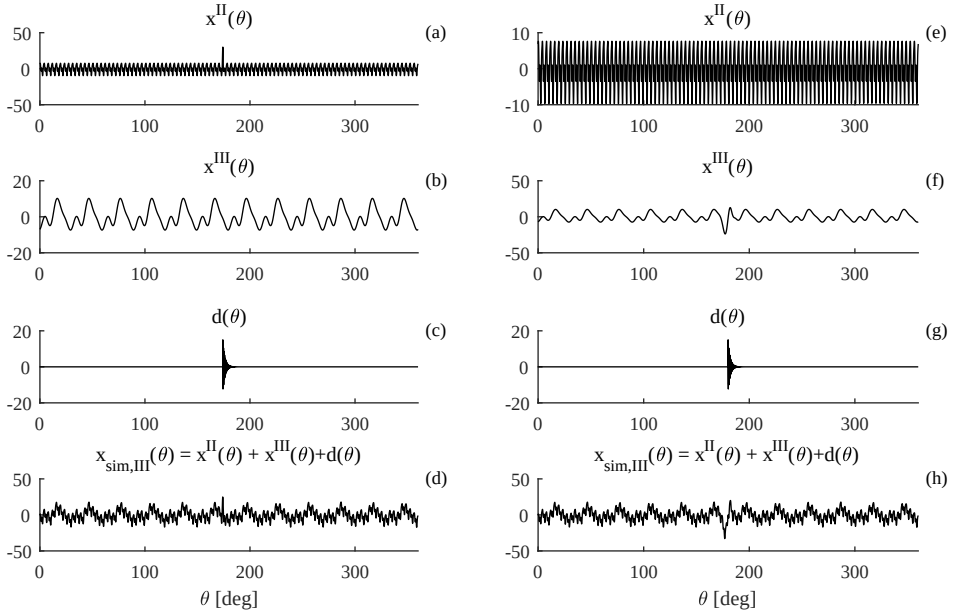

Figure 41: Simulated signals in the angle domain: (d) $x_{sim,II}(\theta)$ and (a-c) its components, (h) $x_{sim,III}(\theta)$ and (e-g) its components.

For the sake of completeness, the estimated PCC values are collected in Figure 44 where the circle symbol refers to c_i^{II} and the star symbol refers to c_i^{III}. In each diagram, the gray horizontal line refers to the threshold corresponding to $PCC = 0.3$. According to the proposed criterion, the representative signals of gear II and gear III are showed in Figures 45 and 46.
The visual inspection of the representative signals shown in Figure 45 highlights that all the considered EMD algorithms has led to satisfying results. In this case, as expected, representative signal M^{II} related to the 93 teeth gear exhibits a localized signal distortion at about $170\,deg$ due to the simulated defect (in agreement to the input data in Table 5) whereas the waveform M^{III} does not show irregularities. It should be remarked that M^{III} estimated by the EMD (Figure 45(d)) is less regular than the others just in correspondence to the angle where M^{II} has the local amplitude/phase modulation. Table 6 collects the statistical indicators estimated by M^{II} and M^{III}. All the indicators return a positive deviation between the faulty gear and the healthy one, with the only exception of the kurtosis when the EMD is performed. This be-

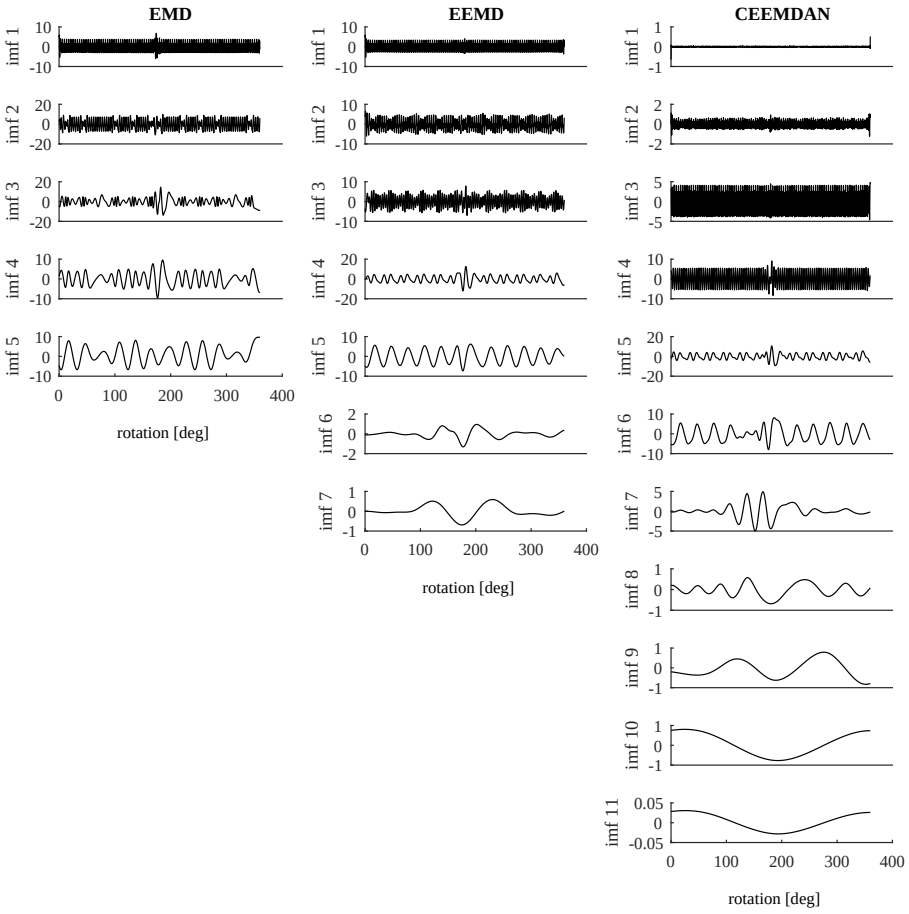

Figure 42: IMF sets of $x_{sim,II}(\theta)$ obtained by using EMD, EEMD and CEEMDAN.

havior is in agreement with the observations previously made by the visual inspection of the signal.

Similar remarks can be mentioned by observing Figure 46. Indeed, M^{III} shows a sudden change of the signal amplitude at about $180\,deg$ that corresponds to the position of the simulated fault (see Table 5). Again, the waveform of M^{II} does not exhibits any abrupt change, although the EMD returns a quiet irregular waveform with respect to the other EMD algorithms. In fact, the indicators collected in Table 7 highlights that negative percentage differences

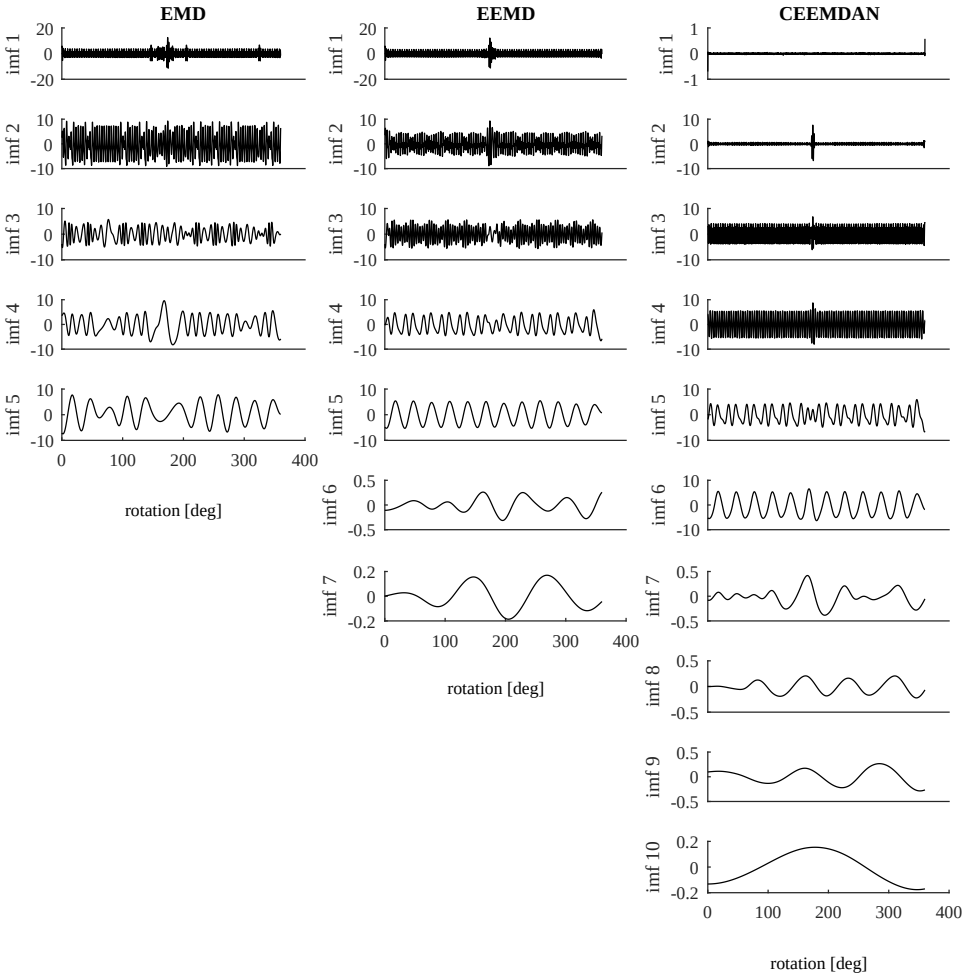

Figure 43: IMF sets of $x_{sim,III}(\theta)$ obtained by using EMD, EEMD and CEEMDAN.

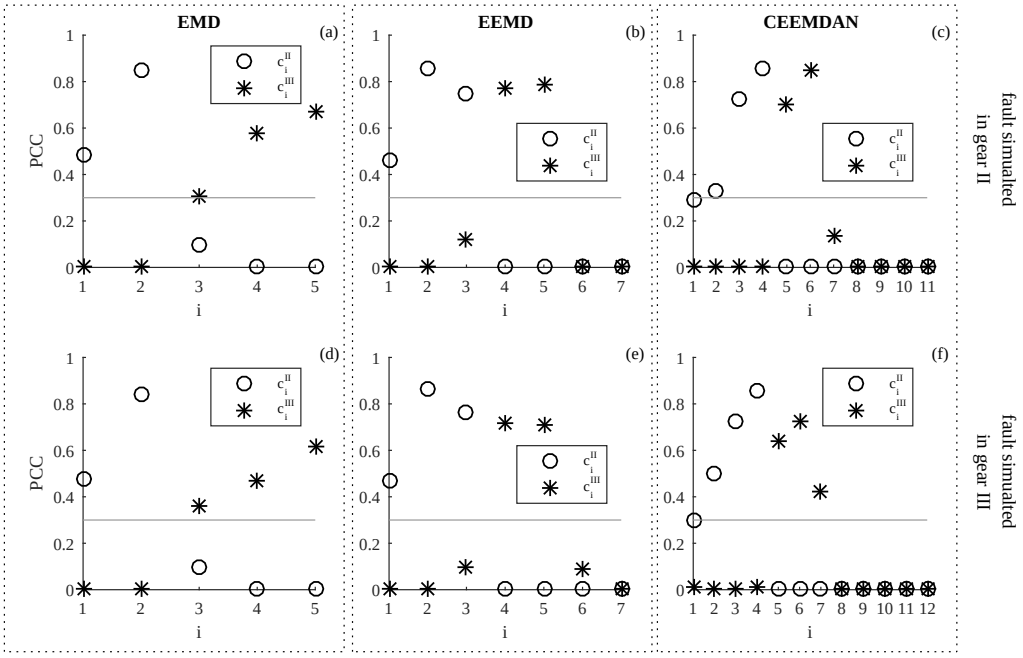

Figure 44: PCC values (a-c) in the case of the simulated signal with localized fault in gear II and (d-e) in the case of the simulated signal with localized fault in gear III.

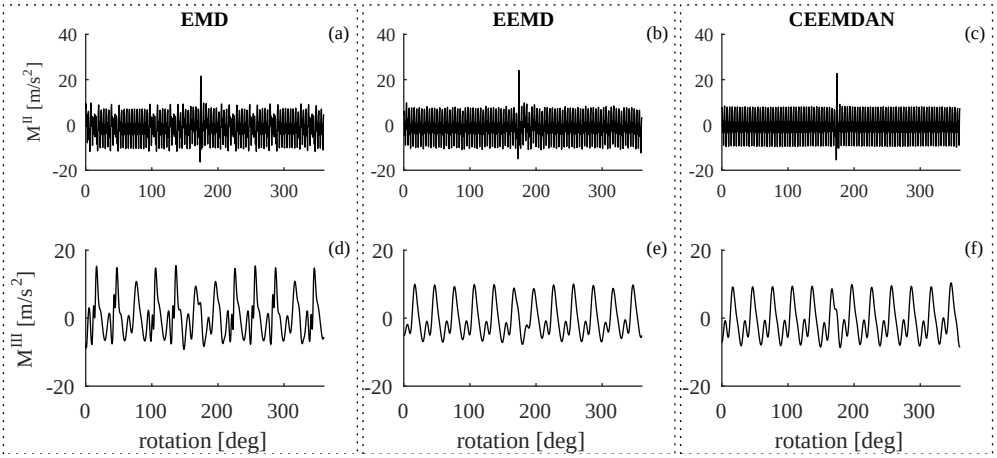

Figure 45: Representative signals for (a-c) gear II and (d-f) gear III in the case of the simulated signal with localized fault in gear II.

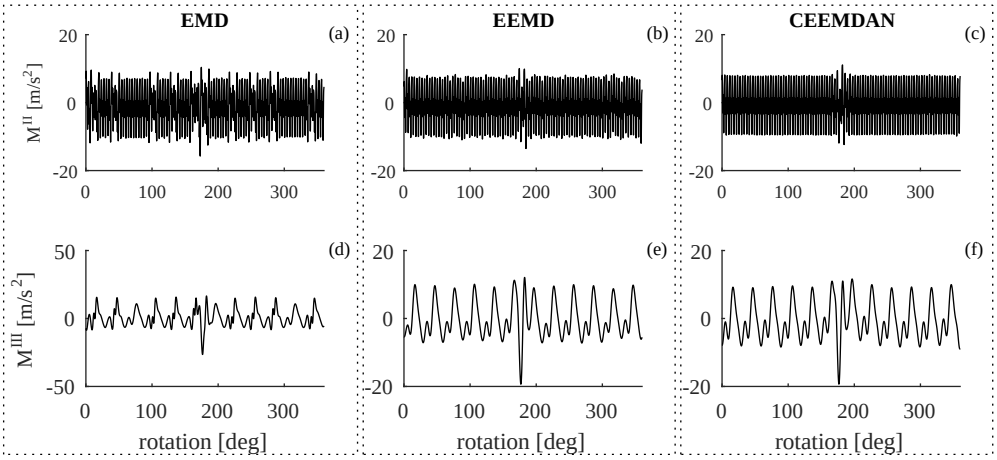

Figure 46: Representative signals for (a-c) gear II and (d-f) gear III in the case of the simulated signal with localized fault in gear III.

Table 6: CIs for the simulated signal with localized fault in gear II.

		kurtosis	CF	CPF	NSVP
EMD	Gear II (faulty)	2.395	4.017	1.854	0.310
	Gear III (healthy)	2.742	2.673	1.083	0.0796
	Gear II vs Gear III [%]	−12.671	50.269	71.244	291.452
EEMD	Gear II (faulty)	2.484	4.494	1.872	0.173
	Gear III (healthy)	2.165	2.014	1.036	0.022
	Gear II vs Gear III [%]	14.713	123.180	80.722	667.777
CEEMDAN	Gear II (faulty)	2.340	4.284	1.857	0.205
	Gear III (healthy)	2.177	1.992	1.027	0.016
	Gear II vs Gear III [%]	7.487	115.058	80.777	1156.891

are present only for the EMD, as expected. However, the method performed using the EEMD and the CEEMDAN has allowed to clearly identify the faulty gear both by visual inspection and by comparing condition indicators.

Finally, the validation of the method by simulated signals has pointed out the following aspects:

Table 7: CIs for the simulated signal with localized fault in gear III.

		kurtosis	CF	CPF	NSVP
EMD	Gear II (faulty)	2.167	2.989	1.625	0.288
	Gear III (healthy)	3.980	4.146	1.579	0.261
	Gear III vs Gear II [%]	83.697	38.733	−2.756	−9.628
EEMD	Gear II (faulty)	2.062	2.569	1.329	0.007
	Gear III (healthy)	2.855	3.578	1.562	0.334
	Gear III vs Gear II [%]	38.482	39.266	17.488	4958.513
CEEMDAN	Gear II (faulty)	2.039	2.357	1.309	0.013
	Gear III (healthy)	2.647	3.428	1.469	0.351
	Gear III vs Gear II [%]	29.847	45.404	12.228	2528.605

- the signal decomposition by means of the EMD is the worst one among the other considered algorithms;
- the faulty gear has been correctly identified in both the simulated cases;
- NSVP is the most sensitive indicator.

3.5 VALIDATION BY EXPERIMENTAL SIGNALS

In the current section, the proposed methodology has been performed in two different experimental cases, discussing the main results. Case 1 concerns the investigation of the method using a dedicated gear test bench while Case 2 regards a more complex transmission mounted on a test rig. The main results have been discussed, focusing on the effectiveness of the proposed methodology performed using actual vibration signals.

3.5.1 *Case 1*

The first experimental case is the same two stage gearbox described in Section 2.6.1 shown in Figure 47a. The investigated gearbox is composed by two stages of helical gears: the first one having 18 and 71 teeth whereas the second one 12 and 55 teeth. Hence, referring to the gearbox scheme in Figure

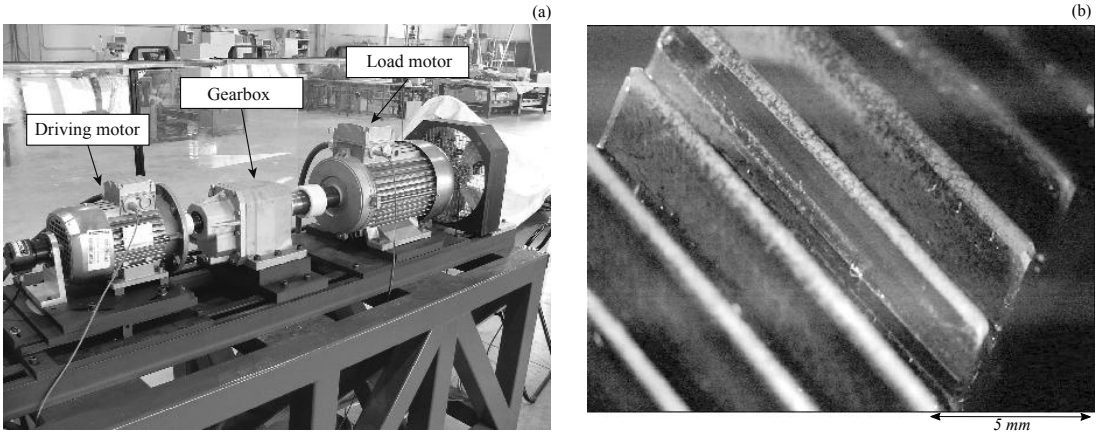

Figure 47: (a) Experimental setup of Case 1 and (b) particular of the spalled tooth.

38, gear II and gear III have 71 teeth and 12 teeth, respectively. The localized fault, i.e. gear tooth spall, has been artificially seeded on the 71 teeth gear, as shown in Figure 47(b). The test has been carried out in steady-state condition at 3600 rpm (referred to the input shaft of the first stage) and nominal load of 48.8 Nm.
The vibration signals in the radial direction have been collected by means of B&K piezoelectric accelerometer placed on the bearing support of the first stage pinion with sampling frequency 12.4 kHz for a total time length of 4 s while the input shaft speed has been measured by a tachometer sensor.
Figure 48 collects the TSA of the measured vibration signal as well as its spectrogram. The TSA has been performed in the angular domain taking into account 4260 points per revolution. The localized fault is easy to recognize on both the diagrams since it appears as a sudden increase of the signal amplitude in a slight rotation range. Thus, even if the presence of the gear tooth spall is obvious, these approaches are not able to identify which gear exhibits the fault.
As done before, three different EMD algorithms have been considered in order to verify the sensitivity of the final results with respect to the adopted EMD method. The signal decomposition has been performed using the same settings as reported in Section 3.4.2 and the results are collected in Figure 49. According to the PCC values collected in Figure 50, the representative signals of gear II and gear III have been computed, as reported in Figure 51.
From the visual inspection of the representative signals in Figure 51 it is not

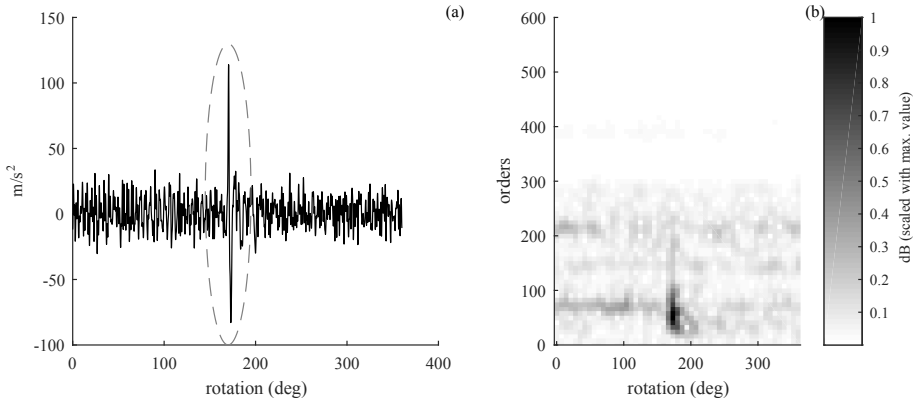

Figure 48: (a) TSA related to the intermediate shaft of Case 1 (the dashed circle highlights the impulsive signal component due to the damaged tooth engagement) and (b) its spectrogram (window length 300 samples and 75 % overlap).

hard to identify the faulty gear. Indeed, the waveform related to the 71 teeth wheel exhibits a large amplitude increase at 170 *deg* that is the effect of the engagement of the faulty tooth. However, Figure 51(d,e) shows a local change of the signal amplitude at about 170 *deg* that corresponds exactly to the angle position of the defect in gear II (clearly visible in Figure 51(a-c) and in the TSA in Figure 48(a)). The diagram related to the CEEMDAN in Figure 51(f) actually display a local change of amplitude too. However it should be noted that such a change occurs at about 250 *deg*, which is not in agreement of the fault position shown on the TSA of the signal.

Unfortunately, the visual inspection of the signal can be open to different interpretations, thus the fault identification is determined by the comparison of condition indicators. Table 8 highlights a significant difference between gear II and gear III, with a minimum percentage difference of 93.872. The proposed CIs (i.e. CPF and NSVP) are the most sensitive to the presence of an impulsive component in the vibration signature as demonstrated by the larger percentage difference with respect to the other traditional CIs.

Finally, in this first experimental case the proposed method is effective on the identification of the faulty gear. Moreover, CEEMDAN is the EMD algorithm that returns the best result taking into account the CIs values as well as the waveform of the representative signals.

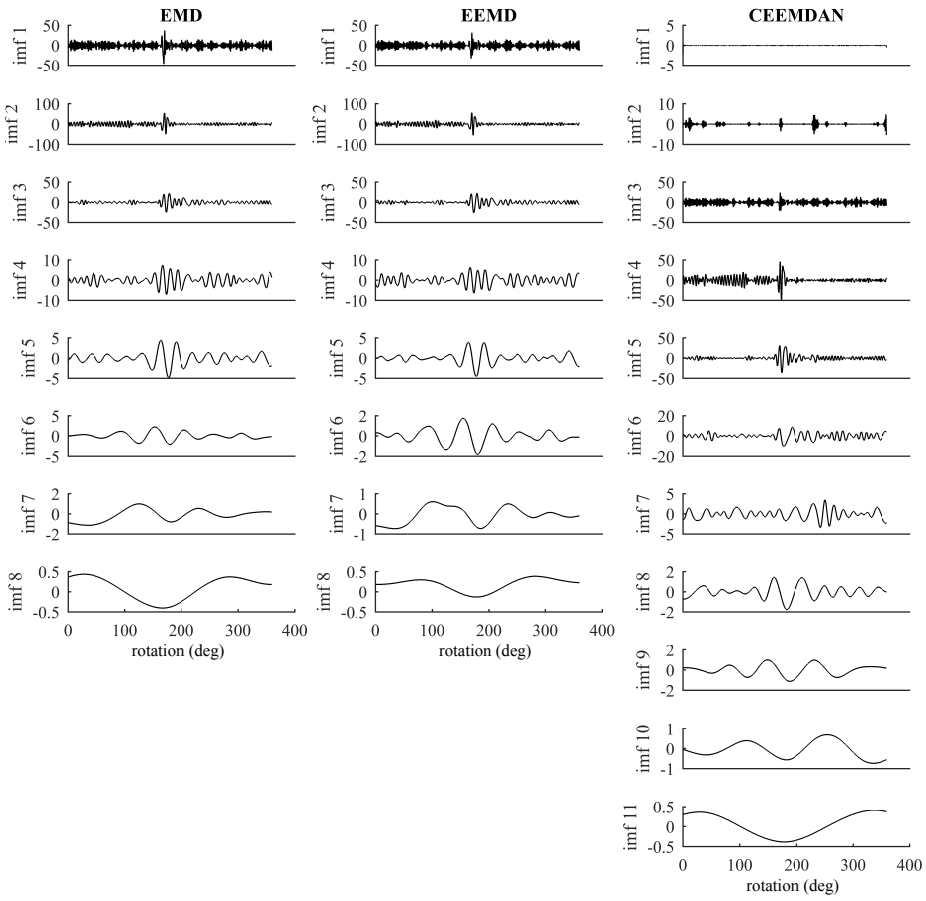

Figure 49: IMF sets of Case 1 obtained by using EMD, EEMD and CEEMDAN.

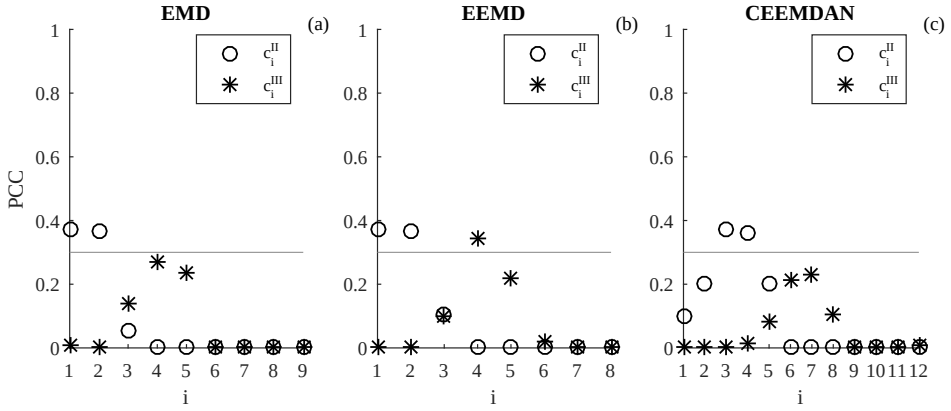

Figure 50: PCC values of Case 1 estimated taking into account (a) EMD, (b) EEMD and (c) CEEMDAN.

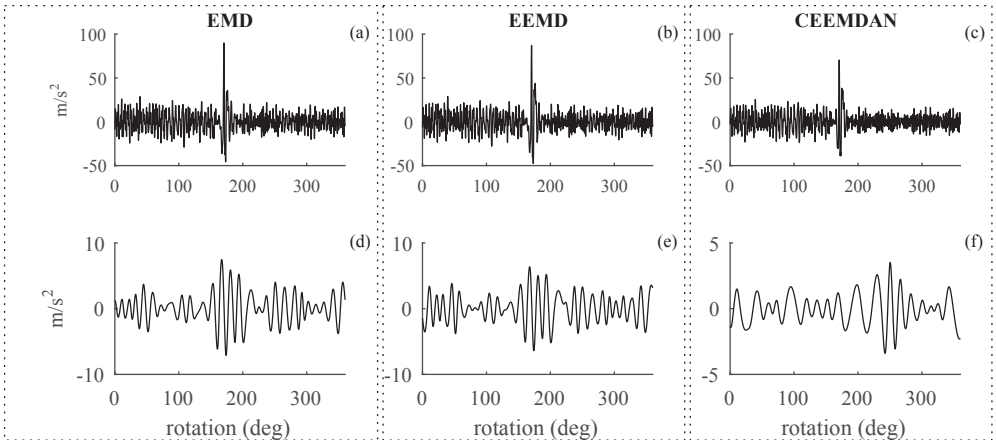

Figure 51: Representative signals of (a-c) gear II and (d-f) gear III for Case 1.

Table 8: CIs for the vibration signal of Case 1, with localized fault in gear II.

		kurtosis	CF	CPF	NSVP
EMD	Gear II (faulty)	10.220	8.785	4.437	1.395
	Gear III (healthy)	3.785	8.021	2.288	0.251
	Gear II vs Gear III (%)	170.043	142.209	93.872	457.089
EEMD	Gear II (faulty)	9.945	7.806	4.444	1.205
	Gear III (healthy)	2.962	2.931	1.942	0.309
	Gear II vs Gear III (%)	235.745	166.309	128.859	290.713
CEEMDAN	Gear II (faulty)	8.031	7.177	4.332	1.139
	Gear III (healthy)	3.141	3.036	2.141	0.112
	Gear II vs Gear III (%)	155.666	136.382	102.324	917.173

3.5.2 *Case 2*

The second case study concerns a more complex gearbox driven by an asynchronous motor. Figure 52 shows the experimental setup: the time domain vibration signal in the radial direction has been acquired by a mono-axial piezoelectric accelerometer (PCB 353B18) with a sample frequency of 25.6 kHz, while the tachometer signal has been simultaneously collected using a tachometer probe with zebra tape. The transmission exhibits an abnormal loudness due to a localized gear fault on the two-stage gearbox just after the input cardan shaft (see Figure 52(b)). The steady-state operational test has been carried out at 600 rpm at the input cardan shaft. Considering the gearbox layout in Figure 38, gear II has 92 teeth whereas gear III has 10 teeth.

Gear II presents a bump on a tooth flank caused by the handling during the surface hardening process. Such a faulty tooth flank engages only in the reverse motion and it has been verified by visual inspection. Furthermore, such a natural defect is clearly visible in the TSA signal performed on the intermediate shaft using 3680 samples per revolution, as reported in Figure 53(a). The presence of the fault is clear also on the spectrogram as well in Figure 53(b). As in Case 1, these signal processing techniques are not able to identify whether the defect is related to the gear of 92 or 10 teeth.

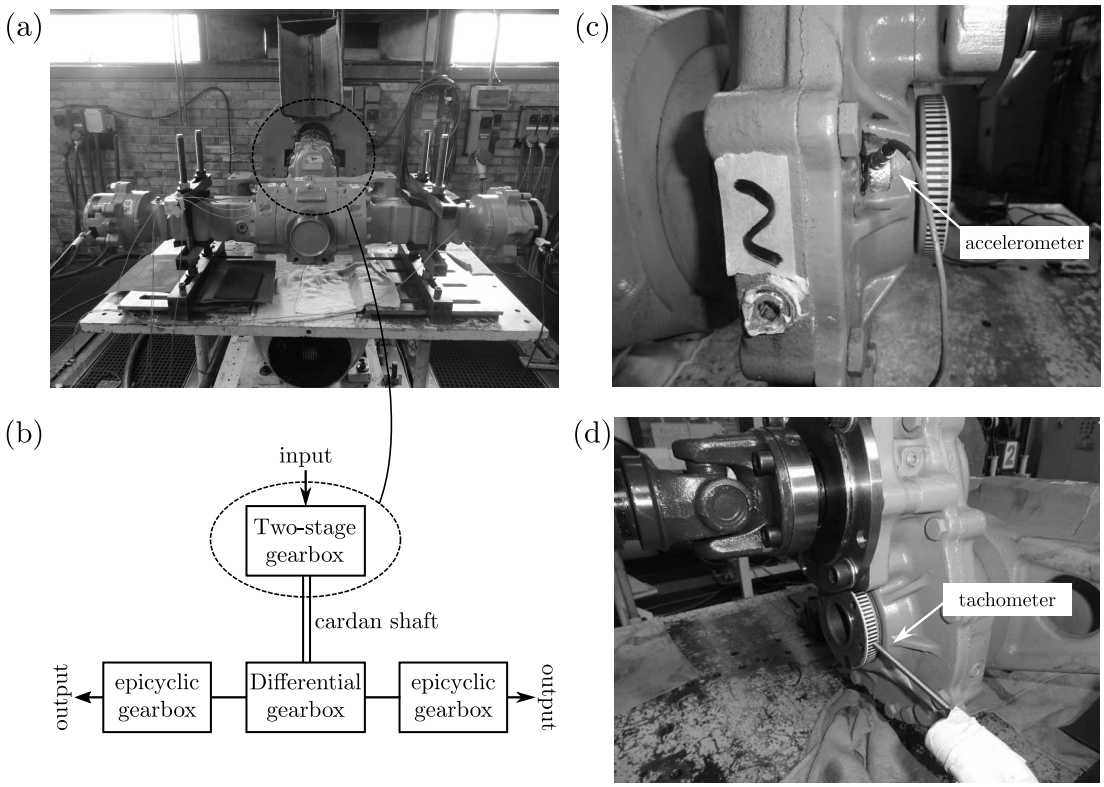

Figure 52: Experimental setup of Case 2: (a) transmission system on the test bench, (b) schematic of the transmission, (c) accelerometer and (d) tacho probe with zebra tape.

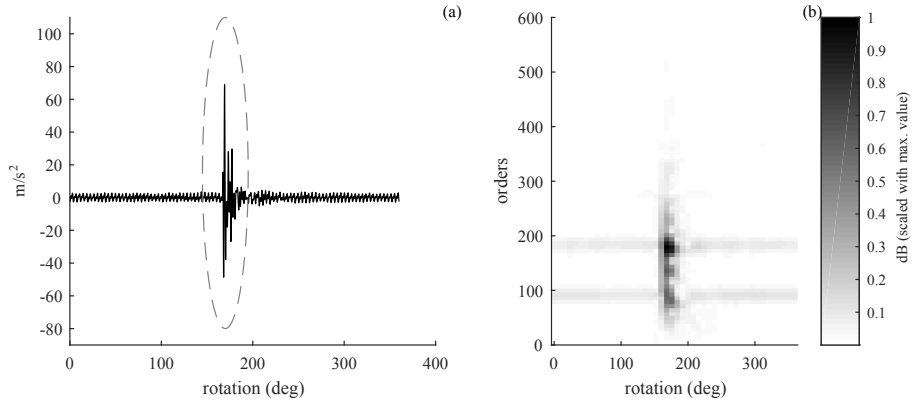

Figure 53: (a) TSA related to the intermediate shaft of Case 2 (the dashed circle highlights the impulsive signal component due to the damaged tooth engagement) and (b) its spectrogram (window length 300 samples and 75 % overlap).

Again, this experimental case study has been investigated by using the same modus operandi of Case 1. For the sake of completeness, signal decomposition results and the PCC values for the estimation of the representative signals are reported in Figure 54 and Figure 55, respectively. By going directly to the visual inspection of the representative signals (Figure 56), it can be noted that in this case the different EMD algorithms have a significant impact on the final results of the methods. From the physical standpoint, the representative signal related to gear II (see Figure 56(a-c)) correctly reflects the presence of the fault at about 170 *deg* due to the localized increase of the signal amplitude. However, this behavior is also present on the representative signal related to gear III computed with the EMD and the EEMD (see Figure 56(d-e)). On the other hand, the representative signals estimated with the CEEMDAN are easy to interpret since the signal related to gear III (Figure 56(f)) does not contain any remarkable local change of amplitude that can be attributed to a localized gear fault. Therefore, the only EMD algorithm that allows a clear visual interpretation of the signals is the CEEMDAN.

The remarks gathered by the visual inspection of the signal can be confirmed by analyzing the CIs collected in Table 9. In fact, the higher percentage differences between the faulty gear and the healthy one are achieved considering the CEEMDAN. Furthermore, it should be note that the results obtained with

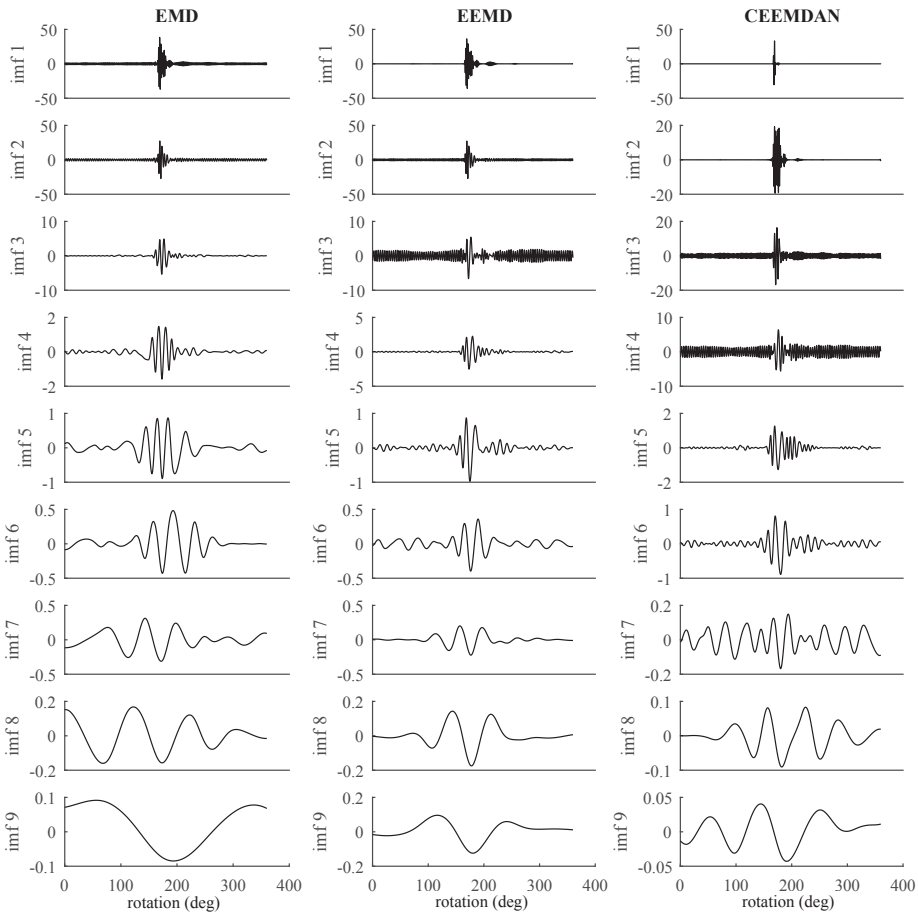

Figure 54: IMF sets of Case 2 obtained by using EMD, EEMD and CEEMDAN.

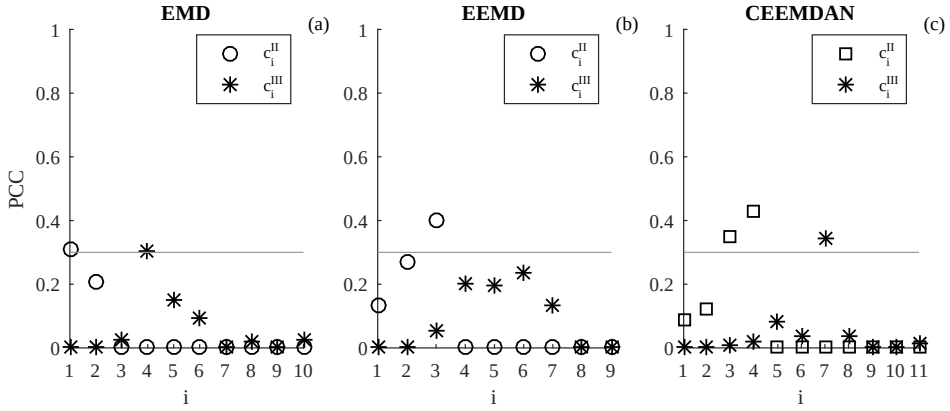

Figure 55: PCC values of Case 2 estimated taking into account (a) EMD, (b) EEMD and (c) CEEMDAN.

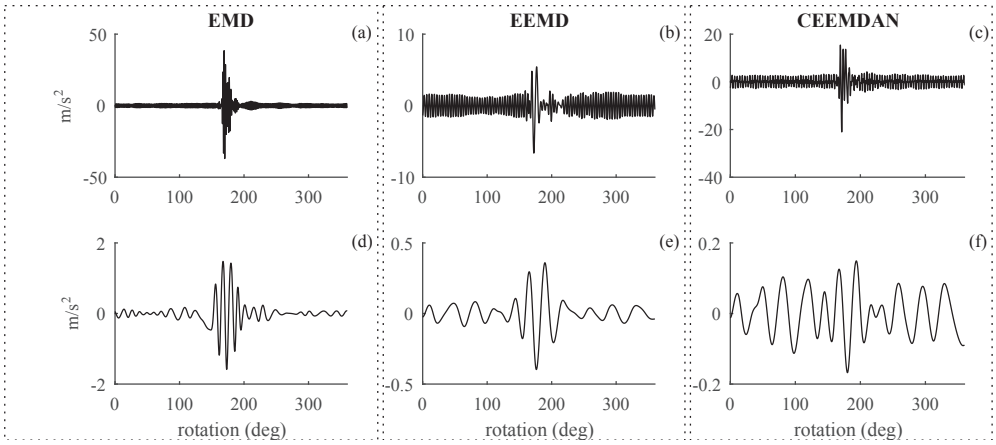

Figure 56: Representative signals of (a-c) gear II and (d-f) gear III for Case 2.

Table 9: CIs for the vibration signal of Case 2, with localized fault in gear II.

		kurtosis	CF	CPF	NSVP
EMD	Gear II (faulty)	48.803	10.910	13.704	0.085
	Gear III (healthy)	12.182	4.979	4.317	0.089
	Gear II vs Gear III (%)	300.604	119.140	217.457	−5.017
EEMD	Gear II (faulty)	6.100	5.304	3.694	0.064
	Gear III (healthy)	7.526	4.072	2.805	0.010
	Gear II vs Gear III (%)	−18.950	30.240	31.677	541.743
CEEMDAN	Gear II (faulty)	19.974	8.444	7.079	0.476
	Gear III (healthy)	2.455	2.712	1.549	0.013
	Gear II vs Gear III (%)	713.512	210.441	357.026	3696.969

the EEMD are not satisfying since the percentage difference are low for the CF and CPF while the kurtosis completely fails on the identification of the faulty gear.
Although this experimental case has been more difficult to handle than the first one, the methodology has provided a correct result when the CEEMDAN is performed. The use of several CIs allows for defining an objective criterion in order to define which gear is faulty, reducing the error due to the user interpretation.

3.6 SUMMARIZING COMMENTS

This chapter has focused on developing a strategy for the identification of localized gear faults in intermediates stages of multi-stage gearboxes. The proposed methodology is constituted of three main ingredients: the TSA, the EMD and a selection criterion of meaningful modes. A comprehensive investigation of the proposed methodology is presented including three different EMD algorithms and a validation with simulated signals and two experimental cases: the first one regards a vibration signal acquired on a dedicated test bench, the second one regards a vibration signal acquired in an industrial context. Moreover, two novel indicators based on the signal energy released within a gear pitch have been heuristically advanced.

On the basis of this activity, the following achievements can be listed:

- a methodology for the identification of localized gear faults in intermediates stages of multi-stage gearboxes has been developed;
- the most effective EMD algorithm turned out to be the CEEMDAN;
- the proposed methodology has been validated using simulated signals and real ones;
- in this application, the new metrics (i.e. CPF and NSVP) emerged to be valid alternatives to the kurtosis.

In this research activity the main original aspect resides on the proposed methodology. De facto, it represents a first attempt to give a solution about the identification of localized gear faults in intermediate stages of multi-stage gearboxes. Moreover, as mentioned in Section 3.1.2, a limited number of works can be found about CEEMDAN. Hence, this work presents another application of CEEMDAN for gear fault diagnosis aiming to extend the comprehension of limits and advantages of such a method.

4

FINAL REMARKS

This thesis has been focused on the impulsive fault identification in rotating machines by using BD algorithms and EMD algorithms in two different but complementary contexts.

Chapter 2 has been devoted to the development of a BD method based on the generalized Rayleigh quotient and solved by means of an iterative eigenvalue decomposition algorithm. A novel second-order cyclostationary criterion, called CYCBD, has been proposed and compared with other BD methods taking into account simulated and real vibration signals.

Considering real signals, the effectiveness of CYCBD has been investigated and discussed, both in qualitative and quantitative terms, in comparison with other BD methods proposed in the literature, first considering the gear tooth spall identification by means of a dedicated experimental campaign. This comparison has led to design a diagnostic procedure based on the proposed cyclostationary criterion for gear tooth spalling in gearboxes operating at constant regimes (or accounting small speed fluctuations). The main advantage of this method is that it requires a limited user interaction by exploiting an indicator based on the relative value of the maximized criterion between the reference condition (healthy) and the current condition. The method robustness has been further demonstrated by means of an extended sensitivity analysis taking into account the effect of the FIR filter length on different critical parameters of the algorithm.

Moreover, the proposed BD method has been applied also for the bearing fault identification using a run-to-failure dataset achieving satisfactory results. In this case, CYCBD provides excellent diagnostic performances with respect to the other BD algorithms in terms of early fault detection and identification.

All the obtained results highlight that the maximized ICS_2 final value can be considered as a robust fault indicator. Specifically, the experimental results, according to the simulated ones, demonstrated the superiority of the proposed criterion dealing with cyclostationary signals in two different experimental cases. In particular, CYCBD overcomes MOMEDA dealing with cyclostationary sources since MOMEDA is based on a criterion sensitive to periodic sources. Concurrently, the cyclostationary criterion used in CYCBD, i.e. ICS_2, appears more consistent with respect to the criterion used in MCKD, namely the correlated kurtosis. CYCBD proved to be effective also in the case of non-constant regime, which represents an open issue until now. CYCBDang has highlighted good performances dealing with vibration signals in variable speed conditions. In such circumstances, MOMEDA and MCKD do not give satisfactory results since they have been designed only for the extraction of equispaced impulse trains.

The main aspect of novelty of this research activity is the formulation of a BD criterion based on second-order cyclostationary maximization by means of a generalized Rayleigh quotient. In this work, the cyclostationary framework in BD algorithms has been explicitly investigated for the first time in rotating machine diagnosis applications from different standpoints. In fact, MCKD is a cyclostationary criterion already presented in the work of McDonald et al. [39] but, de facto, there is no explicit mention of cyclostationarity in that work. A complete study is presented providing the analytical formulation, an extended numerical investigation and two different experimental validations. CYCBD proved to be more consistent and effective for the extraction of cyclostationary sources, also considering the MCKD that is based on a cyclostationary criterion as well. Moreover, the use of a time/angle formulation is another original aspect since it allows for processing vibration signals of machines operating at variable regimes.

Chapter 3 is devoted on the development and validation of a methodology being able to identify localized gear faults occurring in a gear mounted on the intermediate shaft of a multistage gearbox. The goal is to overcome the limit of traditional signal processing techniques that detect just the stage of the faulty gear. For this purpose, a EMD-based methodology has been presented for the local gear fault diagnosis, proposing also two new condition indicators based on the RMS values estimated on the circular pitch rather than the entire vibration signal.

In order to test both reliability and robustness of the methodology, simulated signals and two different real case studies have been analyzed by means of three different EMD algorithms. The first experimental case address a two-stage gearbox having an artificial gear tooth fault whereas the second one concerns a transmission system with a natural defect. The methodology successfully identifies the faulty gear in both the experimental tests, especially when the CEEMDAN is performed. On the basis of this results, the CEEMDAN is the most effective signal decomposition technique, since it returns the clearest results from both the qualitative and quantitative standpoints. Moreover, the proposed CIs - in particular the NSVP - are very sensitive to the presence of a localized change of the vibration signature, simplifying the identification of the faulty gear. On these grounds, this method can be considered reliable on the identification of a faulty gear when the fault occurs in a shaft with multiple gears. Eventually, this diagnosis method is particularly suitable for industrial application since it needs a very limited user interaction.
In this second research activity, the primary original aspect resides on the proposed methodology itself. In fact, as the author is aware, it represents a first attempt to give a solution about the identification of the faulty gear (and not just the faulty stage!) in intermediate stages of multi-stage gearboxes. Moreover, since a very limited number of works are available in the literature about CEEMDAN, this research reports an application of CEEMDAN for gear fault diagnosis aiming to clarify limits and advantages of this method.
This thesis provides also some suggestions for future research works. Regarding the proposed BD algorithm, further criteria could be developed, perhaps considering a different way to maximize the cyclostationarity. Moreover, deeper investigations can be conducted about the effectiveness of CYCBD considering different kind of fault types and regimes. Finally, the method proposed in Chapter 3 is based on EMD algorithms that cannot be investigated from the analytical standpoint. However, a possible idea is to revisit the proposed method using a recent transform, called synchrosqueezed wavelet transforms [116], that decomposes signals in a similar fashion with respect of EMD algorithms but is based on a consistent theoretical foundation.

A

APPENDIX: PROOF OF EQUATIONS

A.1 RELATIONSHIP BETWEEN THE KURTOSIS AND THE DIFFERENTIAL ENTROPY

The differential entropy $\mathbb{H}$ [52] of a random variable x is defined as:

$$\mathbb{H} = -\int f(x) \ln f(x) dx \tag{57}$$

where $f(x)$ is the probability density function (pdf) of x of mean μ and standard deviation σ . If x is zero-mean and of unit variance, the truncated version of the Gram-Charlier expansion of $f(x)$ is given by:

$$f(x) \approx \varphi\left(\frac{x-\mu}{\sigma}\right)\left[1 + \frac{\kappa_3}{3!\sigma^3} H_3\left(\frac{x-\mu}{\sigma}\right) + \frac{\kappa_4}{4!\sigma^4} H_4\left(\frac{x-\mu}{\sigma}\right)\right] \tag{58}$$

where

$$\varphi(u) = \frac{e^{\frac{-u^2}{2}}}{\sqrt{2\pi}} \tag{59}$$

H_m is the Chebyshev-Hermite polynomial of order m and κ_n refers to the cumulant of order n. For the sake of simplicity, the argument of H and φ are neglected hereafter. The expansion reported in Eq. (58) is valid under the hypothesis that $f(x)$ is close to a Gaussian pdf [117]. Eq. (58) can be further simplified if we assume that $f(x)$ is symmetric, which implies that κ_3 is nil.

On these grounds, considering the Taylor's expansion $\ln(1+\psi) \approx \psi - \frac{\psi^2}{2}$, the substitution of Eq. (58) in Eq. (57) gives:

$$\begin{aligned} \mathbb{H} &\approx -\int \varphi \left(1 + \frac{\kappa_4 H_4}{4!}\right) \left[\ln \varphi + \frac{\kappa_4 H_4}{4!} - \frac{1}{2}\left(\frac{\kappa_4 H_4}{4!}\right)^2\right] dx \\ &\approx \int \varphi \ln \varphi + \varphi \frac{\kappa_4 H_4}{4!} - \frac{\varphi}{2}\left(\frac{\kappa_4 H_4}{4!}\right)^2 + \varphi \ln \varphi \frac{\kappa_4 H_4}{4!} + \varphi \left(\frac{\kappa_4 H_4}{4!}\right)^2 - \frac{\varphi}{2}\left(\frac{\kappa_4 H_4}{4!}\right)^3 dx. \end{aligned} \tag{60}$$

Recalling the hypothesis of x approximately Gaussian, this expression can be simplified by noting that:

- κ_4 is small and it's equivalent to the kurtosis if x is zero-mean with unit variance, viz:

$$\kappa_4 = \mathbb{E}\left[\left(\frac{x-\mu}{\sigma}\right)^4\right] = Kurt[x] \tag{61}$$

- the third-order term is infinitely smaller than the second-order terms under the hypothesis;
- the Chebyshev-Hermite polynomials have the property of being orthogonal [117] as follows:

$$\int \varphi(\frac{x-\mu}{\sigma}) H_i(x) H_j(x) dx = \delta_{ij} \tag{62}$$

  where δ_{ij} is the Kronecker delta;

- $\int \varphi \ln \varphi dx$ is a known quantity since it's the entropy of a Gaussian distribution, such as

$$\int \varphi \ln \varphi dx \approx \frac{1 + \ln 2\pi}{2}. \tag{63}$$

Thus, after some manipulation [118], Eq. (60) can be rewritten as:

$$\mathbb{H} \approx \frac{1 + \ln 2\pi}{2} - \frac{1}{48} Kurt[x]^2 \tag{64}$$

which finally gives the link between the kurtosis and the differential entropy.

A.2 OPTIMIZATION PROBLEMS BY USING THE GENERALIZED RAYLEIGH QUOTIENT

The generalized Rayleigh quotient can be used for defining optimization problems, i.e. maximizing or minimizing a given function. Let us define the following optimization problem:

$$\eta(\mathbf{h}, \mathbf{R}_{XWX}, \mathbf{R}_{XX}) = \frac{\mathbf{h}^T\mathbf{X}^T\mathbf{W}\mathbf{X}\mathbf{h}}{\mathbf{h}^T\mathbf{X}^T\mathbf{X}\mathbf{h}} = \frac{\mathbf{h}^T\mathbf{R}_{XWX}\mathbf{h}}{\mathbf{h}^T\mathbf{R}_{XX}\mathbf{h}} \tag{65}$$

where parameter η has to be maximized (or minimized) in function of $\mathbf{h}$, that is a vector of coefficients, while $\mathbf{X}$, $\mathbf{W}$, $\mathbf{R}_{XWX}$ and $\mathbf{R}_{XX}$ are real matrices. This ratio, namely $\eta(\mathbf{h}, \mathbf{R}_{XWX}, \mathbf{R}_{XX})$, is also known as generalized Rayleigh Quotient [119]. Note that this mathematical treatment can be extended in the complex field by substituting transpose matrices with Hermitian matrices. For the sake of conciseness, $\eta(\mathbf{h}, \mathbf{R}_{XWX}, \mathbf{R}_{XX})$ will be called just η implying its dependencies. A further consideration is that assuming $\mathbf{X}$ is a Toeplitz matrix and $\mathbf{W}$ is a diagonal matrix, thus $\mathbf{R}_{XWX}$ and $\mathbf{R}_{XX}$ must be symmetric [53].
Since the problem is to find the critical points of the function reported in Equation (65), the solution can be computed through the Lagrange multipliers method to a canonical Rayleigh Quotient. So, in order to write η in the canonical form, some variable substitutions have to be made. The goal now is to reduce **Rxx** to a identity matrix, hence substituting

$$\mathbf{R}_{XX} = \mathbf{D}^{-1}\mathbf{D} \tag{66}$$

in Equation (65), we obtain

$$\eta = \frac{\mathbf{h}^T\mathbf{X}^T\mathbf{W}\mathbf{X}\mathbf{h}}{\mathbf{h}^T\mathbf{D}^{-1}\mathbf{D}\mathbf{h}}. \tag{67}$$

At this point, given the following equations

$$\mathbf{v} = \mathbf{D}\mathbf{h} \tag{68}$$

$$\mathbf{C} = \mathbf{D}^{-T}\mathbf{R}_{XWX}\mathbf{D}^{-1} \tag{69}$$

the Rayleigh quotient in its canonical is achieved by substituting such equations in Equation (67):

$$\eta = \frac{\mathbf{v}^T \mathbf{C}\mathbf{v}}{\mathbf{v}^T \mathbf{v}}. \tag{70}$$

Critical points of Equation (70) can be determined using the method of Lagrangian multipliers. In other words, the numerator has to be maximized keeping constant the denominator, such as:

$$max(\mathbf{v}^T \mathbf{C}\mathbf{v}) \quad with \quad \mathbf{v}^T \mathbf{v} = 1. \tag{71}$$

Thus, the Lagrangian is defined as:

$$\mathcal{L}(\mathbf{v}) = \mathbf{v}^T \mathbf{C}\mathbf{v} + \lambda(\mathbf{v}^T \mathbf{v} - 1) \tag{72}$$

Substituting Equations (66), (68) and (69) into Equation (72) returns:

$$\mathcal{L}(\mathbf{h}) = \mathbf{h}^T \mathbf{R}_{XWX} \mathbf{h} - \lambda(\mathbf{h}^T \mathbf{R}_{XX} \mathbf{h} - 1). \tag{73}$$

Thus, taking to zero the derivative of Equation (73)

$$\nabla \mathcal{L}(\mathbf{h}, \lambda) = 2(\mathbf{R}_{XWX} - \lambda \mathbf{R}_{XX})\mathbf{h} = 0 \tag{74}$$

the generalized eigenvalue problem with respect to eigenvalues λ and eigenvectors $\mathbf{h}$ can be obtained

$$\mathbf{R}_{XWX} \mathbf{h} = \mathbf{R}_{XX} \mathbf{h} \lambda. \tag{75}$$

According to the min-max theorem , the maximum eigenvalue represents also the maximum value of η and the related eigenvector h represents, in our BD problem, the filter coefficient associated to maximum η. Note that, by definition, $\mathbf{R}_{XWX}$ and $\mathbf{R}_{XX}$ are Hermitian matrices. For real matrices and vectors the Hermitian property is met if and only if the symmetry property is met, as in this case. Moreover, $\mathbf{R}_{XX}$ is also semi-positive definite matrix since the product between a matrix and its transpose is a semi-positive definite matrix. Thus, $\mathbf{h}$ is a vector of real coefficients and λ and is a positive real scalar.
A more direct approach is to take the derivative of Equation (65) with respect to $\mathbf{h}$:

$$\frac{d\eta}{d\mathbf{h}} = \frac{2\mathbf{R}_{XWX}\mathbf{h}(\mathbf{h}^T \mathbf{R}_{XX}\mathbf{h}) - 2\mathbf{R}_{XX}\mathbf{h}(\mathbf{h}^T \mathbf{R}_{XWX}\mathbf{h})}{(\mathbf{h}^T \mathbf{R}_{XX}\mathbf{h})^2}. \tag{76}$$

Setting the first derivative of Equation (76) to zero returns:

$$\mathbf{R}_{XWX}\mathbf{h}(\mathbf{h}^T\mathbf{R}_{XX}\mathbf{h}) = \mathbf{R}_{XX}\mathbf{h}(\mathbf{h}^T\mathbf{R}_{XWX}\mathbf{h}) \tag{77}$$

which is equivalent to

$$\mathbf{R}_{XWX}\mathbf{h} = \mathbf{R}_{XX}\mathbf{h}\frac{(\mathbf{h}^T\mathbf{R}_{XWX}\mathbf{h})}{(\mathbf{h}^T\mathbf{R}_{XX}\mathbf{h})} = \eta\mathbf{R}_{XX}\mathbf{h} \tag{78}$$

This results means that solving this equation for a maximum (minimum) eigenvalue is equal to maximize (minimize) the Rayleigh quotient.

PAPERS CONCERNING THE PHD RESEARCH ACTIVITY

[1] M. Buzzoni, E. Mucchi, and G. Dalpiaz. "Analisi vibrazionale numerica e sperimentale di un trabatto per pasta alimentare." In: *Giornata di studio Ettore Funaioli*. Bologna, 2014, pp. 153–166.

[2] M. Buzzoni, E. Mucchi, and G. Dalpiaz. "Improvement of the vibro-acoustic behaviour of vibratory feeders for pasta by modelling and experimental techniques." In: *Internoise 2016*. Hamburg, 2016, pp. 4005–4013.

[3] M. Buzzoni, M. Battarra, E. Mucchi, and G. Dalpiaz. "Noise and vibration improvements in vibratory feeders by analytical models and experimental analysis." In: *Internoise 2017*. Honk Kong, 2017, pp. 6749–6759.

[4] M. Buzzoni, B. M., E. Mucchi, and G. Dalpiaz. "Motion analysis of a linear vibratory feeder: Dynamic modeling and experimental verification." In: *Mechanism and Machine Theory* 114 (2017), pp. 98–110. ISSN: 0094-114X. DOI: http://dx.doi.org/10.1016/j.mechmachtheory.2017.04.006.

[5] M. Buzzoni, E. Mucchi, and G. Dalpiaz. "Piston slap noise reduction in IC engines : design improvements by advanced signal processing techniques." In: *ISMA2016*. Leuven, 2016.

[6] M. Buzzoni, E. Mucchi, and G. Dalpiaz. "A CWT-based methodology for piston slap experimental characterization." In: *Mechanical Systems and Signal Processing* 86.April 2016 (2017), pp. 16–28. ISSN: 08883270. DOI: 10.1016/j.ymssp.2016.10.005.

[7] M Buzzoni, E Mucchi, G D'Elia, and G Dalpiaz. "Diagnosis of Localized Faults in Multistage Gearboxes: A Vibrational Approach by Means of Automatic EMD-Based Algorithm." In: *Shock and Vibration* 2017 (2017), pp. 1–22. ISSN: 1070-9622. DOI: 10.1155/2017/8345704. URL: https://www.hindawi.com/journals/sv/2017/8345704/.

[8] F. Castellani, M. Buzzoni, D. Astolfi, G. D. Elia, G. Dalpiaz, and L. Terzi. "Wind Turbine Loads Induced by Terrain and Wakes : An Experimental Study through Vibration Analysis and Computational Fluid Dynamics †." In: *Energies* 10.11 (2017), pp. 1–19. DOI: 10.3390/en10111839.

REFERENCES

[9] R. B. Randall. *Vibration-based Condition Monitoring*. John Wiley & Sons Ltd, 2011. ISBN: 978-0-470-74785-8.

[10] R. B. Randall. "A new method of modeling gear faults." In: *Trans. Asme J. Mech. Des.* 104.2 , Apr. 1982 (1982), pp. 259–267. ISSN: 10500472. DOI: 10.1115/1.3256334.

[11] J. Antoni and R. B. Randall. "Differential Diagnosis of Gear and Bearing Faults." In: *Journal of Vibration and Acoustics* 124.2 (2002), p. 165. DOI: 10.1115/1.1456906.

[12] W. D. Mark. "Analysis of the vibratory excitation of gear systems: Basic theory." In: *The Journal of the Acoustical Society of America* 63.5 (1978), p. 1409. ISSN: 00014966. DOI: 10.1121/1.381876.

[13] W. D. Mark, H. Lee, R. Patrick, and J. D. Coker. "A simple frequency-domain algorithm for early detection of damaged gear teeth." In: *Mechanical Systems and Signal Processing* 24.8 (2010), pp. 2807–2823. ISSN: 08883270. DOI: 10.1016/j.ymssp.2010.04.004. URL: http://dx.doi.org/10.1016/j.ymssp.2010.04.004.

[14] W. Wang. "Early Detection of Gear Tooth Cracking Using the Resonance Demodulation Technique." In: *Mechanical Systems and Signal Processing* 15.5 (2001), pp. 887–903. DOI: 10.1006/mssp.2001.1416.

[15] Z. Man, W. Wang, S. Khoo, and J. Yin. "Optimal sinusoidal modelling of gear mesh vibration signals for gear diagnosis and prognosis." In: *Mechanical Systems and Signal Processing* 33 (2012), pp. 256–274. ISSN: 08883270. DOI: 10.1016/j.ymssp.2012.07.004. URL: http://dx.doi.org/10.1016/j.ymssp.2012.07.004.

[16] P. McFadden and J. Smith. "Model for the vibration produced by a single point defect in a rolling element bearing." In: *Journal of Sound and Vibration* 96.1 (1984), pp. 69–82. ISSN: 0022460X. DOI: 10.1016/0022-460X(84)90595-9. URL: http://linkinghub.elsevier.com/retrieve/pii/0022460X84905959.

[17] R. B. Randall and J. Antoni. "Rolling element bearing diagnostics-A tutorial." In: *Mechanical Systems and Signal Processing* 25.2 (2011), pp. 485–520. DOI: 10.1016/j.ymssp.2010.07.017.

[18] J Antoni and R. B. Randall. "A Stochastic Model for Simulation and Diagnostics of Rolling Element Bearings With Localized Faults." In: *Journal of Vibration and Acoustics* 125.3 (2003), p. 282. ISSN: 07393717. DOI: 10.1115/1.1569940. URL: http://vibrationacoustics.asmedigitalcollection.asme.org/article.aspx?articleid=1470582.

[19] J. Antoni, F. Bonnardot, A. Raad, and M. El Badaoui. "Cyclostationary modelling of rotating machine vibration signals." In: *Mechanical Systems and Signal Processing* 18.6 (2004), pp. 1285–1314. DOI: 10.1016/S0888-3270(03)00088-8.

[20] C. Capdessus, M. Sidhamed, and J. Lacoume. "Cyclostationary Processes: Application in Gear Faults Early Diagnosis." In: *Mechanical Systems and Signal Processing* 14.3 (2000), pp. 371–385. ISSN: 08883270. DOI: 10.1006/mssp.1999.1260. URL: http://linkinghub.elsevier.com/retrieve/pii/S0888327099912608.

[21] S. Braun. "The synchronous (time domain) average revisited." In: *Mechanical Systems and Signal Processing* 25.4 (2011), pp. 1087–1102. DOI: 10.1016/j.ymssp.2010.07.016.

[22] V. Sharma and A. Parey. "Gear crack detection using modified TSA and proposed fault indicators for fluctuating speed conditions." In: *Measurement* 90 (Aug. 2016), pp. 560–575. ISSN: 02632241. DOI: 10.1016/j.measurement.2016.04.076.

[23] R. B. Randall. "A history of cepstrum analysis and its application to mechanical problems." In: *Mechanical Systems and Signal Processing* 97 (2017), pp. 3–19. ISSN: 08883270. DOI: 10.1016/j.ymssp.2016.12.026.

[24] P. D. McFadden. "Detecting Fatigue Cracks in Gears by Amplitude and Phase Demodulation of the Meshing Vibration." In: *Journal of vibration, acoustics, stress, and reliability in design* 108.2 (1986), pp. 165–170. ISSN: 07393717. DOI: 10.1115/1.3269317.

[25] G. Dalpiaz, A. Rivola, and R. Rubini. "Effectiveness and Sensitivity of Vibration Processing Techniques for Local Fault Detection in Gears." In: *Mechanical Systems and Signal Processing* 14.3 (2000), pp. 387–412. DOI: 10.1006/mssp.1999.1294.

[26] R. Ricci and P. Pennacchi. "Diagnostics of gear faults based on EMD and automatic selection of intrinsic mode functions." In: *Mechanical Systems and Signal Processing* 25.3 (2011), pp. 821–838. ISSN: 08883270. DOI: 10.1016/j.ymssp.2010.10.002. URL: http://www.sciencedirect.com/science/article/pii/S0888327010003201.

[27] P. D. McFadden. "Examination of a technique for the early detection of failure in gears by signal processing of the time domain average of the meshing vibration." In: *Mechanical Systems and Signal Processing* 1.2 (1987), pp. 173–183. ISSN: 10961216. DOI: 10.1016/0888-3270(87)90069-0.

[28] N. Sawalhi, R. B. Randall, and H. Endo. "The enhancement of fault detection and diagnosis in rolling element bearings using minimum entropy deconvolution combined with spectral kurtosis." In: *Mechanical Systems and Signal Processing* 21.6 (2007), pp. 2616–2633. DOI: 10.1016/j.ymssp.2006.12.002.

[29] W. Wang and A. K. Wong. "Autoregressive Model-Based Gear Fault Diagnosis." In: *Journal of Vibration and Acoustics* 124.2 (2002), p. 172.

[30] J. Antoni and R. B. Randall. "The spectral kurtosis: Application to the vibratory surveillance and diagnostics of rotating machines." In: *Mechanical Systems and Signal Processing* 20.2 (2006), pp. 308–331. ISSN: 08883270. DOI: 10.1016/j.ymssp.2004.09.002.

[31] P. McFadden and J. Smith. "Vibration monitoring of rolling element bearings by the high-frequency resonance technique — a review." In: *Tribology International* 17.1 (Feb. 1984), pp. 3–10. ISSN: 0301679X. DOI: 10.1016/0301-679X(84)90076-8.

[32] J. Antoni. "Cyclic spectral analysis of rolling-element bearing signals: Facts and fictions." In: *Journal of Sound and Vibration* 304.3-5 (2007), pp. 497–529. ISSN: 0022460X. DOI: 10.1016/j.jsv.2007.02.029.

[33] J. Antoni, G. Xin, and N. Hamzaoui. "Fast computation of the spectral correlation." In: *Mechanical Systems and Signal Processing* 92 (2017), pp. 248–277. DOI: 10.1016/j.ymssp.2017.01.011.

[34] J. Antoni. "Cyclostationarity by examples." In: *Mechanical Systems and Signal Processing* 23.4 (2009), pp. 987–1036. DOI: 10.1016/j.ymssp.2008.10.010.

[35] A. Raad, J. Antoni, and M. Sidahmed. "Indicators of cyclostationarity: Theory and application to gear fault monitoring." In: *Mechanical Systems and Signal Processing* 22.3 (2008), pp. 574–587. DOI: 10.1016/j.ymssp.2007.09.011.

[36] R. Randall, J. Antoni, and S. Chobosaard. "The relationship between spectral correlation and envelope analysis in the diagnostics of bearing faults and other cyclostationary machine signals." In: *Mechanical Systems and Signal Processing* 15.5 (2001), pp. 945–962. ISSN: 08883270. DOI: 10.1006/mssp.2001.1415.

[37] P. Borghesani, P. Pennacchi, and S. Chatterton. "The relationship between kurtosis- and envelope-based indexes for the diagnostic of rolling element bearings." In: *Mechanical Systems and Signal Processing* 43.1-2 (2014), pp. 25–43. ISSN: 08883270. DOI: 10.1016/j.ymssp.2013.10.007.

[38] H. Endo and R. Randall. "Enhancement of autoregressive model based gear tooth fault detection technique by the use of minimum entropy deconvolution filter." In: *Mechanical Systems and Signal Processing* 21.2 (2007), pp. 906–919. DOI: 10.1016/j.ymssp.2006.02.005.

[39] G. L. McDonald, Q. Zhao, and M. J. Zuo. "Maximum correlated Kurtosis deconvolution and application on gear tooth chip fault detection." In: *Mechanical Systems and Signal Processing* 33 (Nov. 2012), pp. 237–255. DOI: 10.1016/j.ymssp.2012.06.010.

[40] G. L. McDonald and Q. Zhao. "Multipoint Optimal Minimum Entropy Deconvolution and Convolution Fix: Application to vibration fault detection." In: *Mechanical Systems and Signal Processing* 82 (2017), pp. 461–477. DOI: 10.1016/j.ymssp.2016.05.036.

[41] R. A. Wiggins. "Minimum entropy deconvolution." In: *Geoexploration* 16.1-2 (1978), pp. 21–35. ISSN: 00167142. DOI: 10.1016/0016-7142(78)90005-4.

[42] C. A. Cabrelli. "Minimum entropy deconvolution and simplicity: A noniterative algorithm." In: *Geophysics* 50.3 (1985), pp. 394–413. DOI: 10.1190/1.1441919.

[43] H. Endo, R. B. Randall, and C. Gosselin. "Differential diagnosis of spall vs. cracks in the gear tooth fillet region: Experimental validation." In: *Mechanical Systems and Signal Processing* 23.3 (2009), pp. 636–651. DOI: 10.1016/j.ymssp.2008.08.015.

[44] D. He, X. Wang, S. Li, J. Lin, and M. Zhao. "Identification of multiple faults in rotating machinery based on minimum entropy deconvolution combined with spectral kurtosis." In: *Mechanical Systems and Signal Processing* 81 (2016), pp. 235–249. DOI: 10.1016/j.ymssp.2016.03.016.

[45] J.-Y. Lee and A. Nandi. "Blind Deconvolution of Impacting Signals Using Higher-Order Statistics." In: *Mechanical systems and signal processing* 12.2 (1998), pp. 357–371. DOI: 10.1006/mssp.1997.0144.

[46] J.-Y. Lee and A. Nandi. "Extraction of Impacting Signals Using Blind Deconvolution." In: *Journal of Sound and Vibration* 232.5 (2000), pp. 945–962. DOI: 10.1006/jsvi.1999.2778.

[47] J. Obuchowski, R. Zimroz, and A. Wyłomańska. "Blind equalization using combined skewness-kurtosis criterion for gearbox vibration enhancement." In: *Measurement: Journal of the International Measurement Confederation* 88 (2016), pp. 34–44. DOI: 10.1016/j.measurement.2016.03.034.

[48] Y. Miao, M. Zhao, J. Lin, and Y. Lei. "Application of an improved maximum correlated kurtosis deconvolution method for fault diagnosis of rolling element bearings." In: *Mechanical Systems and Signal Processing* 92 (2017), pp. 173–195. DOI: 10.1016/j.ymssp.2017.01.033.

[49] B. Jelonnek, D. Boss, and K.-D. Kammeyer. "Generalized eigenvector algorithm for blind equalization." In: *Signal Processing* 61.3 (1997), pp. 237–264. DOI: 10.1016/S0165-1684(97)00108-4.

[50] S. Zazo and J. Paez-Borrallo. "A new multichannel blind equalization criterium based on a generalized Rayleigh quotient." In: *1997 IEEE International Conference on Acoustics, Speech, and Signal Processing*. Vol. 5. IEEE Comput. Soc. Press, pp. 3457–3460. ISBN: 0-8186-7919-0. DOI: 10.1109/ICASSP.1997.604608. URL: http://ieeexplore.ieee.org/document/604608/.

[51] R. Ricci, P. Borghesani, S. Chatterton, and P. Pennacchi. "The Combination of Empirical Mode Decomposition and Minimum Entropy Deconvolution for Roller Bearing Diagnostics in Non-Stationary Operation." In: *Volume 1: 24th Conference on Mechanical Vibration and Noise, Parts A and B*. ASME, Aug. 2012, p. 723. DOI: 10.1115/DETC2012-71012.

[52] C. M. Bishop. *Pattern Recognition and Machine Learning (Information Science and Statistics)*. Secaucus, NJ, USA: Springer-Verlag New York, Inc., 2006. ISBN: 0387310738.

[53] B. N. Parlett. *The symmetric eigenvalue problem*. Society for Industrial and Applied Mathematics, 1987. ISBN: 9780898714029.

[54] J.-L. Lacoume, P.-O. Amblard, and P. Comon. *Statistiques d'ordre supérieur pour le traitement du signal*. MASSON, 1997.

[55] B. Kilundu, X. Chiementin, J. Duez, and D. Mba. "Cyclostationarity of Acoustic Emissions (AE) for monitoring bearing defects." In: *Mechanical Systems and Signal Processing* 25.6 (2011), pp. 2061–2072. DOI: 10.1016/j.ymssp.2011.01.020.

[56] S. Delvecchio, G. D'Elia, and G. Dalpiaz. "On the use of cyclostationary indicators in IC engine quality control by cold tests." In: *Mechanical Systems and Signal Processing* 60-61 (2015), pp. 208–228. DOI: 10.1016/j.ymssp.2014.09.015.

[57] P. Borghesani, P. Pennacchi, S. Chatterton, and R. Ricci. "The velocity synchronous discrete Fourier transform for order tracking in the field of rotating machinery." In: *Mechanical Systems and Signal Processing* 44.1-2 (2014), pp. 118–133. DOI: 10.1016/j.ymssp.2013.03.026.

[58] R. B. Randall, J. Antoni, and K Gryllias. "Alternatives to kurtosis as an indicator of rolling element bearing faults." In: *ISMA2016 International conference on noise and vibration engineering*. Leuven, Belgium, 2016.

[59] J. P. Den Hartog. *Mechanical Vibrations*. Dover Pubns, 2003. ISBN: 978-0486647852.

[60] G. Dalpiaz, G. D'Elia, and S. Delvecchio. "Design of a test bench for the vibro-acoustical analysis and diagnostics of rotating machines." In: *The Second World Congress on Engineering Asset Management & The Fourth International Conference on Condition Monitoring*. Harrogate, UK, 2007, pp. 777–792.

[61] G. D'Elia. "Fault detection in rotating machines by vibration signal processing techniques." PhD Thesis. Alma Mater Studiorum Università di Bologna, 2008. DOI: 10.6092/unibo/amsdottorato/952.

[62] G. D'Elia, S. Delvecchio, and G. Dalpiaz. "Gear spall detection by non-stationary vibration signal analysis." In: *ISMA2008 International Conference on Noise and Vibration Engineering*. Leuven, Belgium, 2008, pp. 777–792. ISBN: 9781615671915.

[63] J Lee, H Qiu, G Yu, and J Lin. *Rexnord Technical Services, 'Bearing Data Set', IMS, University of Cincinnati, NASA Ames Prognostics Data Repository*. 2007. URL: http://ti.arc.nasa.gov/project/prognostic-data-repository.

[64] W. Gousseau, J. Antoni, F. Girardin, and J. Griffaton. "Analysis of the rolling element bearing data set of the Centre for Intelligent Maintenance Systems at The University of Cincinnati." In: *the Thirteenth International Conference on Condition Monitoring and Machinery Failure Prevention Technologies*. Paris, FR, 2016.

[65] J. Ben Ali, B. Chebel-Morello, L. Saidi, S. Malinowski, and F. Fnaiech. "Accurate bearing remaining useful life prediction based on Weibull distribution and artificial neural network." In: *Mechanical Systems and Signal Processing* 56 (2015), pp. 150–172. ISSN: 10961216. DOI: 10.1016/j.ymssp.2014.10.014.

[66] B. Assaad, M. Eltabach, and J. Antoni. "Vibration based condition monitoring of a multistage epicyclic gearbox in lifting cranes." In: *Mechanical Systems and Signal Processing* 42.1-2 (2014), pp. 351–367. ISSN: 08883270. DOI: 10.1016/j.ymssp.2013.06.032. URL: http://dx.doi.org/10.1016/j.ymssp.2013.06.032.

[67] D. Baillie and J. Mathew. "A Comparison of Autoregressive Modeling Techniques for Fault Diagnosis of Rolling Element Bearings." In: *Mechanical Systems and Signal Processing* 10.1 (1996), pp. 1–17. ISSN: 08883270. DOI: 10.1006/mssp.1996.0001. URL: http://linkinghub.elsevier.com/retrieve/pii/S0888327096900011.

[68] H. Qiu, J. Lee, J. Lin, and G. Yu. "Wavelet filter-based weak signature detection method and its application on rolling element bearing prognostics." In: *Journal of Sound and Vibration* 289.4-5 (2006), pp. 1066–1090. ISSN: 10958568. DOI: 10.1016/j.jsv.2005.03.007.

[69] M. Malagó, E. Mucchi, and G. Dalpiaz. "Fault detection in heavy duty wheels by advanced vibration processing techniques and lumped parameter modeling." In: *Mechanical Systems and Signal Processing* 70-71 (2016), pp. 141–160. ISSN: 08883270. DOI: 10.1016/j.ymssp.2015.09.043.

[70] J. W. Tukey. *Exploratory data analysis*. Pearson, 1977. ISBN: 978-0201076165.

[71] T. Williams, X. Ribadeneira, S. Billington, and T. Kurfess. "Rolling Element Bearing Diagnostics in Run-To-Failure Lifetime Testing." In: *Mechanical Systems and Signal Processing* 15.5 (2001), pp. 979–993. ISSN: 08883270. DOI: 10.1006/mssp.2001.1418.

[72] S. P. Radzevich. *Dudley's Handbook of Practical Gear Design and Manufacture*. 2nd ed. CRC Press, 2012. ISBN: 9781439866023. DOI: 10.1201/b11842-6.

[73] W. A. Gardner. *Cyclostationarity in communications and signal processing*. IEEE Press, 1994. ISBN: 0-7803-1023-3.

[74] J. Antoni and D. Hanson. "Detection of surface ships from interception of cyclostationary signature with the cyclic modulation coherence." In: *IEEE Journal of Oceanic Engineering* 37.3 (2012), pp. 478–493. ISSN: 03649059. DOI: 10.1109/JOE.2012.2195852.

[75] G. D. Zivanovic and W. A. Gardner. "Degrees of cyclostationarity and their application to signal detection and estimation." In: *Signal Processing* 22.3 (1991), pp. 287–297. ISSN: 01651684. DOI: https://doi.org/10.1016/0165-1684(91)90016-C.

[76] W. Wang and P. McFadden. "Early detection of gear failure by vibration analysis i. calculation of the time-frequency distribution." In: *Mechanical Systems and Signal Processing* 7.3 (1993), pp. 193–203. ISSN: 08883270. DOI: 10.1006/mssp.1993.1008.

[77] H. Oehlmann, D. Brie, M. Tomczak, and A. Richard. "a Method for Analysing Gearbox Faults Using Time–Frequency Representations." In: *Mechanical Systems and Signal Processing* 11.4 (1997), pp. 529–545. ISSN: 08883270. DOI: 10.1006/mssp.1996.0093.

[78] B. P. Bogert, M. J. R. Healy, and J. W. Tukey. "The Quefrency Alanysis of Time Series for Echoes: Cepstrum, Pseudo Autocovariance, Cross-Cepstrum and Saphe Cracking." In: *Symposium on Time Series Analysis*. Ed. by Wiley. New York, 1963, pp. 209–243.

[79] M. E. Badaoui, F. Guillet, and J. Daniere. "New applications of the real cepstrum to gear signals, including definition of a robust fault indicator." In: *Mechanical Systems and Signal Processing* 18.5 (2004), pp. 1031–1046. ISSN: 08883270. DOI: https://doi.org/10.1016/j.ymssp.2004.01.005.

[80] T. Barszcz and R. B. Randall. "Application of spectral kurtosis for detection of a tooth crack in the planetary gear of a wind turbine." In: *Mechanical Systems and Signal Processing* 23.4 (2009), pp. 1352–1365. DOI: 10.1016/j.ymssp.2008.07.019.

[81] J. Antoni. "Fast computation of the kurtogram for the detection of transient faults." In: *Mechanical Systems and Signal Processing* 21.1 (2007), pp. 108–124. ISSN: 08883270. DOI: 10.1016/j.ymssp.2005.12.002.

[82] J. Antoni. "The spectral kurtosis: a useful tool for characterising non-stationary signals." In: *Mechanical Systems and Signal Processing* 20.2 (2006), pp. 282–307. ISSN: 08883270. DOI: 10.1016/j.ymssp.2004.09.001.

[83] N. Huang, Z Shen, S. Long, M. Wu, H. Shih, Q Zheng, N. Yen, C. Tung, and H. Liu. "The empirical mode decomposition and the Hilbert spectrum for nonlinear and non-stationary time series analysis." In: *Proceedings of the Royal Society A: Mathematical, Physical and Engineering Sciences* 454.1971 (1998), pp. 995, 903. DOI: 10.1098/rspa.1998.0193.

[84] B. Boashash. *Time frequency signal analysis and processing*. 1st ed. Elsevier Ltd., 2003. ISBN: 0-08-044335-4.

[85] N. E. Huang. "Introduction to the Hilbert–Huang transform and its related mathematical problems." In: *Hilbert-Huang Transform and Its Applications*. Vol. 5. 2005, pp. 1–26. ISBN: 9812563768. DOI: 10.1142/9789812703347_0001.

[86] G. Rilling and P. Flandrin. "One or Two Frequencies? The Empirical Mode Decomposition Answers." In: *IEEE Transactions on Signal Processing* 56.1 (2008), pp. 85–95. DOI: 10.1109/TSP.2007.906771.

[87] P. Flandrin, G. Rilling, and P. Goncalves. "Empirical Mode Decomposition as a Filter Bank." In: *IEEE Signal Processing Letters* 11.2 (2004), pp. 112–114. DOI: 10.1109/LSP.2003.821662.

[88] Z. He, Y. Shen, and Q. Wang. "Boundary extension for HilbertHuang transform inspired by gray prediction model." In: *Signal Processing* 92.3 (2012), pp. 685–697. DOI: 10.1016/j.sigpro.2011.09.010.

[89] X. Hu, S. Peng, and W. L. Hwang. "EMD revisited: A new understanding of the envelope and resolving the mode-mixing problem in AM-FM signals." In: *IEEE Transactions on Signal Processing* 60.3 (2012), pp. 1075–1086. DOI: 10.1109/TSP.2011.2179650.

[90] S. Loutridis. "Damage detection in gear systems using empirical mode decomposition." In: *Engineering Structures* 26.12 (2004), pp. 1833–1841. DOI: 10.1016/j.engstruct.2004.07.007.

[91] S. J. Loutridis. "Instantaneous energy density as a feature for gear fault detection." In: *Mechanical Systems and Signal Processing* 20.5 (2006), pp. 1239–1253. DOI: 10.1016/j.ymssp.2004.12.001.

[92] J. Cheng, D. Yu, J. Tang, and Y. Yang. "Application of frequency family separation method based upon EMD and local Hilbert energy spectrum method to gear fault diagnosis." In: *Mechanism and Machine Theory* 43.6 (2008), pp. 712–723. DOI: 10.1016/j.mechmachtheory.2007.05.007.

[93] L. Hui, Z. Yuping, and Z. Haiqi. "Wear detection in gear system using Hilbert-Huang transform." In: *Journal of Mechanical Science and Technology* 20.11 (2006), pp. 1781–1789. DOI: 10.1007/BF03027572.

[94] N. E. Huang and Z. Wu. "Ensemble Empirical Mode Decomposition: a Noise-Assisted Data Analysis Method." In: *Advances in Adaptive Data Analysis* 01.01 (2009), p. 1. ISSN: 1793-5369. DOI: 10.1142/S1793536909000047.

[95] J.-R. Yeh, J.-S. Shieh, and N. E. Huang. "Complementary Ensemble Empirical Mode Decomposition: a Novel Noise Enhanced Data Analysis Method." In: *Advances in Adaptive Data Analysis* 02.02 (2010), pp. 135–156. DOI: 10.1142/S1793536910000422.

[96] M. E. Torres, M. A. Colominas, G. Schlotthauer, and P. Flandrin. "A complete ensemble empirical mode decomposition with adaptive noise." In: *2011 IEEE International Conference on Acoustics, Speech and Signal Processing (ICASSP)*. Prague: IEEE, May 2011, pp. 4144–4147. DOI: 10.1109/ICASSP.2011.5947265. URL: http://ieeexplore.ieee.org/lpdocs/epic03/wrapper.htm?arnumber=5947265http://ieeexplore.ieee.org/document/5947265/.

[97] J. Lin and Q. Chen. "Application of the EEMD method to multiple faults diagnosis of gearbox." In: *Proceedings - 2nd IEEE International Conference on Advanced Computer Control, ICACC 2010* 2.1 (2010), pp. 395–399. DOI: 10.1109/ICACC.2010.5486649.

[98] Z. Feng, M. Liang, Y. Zhang, and S. Hou. "Fault diagnosis for wind turbine planetary gearboxes via demodulation analysis based on ensemble empirical mode decomposition and energy separation." In: *Renewable Energy* 47 (2012), pp. 112–126. DOI: 10.1016/j.renene.2012.04.019.

[99] L. Zhao, W. Yu, and R. Yan. "Gearbox Fault Diagnosis Using Complementary Ensemble Empirical Mode Decomposition and Permutation Entropy." In: *Shock and Vibration* 2016 (2016), pp. 1–8. ISSN: 1070-9622. DOI: 10.1155/2016/3891429.

[100] Vanraj, S. S. Dhami, and B. S. Pabla. "Non-contact incipient fault diagnosis method of fixed-axis gearbox based on CEEMDAN." In: *Royal Society Open Science* 4.8 (Aug. 2017), p. 170616. ISSN: 2054-5703. DOI: 10.1098/rsos.170616.

[101] Y. Lei, Z. Liu, J. Ouazri, and J. Lin. "A fault diagnosis method of rolling element bearings based on CEEMDAN." In: *Proceedings of the Institution of Mechanical Engineers, Part C: Journal of Mechanical Engineering Science* 0.28 (2015), pp. 1–12. DOI: 10.1177/0954406215624126.

[102] S. Mohanty, K. K. Gupta, and K. S. Raju. "Vibro-Acoustic Fault Analysis of Bearing Using FFT, EMD, EEMD and CEEMDAN and Their Implications." In: *Advances in Machine Learning and Signal Processing: Proceedings of MALSIP 2015*. Ed. by J. P. Soh, L. W. Woo, A. H. Sulaiman, A. M. Othman, and S. M. Saat. Cham: Springer International Publishing, 2016, pp. 281–292. ISBN: 978-3-319-32213-1. DOI: 10.1007/978-3-319-32213-1_25.

[103] Y. Lei, J. Lin, Z. He, and M. J. Zuo. "A review on empirical mode decomposition in fault diagnosis of rotating machinery." In: *Mechanical Systems and Signal Processing* 35.1-2 (2013), pp. 108–126. DOI: 10.1016/j.ymssp.2012.09.015.

[104] C. Capdessus. "Aide au diagnostic des machines tournantes par traitement du signal." PhD Thesis. Institut National Polytechnique de Grenoble, 1992.

[105] P. D. McFadden and J. D. Smith. "A signal processing technique for detecting local defects in a gear from the signal average." In: *Proceedings of the Institution of Mechanical Engineers, Part C: Journal of Mechanical Engineering Science* 199 (1985), pp. 287–292. DOI: 10.1243/PIME.

[106] L. Cohen. *Time-frequency analysis*. Prentice-Hall PTR, 1995. ISBN: 0-13-594532-1.

[107] A. Tabrizi, L. Garibaldi, A. Fasana, and S. Marchesiello. "Influence of Stopping Criterion for Sifting Process of Empirical Mode Decomposition (EMD) on Roller Bearing Fault Diagnosis." In: *Advances in Condition Monitoring of Machinery in Non-Stationary Operations*. Springer Berlin Heidelberg, 2014, pp. 389–398. ISBN: 978-3-642-39347-1. DOI: 10.1007/978-3-642-39348-8.

[108] G. Rilling, P. Flandrin, P. Gon, and D. Lyon. "On Empirical Mode Decomposition and Its Algorithms." In: *IEEEEURASIP Workshop on Nonlinear Signal and Image Processing NSIP* 3 (2003), pp. 8–11.

[109] Z. Wu and N. E. Huang. "Ensemble Empirical Mode Decomposition." In: *Advances in Adaptive Data Analysis* 1.1 (2009), pp. 1–41. DOI: 10.1515/BMT.2010.030.

[110] M. A. Colominas, G. Schlotthauer, M. E. Torres, and P. Flandrin. "Noise-Assisted Emd Methods in Action." In: *Advances in Adaptive Data Analysis* 04.04 (2012), p. 1250025. DOI: 10.1142/S1793536912500252.

[111] Y. Lei, Z. He, and Y. Zi. "Application of the EEMD method to rotor fault diagnosis of rotating machinery." In: *Mechanical Systems and Signal Processing* 23.4 (2009), pp. 1327–1338. DOI: 10.1016/j.ymssp.2008.11.005.

[112] M. Q. Xu, Y. B. Li, H. Y. Zhao, and S. Y. Zhang. "Application of MSE-EEMD Method in Gear Fault Diagnosis." In: *Applied Mechanics and Materials* 530-531 (2014), pp. 261–265. ISSN: 1662-7482. DOI: 10.4028/www.scientific.net/AMM.530-531.261.

[113] M. A. Colominas, G. Schlotthauer, and M. E. Torres. "Improved complete ensemble EMD: A suitable tool for biomedical signal processing." In: *Biomedical Signal Processing and Control* 14.1 (2014), pp. 19–29. DOI: 10.1016/j.bspc.2014.06.009.

[114] J. Dybała and R. Zimroz. "Rolling bearing diagnosing method based on empirical mode decomposition of machine vibration signal." In: *Applied Acoustics* 77 (2014), pp. 195–203. DOI: 10.1016/j.apacoust.2013.09.001.

[115] G. D'Elia. "Fault detection in rotating machines by vibration signal processing techniques." PhD Thesis. Università degli Studi di Bologna, 2008, p. 113. DOI: 10.6092/unibo/amsdottorato/952.

[116] I. Daubechies, J. Lu, and H.-T. Wu. "Synchrosqueezed wavelet transforms: An empirical mode decomposition-like tool." In: *Applied and Computational Harmonic Analysis* 30.2 (Mar. 2011), pp. 243–261. ISSN: 10635203. DOI: 10.1016/j.acha.2010.08.002. eprint: 0912.2437.

[117] A. Hyvarinen, J. Karhunen, and E. Oja. *Independent Component Analysis*. John Wiley & Sons, Inc., 2001. ISBN: 978-0-471-40540-5.

[118] M. C. Jones and R Sibson. "What is Projection Pursuit?" In: *Journal of the Royal Statistical Society* 150.1 (1987), pp. 1–37.

[119] B. N. Parlett. *The symmetric eigenvalue problem*. SIAM, 1998. ISBN: 0-89871-408-8. DOI: 10.1201/b11842-6.